Analysis of the Mechanical Reaction of Human Endothelial Cells to a Single Constant or Transient Uniaxial Strain

Dissertation

zur

Erlangung des Doktorgrades (Dr. rer.nat.)

der

Mathematisch-Naturwissenschaftliche Fakultät

der

Rheinische Friedrich-Wilhelms-Universität Bonn

vorgelegt von

Zhanna Santybayeva

aus Almaty, Kazakhstan

Bonn, 2013

Angefertigt mit Genehmigung der Mathematisch-Naturwissenschaftlichen Fakultät der Rheinischen Friedrich-Wilhelms-Universität Bonn

1. Gutachter: Prof. Dr. Rudolf Merkel

2. Gutachter: Prof. Dr. Ulrich Kubitscheck

Tag der Promotion: 13.02.2014

Erscheinungsjahr: 2014

Zusammenfassung

Eine Vielzahl von adhärenten Zelltypen ist ständig verschiedenen mechanischen Belastungen ausgesetzt. Vaskuläre Endothelzellen, Alveolarzellen und Zellen des Magen-Darm-Tracks erfahren beispielsweise periodische Deformationen durch den Blutkreislauf, Atmung und Peristaltik. Die Zellen können diesen Belastungen standhalten, indem sie die Deformation erkennen und durch biochemische oder mechanische Rückkopplung entsprechend reagieren. Diese Fähigkeit wird Mechanosensitivität genannt und ist von entscheidender Bedeutung für die normale Zellfunktion, Proliferation und das Überleben. Die Weiteren ist die Mechanosensitivität wichtig in pathogenen Prozessen wie Krebs, Atherosklerose und Plaquebildung [1]. Die mechanische Zellantwort besteht im Umbau der internen spannungs-aufnehmenden und spannungs-erzeugenden Strukturen wie z.B. im Aktomyosin-Zytoskelett und in den fokalen Adhäsionen. Das hochdynamische Aktinnetzwerk besteht aus einzelnen Aktinfilamenten und Aktinbündeln, die durch Kreuzvernetzer wie α-Actinin zusammen gebunden sind. Mit Hilfe des kontraktilen Aktomyosin-Apparats kann das Netzwerk die Kräfte an die zellulären Adhäsionsstellen vermitteln. Letztere sind mit den Transmembranrezeptoren verbunden, die sich an der Außenseite der Zelle, z.B. an die extrazelluläre Matrix oder an benachbarte Zellen befestigen. Somit werden intern erzeugte Kräfte auf die Umgebung der Zelle übertragen, wodurch der gesamte Prozess der Kraftaufnahme reziprok ist.

Die vaskulären Endothelzellen sind dafür bekannt, auf mechanische Reize reagieren zu können, die in ihrer physiologischen Umgebung entstehen [2], wie zum Beispiel auf Scherströmung und Druck der pulsierenden Bewegung des Blutes durch das Blutgefäß oder auf eine angelegte radiale Kompression der glatten Muskulatur um die Vene. Außerdem erfassen Endothelzellen die Steifigkeit der zugrunde liegenden Basalmembran, was ihnen die Fähigkeit verleiht, bei Entzündungen oder Atherosklerose entgegenzuwirken [3]. Daher war es unser Ziel, die mechanische Reaktion der Endothelzellen auf äußere Belastung zu analysieren. Hierfür wurden die Zellen auf einem elastischen Substrat mit passender Elastizität kultiviert und einer uniaxialen Dehnung ausgesetzt, um *in vivo* Bedingungen nachzuahmen.

Um diese Experimente zu realisieren, ist ein neuer Aufbau einschließlich geeigneter Software entwickelt worden. Der Aufbau kombiniert die Lebendzellmikroskopie unter

nahezu physiologischen Bedingungen, die Zellkraftmikroskopie und die Substrat-Dehnung. Zwei Arten der Dehnungsprotokolle wurden verwendet: eine konstante 20% Dehnung und eine transiente 20% Dehnung. Die Zellen wurden vor und nach der Dehnung optisch abgebildet. Die Zugkräfte der Zellen wurden über die numerische Lösung des Boussinesq-Problems des elastischen Halbraumes abgeschätzt [4]. Darüber hinaus wurden geometrische Parameter wie Fläche, Orientierung, Ausdehnung und Aspektverhältnis der Zellen vermessen. Die zwei Dehnungsprotokolle verursachten zwei verschiedene Zellreaktionen. Die transiente Dehnung induzierte einen abrupten Abfall der Zellkräfte um 20%, die sich innerhalb von 5 min wieder vollständig auf das Vordehnungsniveau ausglichen. Andere visuelle Änderungen des Verhaltens von Zellen wurden nicht beobachtet. Die Zellen änderten weder ihre Ausrichtung noch Morphologie nach der transienten Dehnung. Im Gegensatz dazu führte eine konstante Dehnung zu einem plötzlichen Anstieg der kontraktilen Kräfte von bis zu 150%. Nach dem Strecken erhöhten sich diese Kräfte für etwa weitere 10 min. Danach fielen sie entweder allmählich ab oder blieben auf dem maximalen Niveau stehen. In diesem Dehnungsprotokoll zeigten überraschenderweise 90% der beobachteten Zellen Kräfte, die sich nicht bis zum Ende der Beobachtungszeit (70-100 min) auf das Vordehnungsniveau entspannten. Gleichzeitig wurden Zellorientierung und Ausdehnung während Messungen nach dem Strecken beibehalten: die Zellen folgten einfach der Verformung des Substrats. Obwohl die Resultate im Einklang mit früheren Befunden sind, motivieren diese Ergebnisse zukünftige Untersuchungen der genauen beteiligten subzellulären Prozesse.

Die zwei Arten der Experimente erzeugten verschiedene mechanische Zellreaktionen. Die Zellantwort war universell in jedem Dehnungsprotokoll: alle Zellen zeigten die gleiche Reaktion, unabhängig von der Vorspannung der Zelle. Die Änderung der kontraktilen Kräfte bedeutet, dass die Aktomyosin-Aktivität sich gemäß der angelegten Spannung anpasst. Die Zellorientierung blieb in diesen Dehnungsexperimenten konstant. Dies bedeutet, dass eine längere und wiederholte externe mechanische Belastung notwendig ist, um die Zellorientierung entweder in Richtung minimaler Dehnung oder Belastung zu ändern, wie es in zyklischen Dehnungsexperimenten gezeigt wurde. Diese Beobachtungen motivieren weitere Untersuchungen der Aktomyosin- und Aktinkreuzvernetzer-Kinetik unter einzelner Dehnung oder Kompression, sowie der schrittweisen Änderung der Kontraktilität und Orientierung der Zelle unter zyklischer Dehnung.

Abstract

Many adherent cell types are continually exposed to a variety of mechanical stresses. For instance, vascular endothelial cells, alveolar cells, and cells of gastrointestinal tract experience periodic strains due to blood circulation, breathing and peristaltic activity. In order to withstand those stresses, cells have to be able to perceive them and to react accordingly through a biochemical or mechanical feedback. This ability, called mechanosensitivity, is crucial for normal cell function, proliferation, and survival. Mechanosensing is believed to be important in such processes as cancer, atherosclerosis and plaque formation [1]. In particular, mechanical cell response is manifested in modulation of the internal stress-bearing and stress-generating structures as actin cytoskeleton and focal adhesions. The highly dynamic actin network consists of single filaments and actin bundles, connected by a variety of cross-linking proteins like α-actinin. The filaments transmit forces produced by the contracting actomyosin machinery to the cellular adhesion sites. The latter connects to transmembrane proteins anchoring to the outside of the cell, be that extracellular matrix or neighbouring cells. Thus, internally generated forces are transmitted to the environment of the cell, implying that the whole process is reciprocal.

In this work the mechanical response of vascular endothelial cells was studied. These cells are known to be responsive to mechanical stimuli present in their physiological environment [2], where they are exposed to shear flow and pressure of the pulsating movement of blood through the vessel, and radial compression created by the smooth muscle tissue encircling the vein. Besides, endothelial cells sense the stiffness of the underlying basal membrane which is essential at counteracting in case of inflammation or atherosclerosis [3]. Therefore, we aimed to examine the mechanical response of vein endothelial cells to an external stress. Here, cells cultivated on an elastic substratum of suitable elasticity were exposed to a uniaxial stretch in order to mimic *in vivo* conditions.

To realize these experiments, a new setup and suitable software have been developed. The setup successfully combined live cell imaging at close to physiological conditions, traction force microscopy, and substrate stretching. Two kinds of stretch protocols were used: a constant 20% strain (also called stretch-and-hold) and a transient 20% (stretch-and-release).

Cells were imaged before and after stretching for comparison. Cell traction forces were calculated by solving the Boussinesq problem for infinite layers with the help of a Fourier transform method combined with regularization [4]. In addition, such geometrical parameters as cell area, orientation, elongation and aspect ratio were measured. The two kinds of strain protocols prompted two different cell reactions. Transient strain induced an abrupt drop of cell forces by 20% that recovered completely to the pre-stretch level within 5 min. No other visual changes of the cell behaviour were detected. Cells did not change their orientation or morphology after the stretch-release cycle. In contrast, constant strain evoked a sudden rise of contractile forces by up to 150%. These forces continued to increase for about 10 min after stretching. After that they either decreased gradually or remained at the maximal level. Surprisingly, in this strain protocol 90% of the observed cells exhibited forces that did not relax to the pre-stretch levels until the end of observation (70-100 min). At the same time, cell orientation and elongation persisted throughout measurements after stretching: cells simply followed the deformation of the substrate.

The two types of experiments resulted in different kinds of mechanical response of the cell. The cell response was universal under each strain type: in practice, all cells displayed the same reaction, independently of the cell pre-stress history. The change in contractility indicated that the actomyosin activity adapted according to the applied stress. The cell orientation upon the stretch persisted in these single stretch experiments. This implies that a longer and a repetitive exposure to external loads is necessary to induce cell reorientation in either minimum stress or minimum strain direction as in cyclic stretch experiments. These observations motivate further investigations of the cell actomyosin and actin cross-linker kinetics upon single stretch or compression, as well as of gradual change of cell contractility and orientation in cyclic stretch experiments.

Dedication

To my parents and my little brother

Acknowledgement

I am deeply grateful to my supervisor Prof. Dr. Rudolf Merkel for accepting me in the field with zero experience in the cell culture work, and believing I would manage to learn, for help and advice, and all the productive discussions together with Dr. Bernd Hoffman.

Dr. Norbert Kirchgessner, Dr. Ronald Springer, Georg Dreissen for programming tips and implementations, for facilitating analysis, tea-times, and serious and fun discussions. Wolfgang Rubner, Johannes Fleischhauer, Werner Hüttner for giving hand in the hardware and electronics matters. The IT crowd for the updates and fixing computer problems.

Claudia Klamandt for always helping with documents, sympathy, and nice chats in between the work.

Special thanks to my office-mate Kevin Küpper for giving important advice concerning the lab and everyday life, and for the very first corrections, and Alex Zielinski for always helping around in the lab and with cells. It has been a great pleasure to work with Christian Kleusch, Cornelia Monzel, David Kirchenbüchler, and all the colleagues, that I thank for being so friendly and supportive. Nico, Simone and Nils for sharing the valuable experience of the lab work.

Thorsten Auth and my friends from the Biosoft for giving a chance to learn many important things about and around science, and to upgrade soft skills. Many thanks to my friends and scientific acquaintances, who kept me going, by sharing their successes and fails, their opinions and challenges, and more importantly, for all the chocolate and waffle breaks by the lake.

I thank my colleagues and friends who found the time to review the text of the dissertation, even though they were very busy themselves. I'd like to thank everyone for helpful suggestions and constructive criticism of the work. My super gratitude to my super friend Simón Poblete, who read and reviewed this work, until it reached a reasonable level of readability, for all fruitful discussions and interesting and inspiring stories. All hail to the coffee and Radio 6 Music!

I express my greatest gratitude to my greatest parents and little brother for all the irreplaceable support during all these years.

Table of Contents

List of Figures

1. Introduction

For survival and proper function, adherent cells have to actively respond and adapt to biochemical and mechanical cues of the surrounding extracellular matrix or neighbouring cells. The mechanical reaction of endothelial cells to uniaxial strains is of primary interest in this work. The cells are able to alter their internal stresses and forces they apply in order to withstand mechanical loads. Cell forces can be detected and evaluated with appropriate traction force techniques.

1.1 Cell Mechanosensitivity

Primary human umbilical vein endothelial cells (pHUVECs) were studied in the current work. Among the assortment of adherent cells, vascular endothelial cells (VECs) are of great interest, because they naturally undergo a variety of mechanical stresses (Figure 1.1). Smooth muscle cells covering the vein contract periodically to advance the blood through. At the same time, blood presses on the walls of veins and shears the endothelium when flowing. Furthermore, the cells are exposed to stresses applied by adjacent tissues. While forming an inner lining of blood vessels, endothelial cells actively participate in many processes, such as hemostasis, thrombosis, and vascular resistance [5].

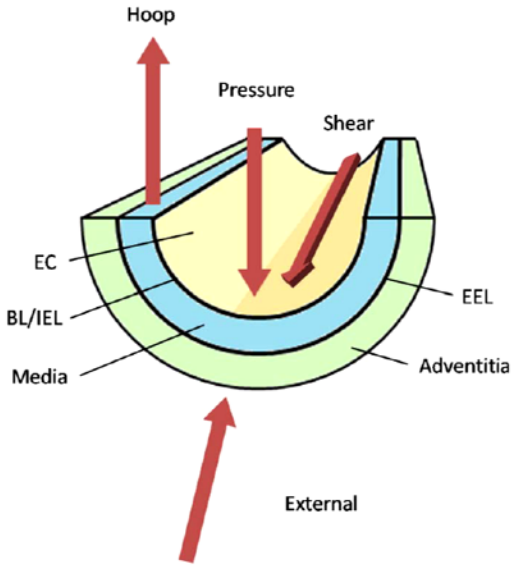

Figure 1.1. Cartoon of a blood vessel with applied forces [6]. EC – endothelial cells, BL – basement lamella, IEL and EEL – internal and external elastic laminae.

It has been extensively demonstrated that endothelial cells sense structure, stiffness, stress, and deformations of the underlying matrix [7]–[12]. Cell body orientation follows

patterns on the surface they adhere to (Figure 1.2. a). In addition, these cells sense the rigidity of their substratum, a property that is essential in tubulogenesis [13] (Figure 1.2. b) and in pathogenic processes, like atherosclerosis [3]. Furthermore, the cells actively rearrange themselves and their inner structures as a result of application of external forces (Figure 1.2. c).

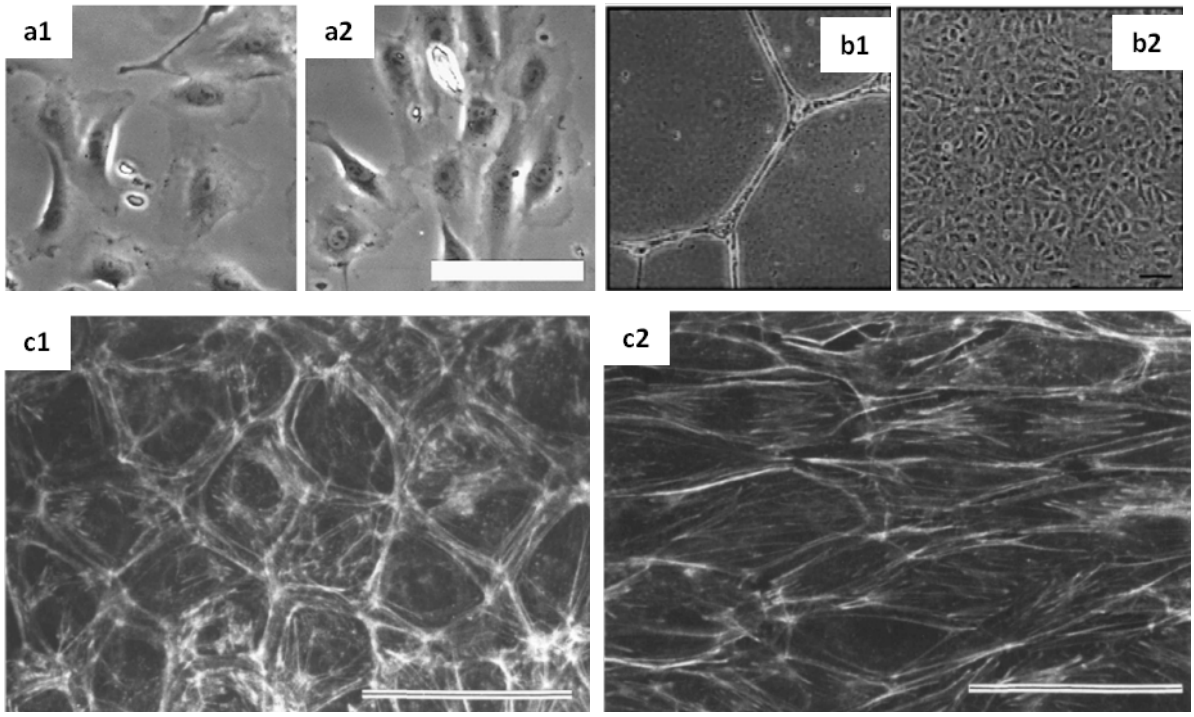

Figure 1.2. VECs mechanosensitivity. (a) HUVECs cultured on different topology [10]. (a1) On a flat surface have no preferred orientation, (a2) on a ridged surface cells align along the seams. Scale bar 100 µm. (b) HUVECs cultured on gels of different stiffness [13]. (b1) Grown on matrigel containing heat-denatured type I collagen, and (b2) polymeric type I collagen. Scale bar 25 µm. (c) Monolayers of rhodamine phalloidine stained bovine aortic endothelial cells [2]. (c1) No-stress control state. (c2) After 24 h exposure to 3 Pa shear stress. Scale bars 50 µm.

In this work, two kinds of strain protocols were applied: a transient and a constant uniaxial stretch. A similar research on various cell types showed, that the cells respond to stretch either by prompt fluidization of their cytoskeleton followed by its reinforcement or only by stiffening of the cytoskeleton and reinforcement [14]–[18]. In attempt to resolve this discrepancy it was speculated, that response of cells depends primarily on their cytoskeletal prestress: stiffer cells react by fluidizing and softer cells reinforce in order to comply with the applied stresses [19]. Other obvious explanations included dependence on the cell type, experimental setup, etc. However, the exact mechanisms of the cell reaction remain unclear although some clues have been suggested, in which the main role is given to the contractile actomyosin network.

1.2 Contractile Actin Cytoskeleton

Cell integrity and shape are supported by its cytoskeleton, which is made up of three types of filaments: actin filaments, intermediate filaments, and microtubules. Since actin filaments together with motor proteins are the force-generating structures, they are of major importance in this work. Actin filaments are highly dynamic structures made up of a globular protein actin. They assemble and disassemble in a way that allows the cell to react very fast to the changing conditions of the environment. Single actin filaments connected by cross-linking proteins like α-actinin form actin bundles. Several bundles assemble into more stable and thicker stress-fibres linked by a motor-protein non-muscle myosin. When the latter changes its conformation by ATP (adenosine triphosphate) hydrolysis, an event known as a *power stroke,* it causes stress fibre contraction.

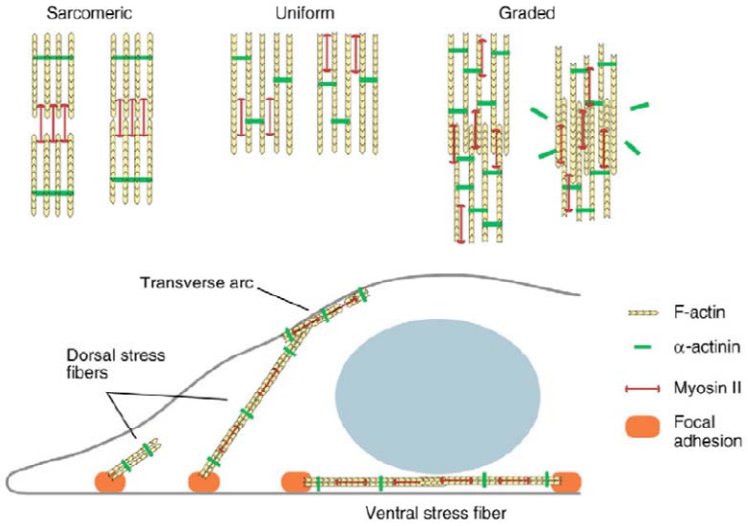

Figure 1.3. Actin stress-fibre structure in non-muscle cells [20]. Depending on the location and function, three main types of actin stress-fibres have been distinguished: ventral, transverse, and dorsal SF.

The structural organization of stress fibers varies depending on the location and their direct function (Figure 1.4) [20], [21]. For instance, ventral SF have either graded structure or sacromeric-like structure similar to that of muscle cells, so that they are able to extend or contract, e.g. under changing tension (Figure 1.3). The ends of actin stress fibres connect to adhesion protein complexes, creating an active framework of a cell, and defining its internal stress, or called otherwise *prestress* [22], [23]. It was shown that actin filaments and entire stress fibers are themselves able to function as mechanosensors, for instance, by inhibiting binding of fiber severing proteins as cofilin under strain, or by means of focal adhesion associated proteins, like zyxin and talin [24], [25].

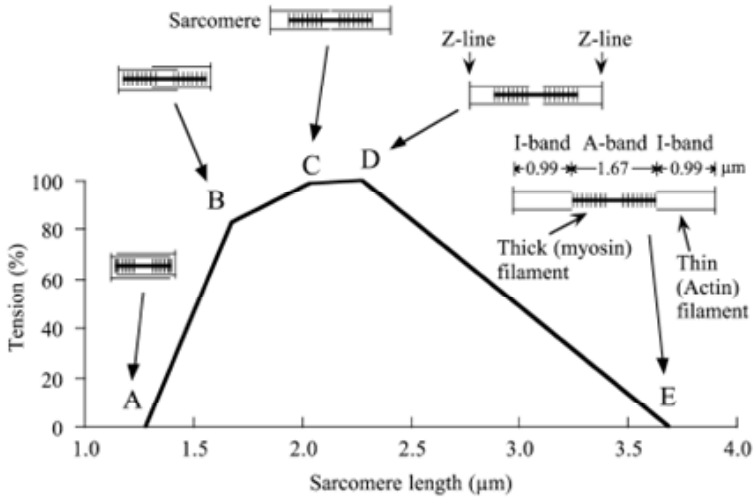

Figure 1.4. Length change of a muscle sacromere under tension. [26] The structure elongates upon increased strain.

Adhesion sites connect to the outside of the cell via transmembrane receptors of integrin family. Thus, cell traction forces are transmitted to the extracellular matrix (ECM, a network of proteins, such as fibronectin and collagen, and polysaccharides that compose intercellular space) or adjacent cells.

1.3 Cell Traction Forces

Various methods of cell force detection have been developed. One of the first introduced methods used wrinkling of a thin film to which cells adhered as a measure of applied force [27] (Figure 1.5 a). However, this led to highly demanding calculations because of the non-linearity of deformations. Other methods involve 3-dimensional microstructures, e.g. micropillars [28], from which deflection cell forces are evaluated (Figure 1.5 b). However, the structure might not exactly mimic the natural environment of cells. Other methods, induce local deformations of a cell, such as micropipette aspiration (Figure 1.5 c), pulling on a magnetic bead, to which a cell created contact, etc. [29]–[31]. The reported cell force magnitude is in pN to nN range, depending on the cell type and cell activity.

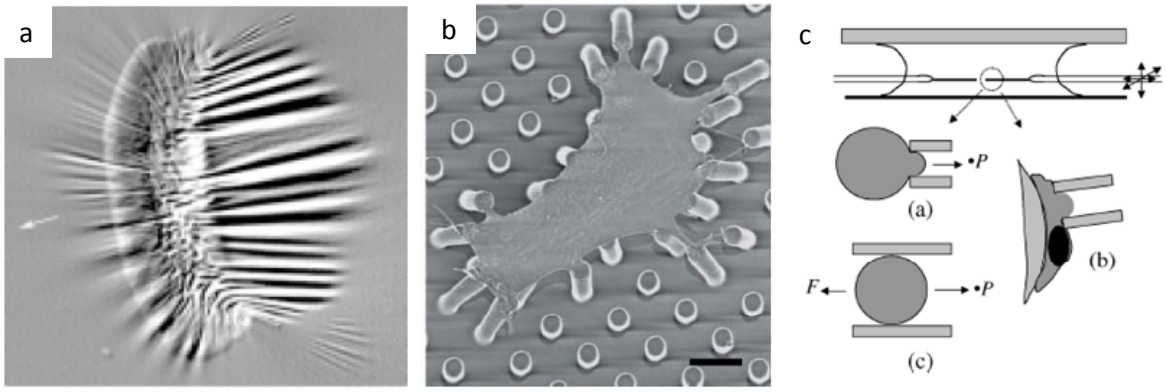

Figure 1.5. Cell traction force techniques. (a) Wrinkling of a thin elastic lamella [32]. (b) Micropillars deflection [33]. (c) Micropipette aspiration [29].

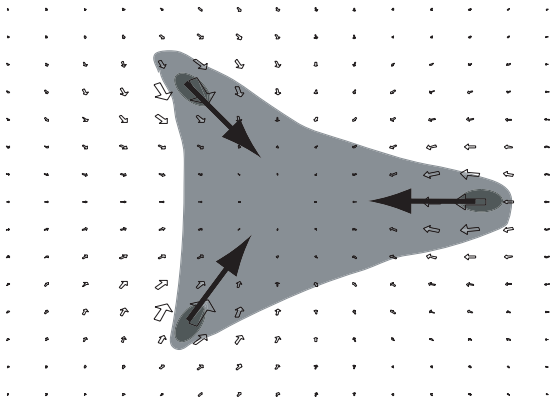

Figure 1.6. Deformation of the substrate by a cell. When adhered to a flat surface (dark grey ellipses are adhesion sites) cells deform the upper layers by applying traction forces (dark arrows). Open arrows represent deformation vectors. [34].

In the current work, the deformation of a flat substrate by a cell is used for cell force detection (Figure 1.6). When a cell creates adherent contacts to an elastic surface, it deforms its upper layers. In order to detect these deformations, fluorescent microscopic markers (beads) are incorporated into the upper layer of the substrate material, so that beads displace together with it. By comparing images of a relaxed substrate and those where cell was applying force, one can evaluate cell forces. In order to get an image of a relaxed substrate, the cell has to be detached from it mechanically or chemically (see Section 2.1). This method of cell traction force calculation was first proposed by M. Dembo and Y.-L.Wang [6], and improved by introducing a regularization of the solution by S. Houben and colleagues [34].

For simplicity, it is assumed that the material of the substrate is linear, isotropic, and homogeneous, and that the deformation is homogeneous throughout the substrate. Knowing the properties of the material (thickness, Young's modulus and Poisson's ratio) traction forces can be calculated from these deformations. The linearity assumption permits to use the Hooke's law in a first approximation. Young's elastic modulus characterizes stiffness of

elastic materials. It is a measure of how much force per area (stress σ) should be applied to deform a substrate to certain magnitude (strain ε), and is defined as:

$$E = \frac{\sigma}{\varepsilon} = \frac{F/A}{\Delta l/l} \tag{1}$$

where F is the applied force, A is the cross-sectional area to which force is applied, Δl is the elongation and l is the initial length of the object of interest (Figure 1.7 a).

Suppose, a rod made of an isotropic elastic material is being stretched along one direction. It will compress in two other dimensions perpendicular to the force application. The ratio between the transverse compression and the axial stretch is called Poisson's ratio (Figure 1.7 b):

$$\nu = -\frac{\varepsilon_\perp}{\varepsilon_\parallel} = -\frac{\varepsilon_y}{\varepsilon_x} = -\frac{\varepsilon_z}{\varepsilon_x} \tag{2}$$

where axial and transverse strains are the relative changes in length: $\varepsilon_x = \frac{\Delta x}{x}, \varepsilon_y = \frac{\Delta y}{y}, \varepsilon_z = \frac{\Delta z}{z}$.

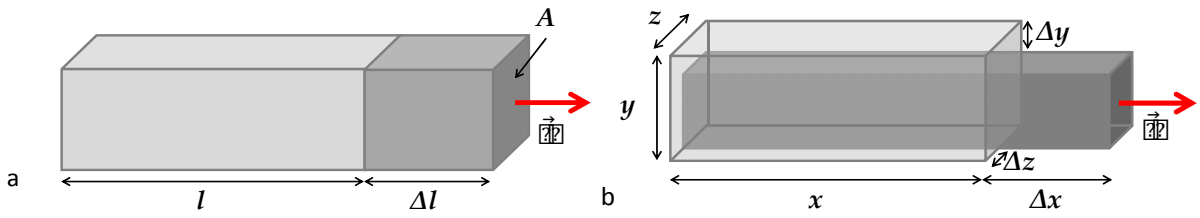

Figure 1.7. Young's modulus and Poisson's ratio. (a) Force applied to the cross-sectional area of a bar causes change in the length. The ratio between stress and strain is Young's modulus. (b) Stretching a rod along x-axis results in compression in y and z. The ratio between axial and transverse strains is Poisson's ratio.

Force estimation assumes that the thickness of the substrate is infinite (>100 μm, or larger than the lateral size of a cell) compared to deformations [7], [35], and therefore forces are constrained to the surface, or said to be tangential. The deformations of the substrate are related to the forces through a Green's tensor in the Fredholm's integral equation of the first kind:

$$\vec{u}(x,y) = \int \vec{\vec{G}}(x-x',y-y')\vec{f}(x',y')dx'dy' \tag{3}$$

where $\vec{u}$ represents the deformation field, and $\vec{\vec{G}}$ is the Green's tensor, that relates surface displacements $r = \sqrt{(x-x')^2 + (y-y')^2}$ with (x, y) initial coordinates, and (x', y') – displaced coordinates, and material properties (Poisson's ratio, ν, and Young's modulus, E):

$$\vec{\vec{G}} = \frac{1+\nu}{2\pi E r}\begin{pmatrix} \frac{2\nu x^2}{r^2} + 2(1-\nu) & \frac{2\nu xy}{r^2} & -\frac{1-2\nu}{r}x \\ \frac{2\nu xy}{r^2} & \frac{2\nu y^2}{r^2} + 2(1-\nu) & -\frac{1-2\nu}{r}y \\ \frac{1-2\nu}{r}x & \frac{1-2\nu}{r}y & 2(1-\nu) \end{pmatrix} \tag{4}$$

The expression (3) is a classical example of an ill-posed problem in numerical analysis, for more than one solution exists for the same dataset: the same displacement field can result in different deformations and forces. Moreover, the solution is very sensitive to minor changes in the data. The solution was first elaborated by Boussinesq for a semi-infinite substrate [7]. Ideally, the expression (3) can be solved in two steps. The right-side of the equation is a convolution of two functions. In Fourier space deconvolution is simply a product of the two variables, and hence the solution for $\vec{f}$ is found in a rather straightforward way by system of linear equations. However, any real measurement is not error-free. The uncertainty emerges from the measurement inaccuracy, noise and limited spatial resolution of the detection system, etc. Therefore, the validity of each solution must be checked through a regularization procedure [4], [36], [37]. The best-known regularization procedure is *Tikhonov regularization* that is similar to the least-squares method and minimizes the residual and penalty norms:

$$f_\lambda = argmin\left\{ \left\|G\tilde{f} - \tilde{u}\right\|^2 + \lambda\left\|I\tilde{f}\right\|^2 \right\} \tag{5}$$

where λ is the regularization parameter, I – identity operator, $\tilde{f}$ and $\tilde{u}$ are the calculated forces and measured deformations, respectively.

A convenient measure of the whole cell mechanical activity that is conventionally used in force evaluations is the first generalized moment [34]:

$$M = \sum_i \begin{pmatrix} x_i f_{i,x} & y_i f_{i,x} \\ x_i f_{i,y} & y_i f_{i,y} \end{pmatrix} \tag{6}$$

This matrix can be diagonalized assuming the torque is zero, and its trace gives the sum of its eigenvalues, i.e. the contractile moments: $\lambda_1 + \lambda_2 = \sum_i x_i f_{i,x} + \sum_i y_i f_{i,y}$. The net force applied by a stationary cell on the surface is zero. Therefore, calculating forces only inside a cell outline gives a more stable and reasonable solution.

2. Materials and Methods

In the current work primary human umbilical vein endothelial cells (pHUVECs) were chosen as a model of study (Section 2.1). Adhered to flat silicone elastomeric substrates (Sections 2.2 and 2.5) they were subjected to constant or transient uniaxial strain protocols (Section 2.6). The short and long term mechanical response of cells was observed and quantified with the help of the developed setup and software (Sections 2.3 and 2.4, respectively).

2.1 Cell Culture

Primary HUVECs, originated from various donors, were supplied by *Lonza* (*Cologne, Germany*) with an attributed passage number *P0*. In this study cells in passages 2-6 were used. Primary HUVECs were cultured in endothelial growth medium EGM-2 (*Lonza, Cologne, Germany*; see Appendix B for details) under physiological conditions (37 °C, 5% CO_2 and 95% humidity; *Heracell 150i, Thermo Scientific, Germany*). To be transferred from culture to substrates (see Section 2.2), cells were trypsinized. To do so, they were rinsed with phosphate buffered saline solution (PBS; see Appendix B) and incubated in 1 ml (for a 35 mm tissue culture dish) of 5% trypsin-EDTA solution (TE; see Appendix B; *Sigma-Aldrich, Munich, Germany*) for 4 min at 37 °C. When cells detached, 2 ml EGM-2 were added to the suspension to block trypsin digestion. The suspension was centrifuged for 3 min at 200 g (*Heraeus Labofuge 400, Thermo Scientific, Germany*), and the pellet was resuspended in 1 ml EGM-2 for further passaging or transfer. Approximately 1,500 cells were seeded in 200 µl medium per substrate, so that by the time of acquisition there were single-lying cells (around 2,500 cells per sample). After 2 h of incubation, when cells formed stable contacts to the substrates, 7 ml of EGM-2 were added for further 24 h incubation.

Before the experiment started, the substrates were washed with PBS to get rid of cell debris. For imaging, samples were immersed in 20 ml EGM-2 with 20 mM HEPES (buffering agent, 4-(2-hydroxyethyl)-1-piperazineethanesulfonic acid; S*igma-Aldrich, Munich, Germany*), in order to supply cells with sufficient nutrients during the whole experiment without excessive evaporation. The latter supported pH of the medium at a physiological level (pH 7.2) during the whole experiment. pH and osmolarity of once used media were measured. These measurements showed that the same medium could be used for two or three further experiments (pH and osmolarity ranged in 7.0-7.6 and 0.300-0.380 osmol/kg,

respectively). Moreover, random samples of the media were checked for contamination of bacterial or fungal origin. No contamination was detected.

2.2 Substrate Manufacturing and Treatment

Flat ribbon-like (Figure 2.1 c) silicone elastomeric substrates were made of cross-linked polydimethylsiloxane (PDMS, prepared from a two-component liquid *Sylgard 184, Dow Corning, Wiesbaden, Germany*). The material exhibits physical and chemical properties, necessary for the experiment. It is biocompatible, incompressible (Poisson's ratio ~0.5) and absorbs insignificant amount of water when immersed [34]. Moreover, its stiffness can be tuned over a wide range of values (from several kPa to few MPa) by mixing the cross-linker and the base in different ratios. The procedure for calibration of the Young's elastic modulus was developed by C. M. Cesa and co-workers [34], and every batch was calibrated by N. Hampe (*ICS-7, FZ Juelich*) according to this procedure. The substrates used in the current work had a Young's modulus of 30 kPa. They were manufactured according to the moulding and curing protocol [34]. The cross-linker was stirred thoroughly with the base in a 1:45 mass-ratio. The PDMS mixture was degassed and poured into moulding forms (Figure 2.1 a, b).

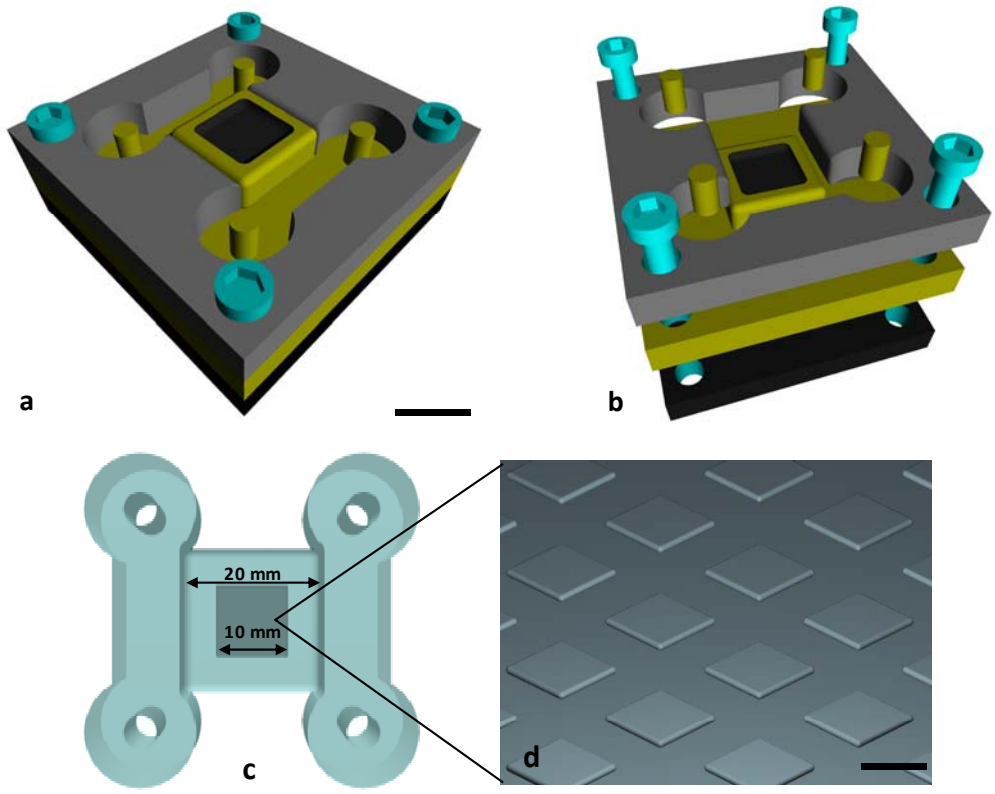

Figure 2.1. (a, b) Cartoons of a mould. Scale bar 10 mm. (c) A substrate with (d) a close-up of the 100 nm high microstructure with 3.5 µm lattice constant and 2 µm size on the substrate. Scale bar 2 µm.

The polyvinylchloride moulds had silicon wafers with a microstructure in the central part (Figure 2.1) to ensure that the imaged surface was flat, and to enable fluorescent beads incorporation. Primary HUVECs were able to recognize even 300 nm deep features on 50 kPa substrates (Figure 2.2 a), but did not sense 100 nm structure on a softer (30 kPa) surface (Figure 2.2 b). In this case, the rectangular microstructure, fabricated by photolithography, was 100 nm deep and with a 3.5 μm lattice constant (Figure 2.1 d).

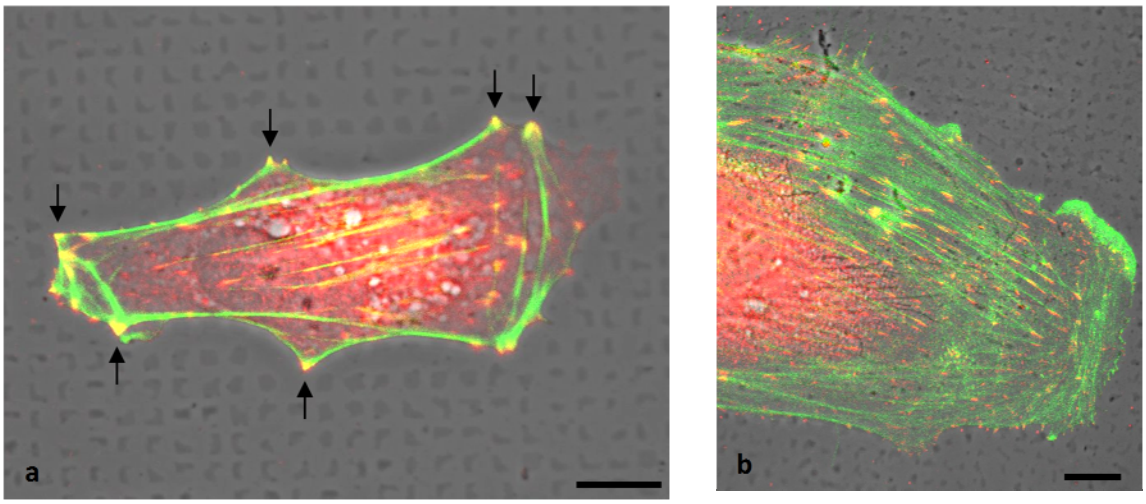

Figure 2.2. Composite fluorescence micrographs of pHUVECs. The cells were grown on the microstructured substrates of 50 kPa with 300 nm deep structures (a) and 30 kPa with 100 nm deep structures (b). They recognized the pattern on a stiffer surface and formed focal adhesions on the structures (a). Immune staining: red – vinculin, green – actin (Alexa 488-Phalloidin). Scale bars 10 μm.

In order to perform cell traction force microscopy (CTFM), fluorescent microscopic markers were embedded in the surface of substrates (Figure 2.3). Carboxylate-modified red (580 nm excitation/605 nm emission wavelengths) 100 nm microspheres (2% solid *FluoSpheres, Invitrogen, Karlsruhe, Germany*) were combined with 1 ml of uncross-linked 1:45 PDMS mixture. Prior to moulding, a drop of the beads-PDMS mix was spread over the wafer surface, so that a thin layer covered it. Excess was removed with a dust-free tissue (*Kimtech, Kimberly-Clark Professional, Irving, TX, USA*). Each mould was then filled with approximately 3.5 g of the 1:45 PDMS mixture, and cured at 60 °C for 16 h. The cross-linked silicone rubber was removed carefully from the forms with the help of filtered isopropanol (*Merck, Darmstadt, Germany*).

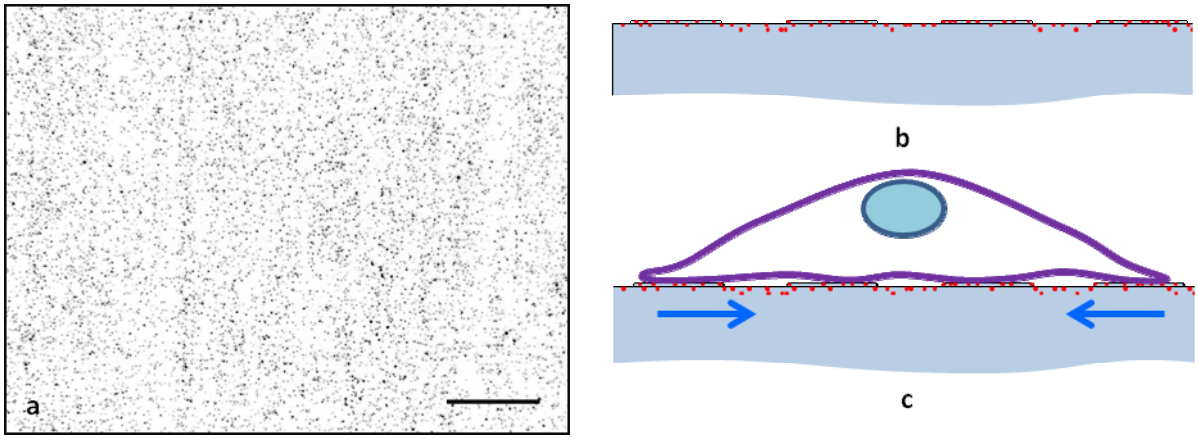

Figure 2.3. Fluorescent beads on the cross-linked PDMS substrates. (a) Inverted fluorescence micrograph of beads spread over a micropatterned surface. Scale bar 40 µm. (b) Cartoon of the substrate side cut: beads are embedded in the upper layer of the cross-linked material. (c) Cell tractions cause deformation of the upper layer of the substrate and thus bead displacements.

For the experiments, the substrates were stretched over on metal holders, and fixed with bent clamps (Figure 2.4). The advantage of using these clamps was that substrates attached more tightly to the holders. All substrates were pre-stretched by 1 mm (the inner part of the substrate is 2x2 mm^2) to prevent sagging, and thus unnecessary distortions.

In order to supply cells with sufficient medium two kinds of basins (Figure 2.4) were manufactured from acrylic glass. Both were able to contain a substrate on the holders. The first had a smaller volume (310 ml), and was designated for incubation in cell culture. The other was larger (380 ml) allowing the sample to move during the experiment.

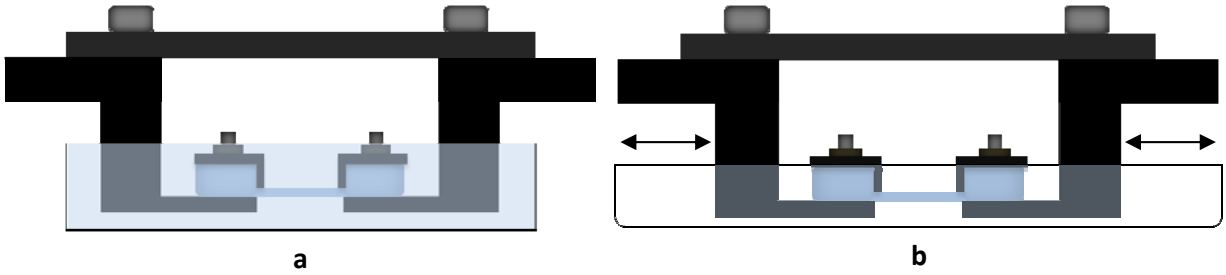

Figure 2.4. Cartoon of substrates clamped onto holders in a basin for incubation (a) and a basin for experiment (b).

Before seeding cells, holders with substrates, basins, and *Parafilm* (*Pechiney Plastic Packaging Company, Chicago, Illinois*) were disinfected with 70% ethanol solution. After drying, substrates were coated with 2.5 µg/cm^2 fibronectin solution in PBS (*BD Biosciences, Heidelberg, Germany*) and incubated at 37 °C for 30 min. Cells were seeded as described in Section 2.1. The samples were wrapped in *Parafilm* to reduce evaporation, and kept in the cell culture incubator until the beginning of the experiment.

2.3 Microscopy Setup

The setup was specifically designed and developed by the author of the thesis for live cell imaging during stretch experiments. The general idea behind the setup was to be able to find a cell on the substrate before and right after stretch was applied, and to perform imaging of the entire event.

The choice fell on an upright microscope (*Axiotech Vario*, *Carl Zeiss Inc., Jena, Germany*), for the thickness of the samples was larger than any inverted microscope was able to resolve (>350 μm). Consequently, imaging had to be performed from above the sample. Moreover, the microscope is robust and, at the same time, adaptable to additional equipment, necessary for the experiment. Its body was connected to a 380 mm high stand via a coarse z-focus system, and could slide 115 mm up- and downwards, providing an easy access to the underlying devices (Figure 2.5).

The Z-stage (P-725.1CD, *PI, Karlsruhe/Palmbach, Germany*) is a fast piezo-based device with the travel range of 100 μm, and the closed-loop resolution of 0.65 nm. It was fitted between the microscope's objective mount and the objective itself, making the latter dynamic. The stage is equipped with a programmable controller, facilitating the use of different focusing algorithms.

The illumination was supplied by a 120 W metal halide short arc lamp (*X-Cite 120, EXFO, Quebec, Canada*) with a broad emission spectrum. In all experiments a LUMPLFLN 40x (*Olympus Corp., Tokyo, Japan*) water immersion objective with numerical aperture 0.8 and working distance 3.3 mm was used.

A home-built incubator was designed such that the devices inside it could be easily accessed. A heating unit (*PeCon GmbH, Erbach, Germany*) kept temperature at a physiological level (37 °C) around the sample. No CO_2-level controlling system was employed (see Section 2.1).

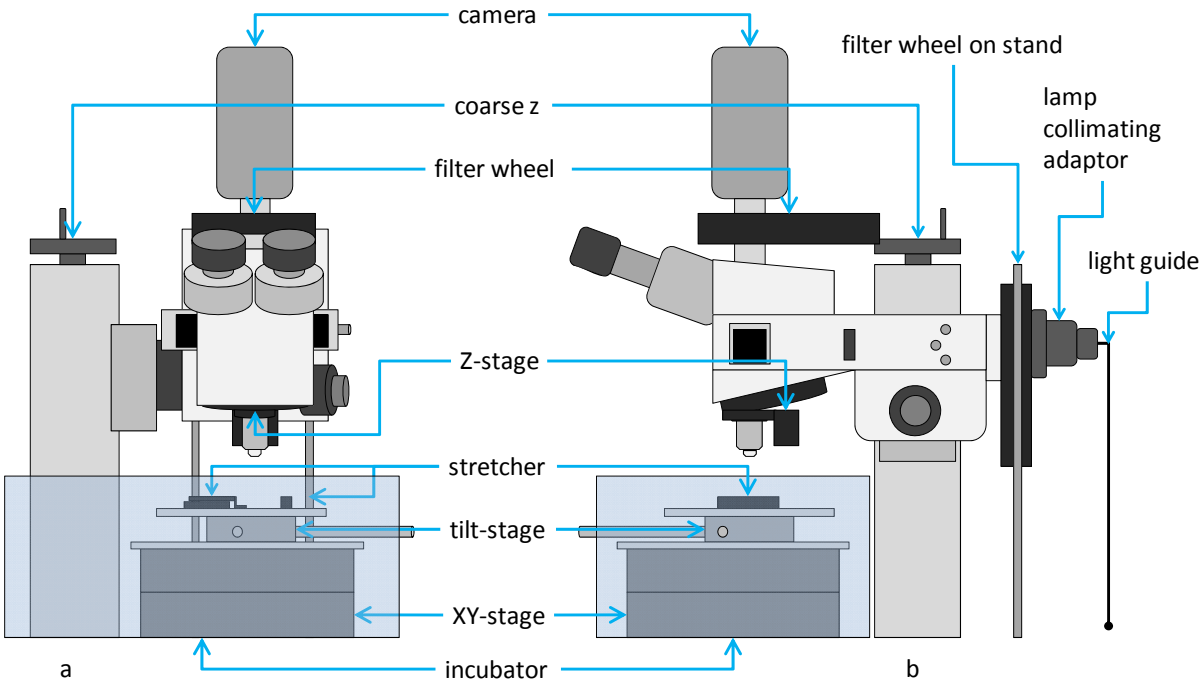

Figure 2.5. Cartoon of the setup: (a) front view, (b) side view. The microscope sits on a coarse z-stand. The lamp is connected to the excitation filter wheel by light guide, that has an additional support, and the camera is fixed directly onto the emission filter wheel. The z-stage connects the objective and the microscope. The stretcher rests on the tilt and XY-stages, covered by an incubator.

Two motorized filter wheels (500-HF110, *Prior Scientific GmbH, Jena, Germany*) for excitation and emission light were mounted directly to the microscope body. To reduce swaying of the microscope, the excitation filter wheel was installed on an additional vertical dual track, however, not firmly, so the wheel could slide along it freely. Both filter wheels have 10 positions for 25 mm round optics, and a maximum switch time between the adjacent positions of 55 ms. Depending on the experimental needs various excitation and emission filters could be fitted in the necessary order for a faster acquisition. In this work, for bright field imaging the excitation filter was a 5% transmittance optical glass (*Schott AG, Mainz, Germany*). To reduce the destructive effect of blue light on cells [38] a 2 mm thick blue filter (GG 475 nm; *Schott AG, Mainz, Germany*) was placed in addition to the 5% transmittance filter. For fluorescence imaging, an excitation band pass filter for green light (556/25 nm) was mounted. The emission band pass filter was in red (630/98 nm). No shutter was used in this work, since its opening and closing would have caused sway of the whole microscope body, thus affecting the measurement. Instead, when no images were acquired, the light was blocked by a non-transmitting blackened metal plate, fitted in the filter wheel between the two excitation filters.

Most of the substrates could not be positioned ideally parallel to the acquisition plane, thus a tilt correction was necessary. The tilt stage (M-044.00, *PI, Karlsruhe/Palmbach, Germany*)

was mounted under the linear stage plate, such that the whole sample could be inclined for ±7° around two rotational axes (Figure 2.6).

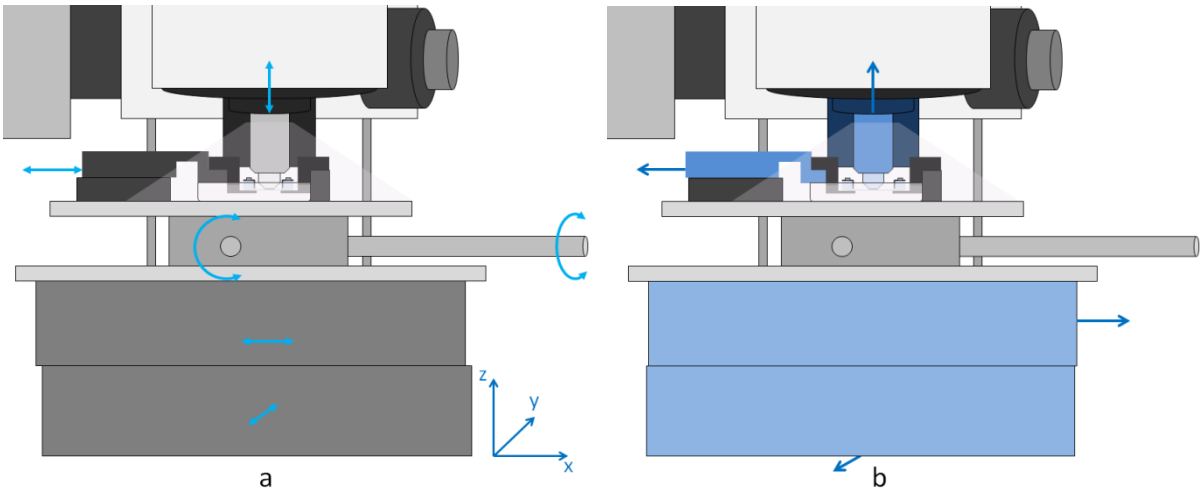

Figure 2.6. Detailed cartoon of the setup. The silicone substrate with cells is fixed on the stretcher. The tilt stage can incline the sample around two rotational axes. The XY-stage moves the stretcher and tilt stage in x- and y-directions. The basin contains sufficient amount of cell medium (a) Before stretch was applied; arrows show stretch direction, and according x-, y-, z-, and tilt-corrections, (b) after stretch application. Devices that changed their positions are coloured blue.

Substrates on holders were fixed on a linear stage, hereafter referred as the "stretcher". This device moves along one axis thus stretching or compressing samples. To move the entire sample an XY-stage was mounted under the stretcher.

The XY-stage and the stretcher are based on a stepper motor, MDrive (KT 205 and MT 63, *Steinmeyer GmbH, Albstadt, Germany*). Their controllers could be programmed using MCode commands [39]. The speed of the stretcher motor was set to 2 mm/s. The speed of the XY-stage was calculated from the speed of the stretcher, the stretch amplitude, and the jog distance in x-axis, and set such that the same region of a sample remained in the field of view of the camera. The user-defined microstep resolution (number of steps that complete one full motor rotation; denoted as "µst") of the XY-stage was set to 12800 µst/mm, and 20032 µst/mm of the stretcher.

A 12 bit CCD camera (SensiCam qe, *pco.imaging AG, Kelheim, Germany*) with a physical pixel size 6.45x6.45 µm² was connected to the emission filter wheel via a C mount. The setup equipped with a 40x water immersion objective delivered sample size of 175x175 nm² per pixel, as defined from an image of a standard calibration scale. The theoretical xy-resolution of the setup was ~330 nm for green (530 nm) and ~378 nm for red (608 nm) light. The field of view was 240.8x180 µm², being large enough to contain a single cell.

To reduce evaporation of the cell medium during the experiment, a plastic wrap folded in double of roughly 25x16 cm^2 was attached with a paper tape to the objective and around the stretcher, forming a protective tent.

2.4 Software

At different stages of the experiment suitable software and integrated development environment (IDE) were involved. The main experiments were operated by Micro-Manager 1.4 [40], image processing during acquisition was done with the help of ImageJ 1.44p [41], [42] macros and plug-ins, and the primary data processing and visualization were done in ImageJ, MATLAB 7.11 (*MathWorks, Natick, MA, USA*) and Origin 8.1 G (*OriginLab, Northampton, MA, USA*). Cell force analysis was performed using a MATLAB 7.14 standalone (*MathWorks, Natick, MA, USA*). Statistical tests were performed using R 3.0.2 (*The R Foundation for Statistical Computing, 2013*).

2.4.1 Acquisition Software

Open source software Micro-Manager 1.3 and its later version Micro-Manager 1.4 (MM) proved to be suitable and flexible as a main tool for controlling the set-up. MM was employed for imaging together with ImageJ (IJ), a Java-based image processing application. All experiment sequences were scripted by the author with the help of the lightweight source interpreter BeanShell [43], inbuilt in MM. The IJ built-in compiler was used for writing plug-ins and macros, which could be called in MM scripts during acquisition to perform image processing on the fly. All devices used in the current work had MM device adaptors, except the stretcher and the XY-stage, that were communicated through COM-ports. User friendly GUIs and scripts were developed for each type of experiment (see Appendix C).

2.4.2 Autofocus

The sample was drifting in z-axis, because of the cell medium evaporation. Generally, the drift was less than 10 μm in a 100 min experiment. It was possible to correct it automatically with an MM plug-in. The original built-in autofocus plug-in [44] was modified to comply with the Z-stage parameters and experimental requirements. NetBeans IDE 7.2.1 was employed to adapt and compile the new autofocus plug-in. To increase processing speed only part of images was regarded. Each image was cropped from the center. Crop ratios of

0.25-0.3 gave a reasonably fast and precise focusing. The search range was reduced to 6 µm in the loop acquisition for time and illumination concerns. All autofocus settings are shown in the Appendix C.

2.4.3 Reference Image Correction

Due to the high thermal expansion coefficient of cross-linked PDMS (310 ppm/K [45]), temperature change by 0.1 °C caused a 2 cm long substrate to expand or shrink by approximately 0.6 µm. Considering that the precision of the heating system could not be less than 0.1 °C, this effect was unavoidable, and deteriorated data quality.

Images of fluorescent beads on a substrate without a cell, or so called null-force reference images, were subjected the most to the effect of thermal expansion and rotation. They were acquired after cells were chemically removed from substrates (see Section 2.6), and during these manipulations the samples had to be exposed to the outer environment. Reference images had to be fitted to the images of beads with cells, in order to get rid of the distortions. Only the areas unaffected by a cell were taken into account. Rectangular regions of interest (ROIs) were manually set around the cell in order to exclude areas, deformed by it, ensuring that sufficient number of beads was inside them (Figure 2.7).

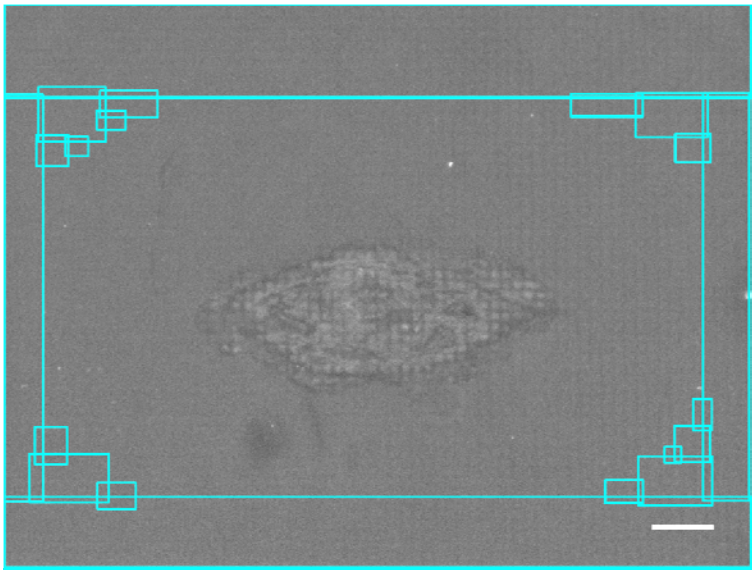

Figure 2.7. Bright field micrograph of a cell. Overlapping ROIs were set manually around the cell so that areas deformed by the cell's tractions were not included. Scale bar 20 µm.

All data points, i.e. coordinates of the positions of beads, inside the ROIs were used for the linear least squares fit of the form:

(7)

Here x, y are coordinates of an object in the corrupt image, x', y' are coordinates in the image, to which fit is performed, coefficients a, b, d, and e represent rotation, skew, and resize, c and f – linear drift. Note, that in this case the coefficients $c, f \to 0$, because of already performed translational drift correction during CFA (Section 2.4.4). The coefficients a, b, c, d, e, f are found through the least squares for all data points inside the ROI:

$$\frac{\partial}{\partial a,b,c}\left[\sum_{i=1}^{N} x_i' - \left(a\sum_{i=1}^{N} x_i + b\sum_{i=1}^{N} y_i + c\right)\right]^2 = 0 \tag{8.1}$$

$$\frac{\partial}{\partial d,e,f}\left[\sum_{i=1}^{N} y_i' - \left(d\sum_{i=1}^{N} x_i + e\sum_{i=1}^{N} y_i + f\right)\right]^2 = 0 \tag{8.1}$$

From Eq. (7) and (8) a system of six linear equations is inferred:

$$\begin{pmatrix} \sum_{i=1}^{N} x_i' x_i \\ \sum_{i=1}^{N} x_i' y_i \\ \sum_{i=1}^{N} x_i' \end{pmatrix} = \begin{pmatrix} \sum_{i=1}^{N} x_i^2 & \sum_{i=1}^{N} x_i y_i & \sum_{i=1}^{N} x_i \\ \sum_{i=1}^{N} x_i y_i & \sum_{i=1}^{N} y_i^2 & \sum_{i=1}^{N} y_i \\ \sum_{i=1}^{N} x_i & \sum_{i=1}^{N} y_i & \sum_{i=1}^{N} 1 \end{pmatrix} \begin{pmatrix} a \\ b \\ c \end{pmatrix} \tag{9.1}$$

$$\begin{pmatrix} \sum_{i=1}^{N} x_i y_i' \\ \sum_{i=1}^{N} y_i y_i' \\ \sum_{i=1}^{N} y_i' \end{pmatrix} = \begin{pmatrix} \sum_{i=1}^{N} x_i^2 & \sum_{i=1}^{N} x_i y_i & \sum_{i=1}^{N} x_i \\ \sum_{i=1}^{N} x_i y_i & \sum_{i=1}^{N} y_i^2 & \sum_{i=1}^{N} y_i \\ \sum_{i=1}^{N} x_i & \sum_{i=1}^{N} y_i & \sum_{i=1}^{N} 1 \end{pmatrix} \begin{pmatrix} d \\ e \\ f \end{pmatrix} \tag{9.2}$$

The solutions give transformation coefficients a, b, c, d, e, and f. The new reference image emerges by transforming the initial reference image (Figure 2.8). For each time step, new beads positions were calculated according to Eq. (7). χ^2-test was performed for the calculated beads positions outside the ROI to verify the fit. Fits with χ^2<10 nm^2 were accepted.

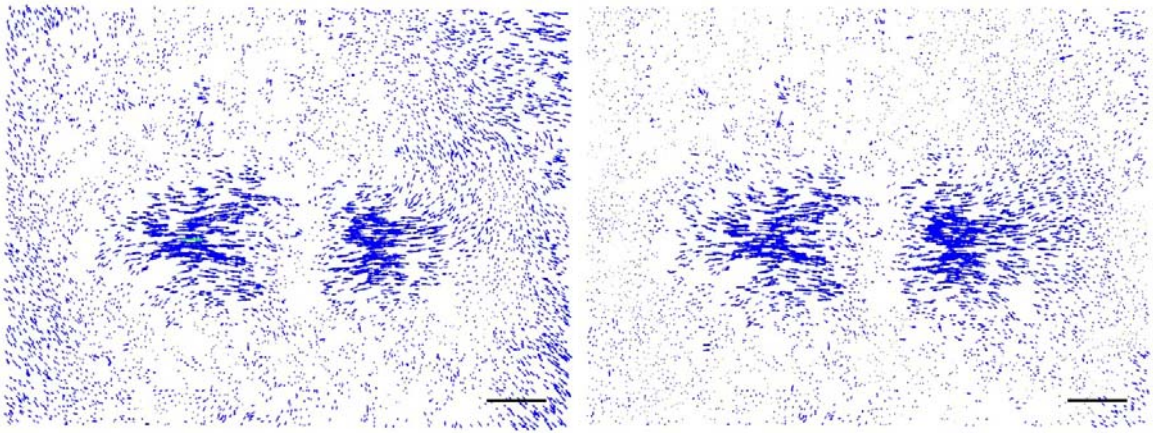

Figure 2.8. Displacement vector field before (left) and after (right) the bead positions correction. Arrows length enlarged 30 times. Scale bars 20 µm.

The image correction routine was coded in MATLAB 7.14. The code was refined and built in by Dr. R. Springer (*ICS-7, FZ Jülich, Germany*) to the main standalone program for cell force analysis.

2.4.4 Cell Force Analysis

The algorithms for cell force analysis (CFA) were developed in MATLAB and are described in detail in [4]. The program was further corrected and complemented by Dr. R. Springer (*ICS-7, FZ Jülich, Germany*). The image processing steps are presented schematically in Figure 2.9.

The input data consisted of a time-stack of images of a cell (Figure 2.9 a), a corresponding time-stack of images of fluorescent beads (Figure 2.9 b) and a reference image (Figure 2.9 c). To restrict force estimation to a single cell, the cell outlines were manually selected using the first time-stack (Figure 2.9 d). The images of beads contained the most important information for this analysis: by comparing them with the reference image, substrate deformations created by this cell could be deduced.

The procedure of finding cell traction forces consisted of four major steps. Firstly, the positions of beads were found in the reference image (Figure 2.9 e). A manually selected sample bead was convolved with two dimensional Gaussians of different radii. Each of the resulting templates was searched for through the entire image by normalized cross-correlation. Whenever correlation was locally the highest, a position of a bead was registered with a predefined threshold to eliminate noise. In the second step a translational xy-correction was made over a larger search length (Figure 2.9 f). The drift was very large (up to 50 µm) in these measurements due to the properties of the substrate material and experimental course. The drift correction was performed by finding average displacements of small but with distinctly patterned regions outside the action of the cell. Thirdly, after the drift correction, a larger template was set around each of the found beads in the reference image (Figure 2.9 g). Each of these templates was searched in the time-stack by cross-correlation together with the reference image correction as described above (Figure 2.9 h).

Displacement vector fields (DVF) were calculated from the bead positions in the reference image and in the time-stack (Figure 2.9 j). Knowing the properties of the substrate material (Young's elastic modulus and Poisson's ratio) and DVF, deformations (Figure 2.9 k) and forces (Figure 2.9 l) could be estimated (see Section 1.3).

Regularization parameter could vary within the same data set depending on the data quality (Figure 2.9 i). To make a consistent comparison of the estimated deformations and forces, their values were rescaled according to a single regularization parameter. Data necessary for further analysis (sum of eigenvalues, angle between eigenvectors, and results of a χ^2-test) were available in .mat files.

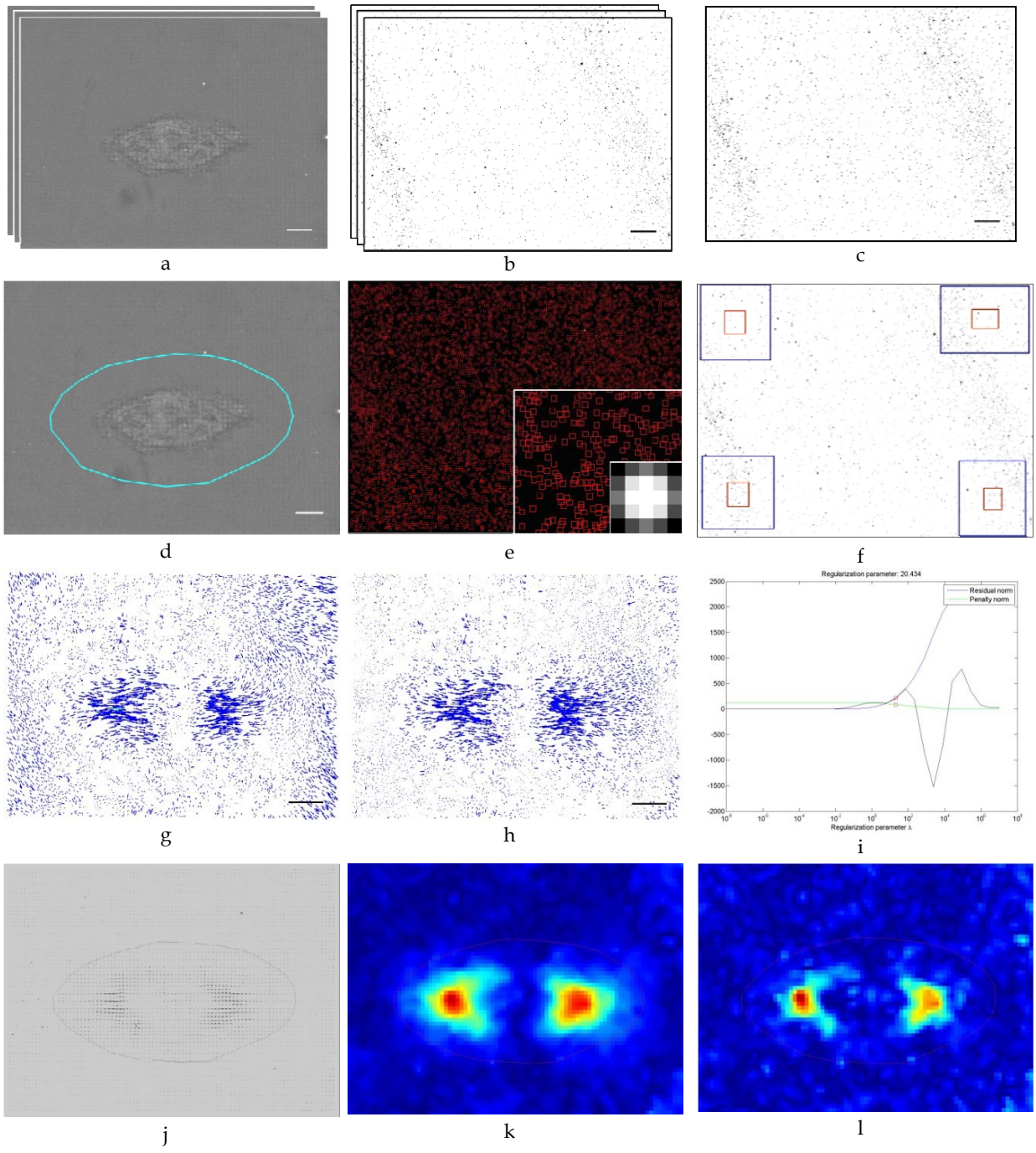

Figure 2.9. Cell force analysis image sequence. Time-stacks of images of a cell (a), of beads (b), and a reference image (c). (d) Manually selected cell outline. (e) Beads positions are found by normalized cross-correlation of a selected bead template (greyscale image lower right) throughout the image. (f) The correction of xy-drift is performed by cross-correlation of the areas unaffected by a cell (red rectangles) in the selected search area (blue rectangles). (g) Displacement vector field is calculated from the beads positions. (h) The same displacement vector field after reference image correction. (i) The regularization parameter is found together with (j) mapped deformation vector field, (k) colour-coded deformation field, and (l) colour-coded force field. Scale bars 20 µm.

2.4.5 Strains and cell orientation

The substrate strain was determined using a MATLAB standalone written by G. Dreissen (*ICS-7, FZ Jülich*). Two or more lines along x- and y-axes were set manually such that they were connecting distinct patterns on the image with beads. Square ROIs around end points of the lines were found in each of the time-stack images of beads by cross-correlation (Figure 2.10 a, b). Search length and correlation threshold were chosen depending on the drift length and deformation magnitude.

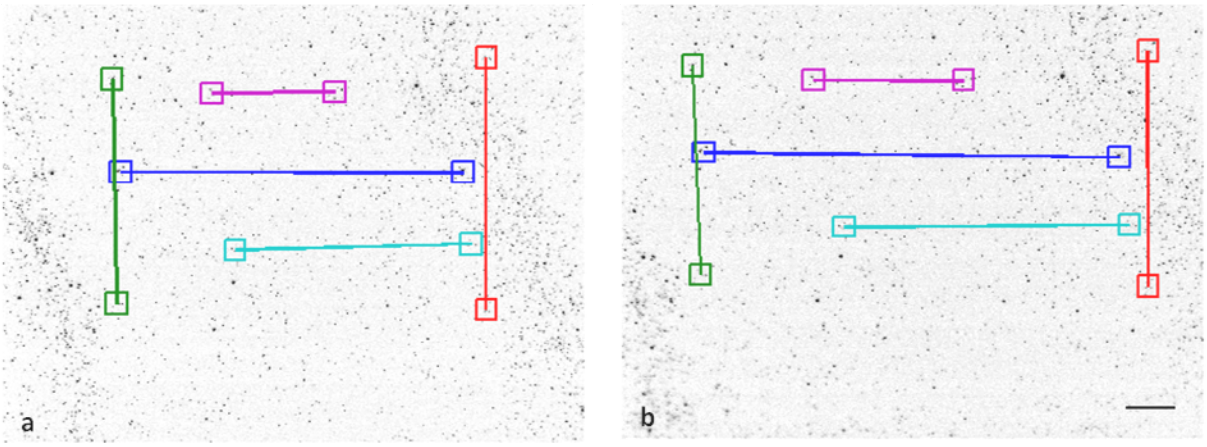

Figure 2.10. Inverted micrographs of fluorescent beads. (a) Lines are manually set between regions with distinct patterns on an image before stretch. (b) The features are found in consecutive images after stretch by cross-correlation. Here, the blue line is elongated by 21.7%, magenta 21.5%, cyan 21.7%, the green line is compressed by 5.8%, and red by 6.2%. This gives on average 21.6% axial strain and 6% transverse compression. Scale bar 40 µm.

To find the elongation and orientation of a cell, a combination of an IJ macro and a MATLAB script was used. Images of a cell before and after stretching were loaded in a single time stack to IJ. The stack was converted to RGB for better visualization. Cell outlines were manually drawn using a polygon selection (Figure 2.11 a, b). The macro saved coordinates of the selections and computed areas of the cell in each image. The MATLAB script loaded the coordinates and calculated the best fitting ellipses [46] (Figure 2.11 c, d). The output parameters (namely, coordinates of ellipse center, major and minor axes, and angles between the major axis and the x-axis) allowed monitoring cell strain and orientation before and after stretch was applied.

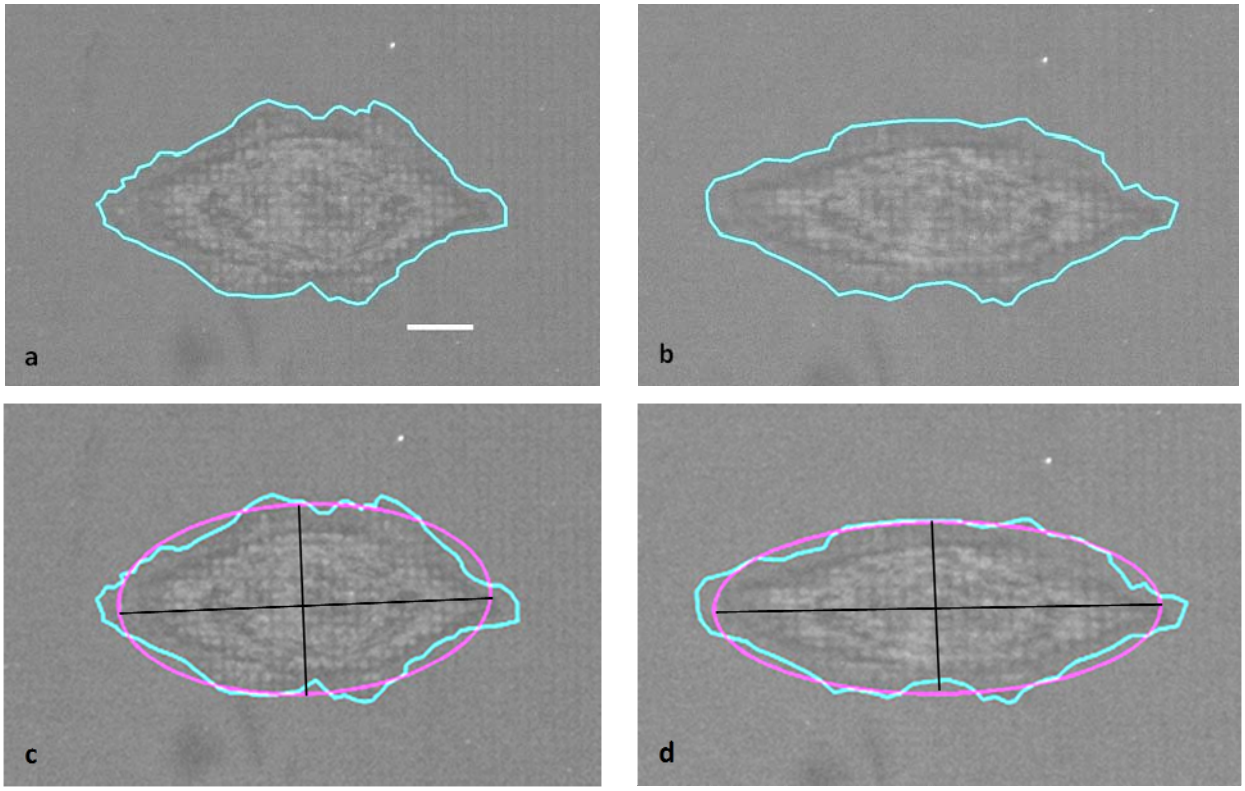

Figure 2.11. Bright field micrographs of a cell before (on the left) and after (on the right) stretching. (a, b) The cell with manual polygon selections using IJ macro; (c, d) ellipsoid fits to the polygonal selections were done in MATLAB. The cell is strained by 16.5% and compressed by 3.2%. Scale bar 20 μm.

2.5 Calibration Measurements

When the substrate was stretched, it deformed in all three dimensions: it elongated in the direction of stretch (x) and contracted in other two dimensions (y and z), such that a spot of interest shifted (Figure 2.12 a, b). Therefore, appropriate corrections in all dimensions had to be performed to observe the same ROI throughout the experiment.

2.5.1 X- and Y-Corrections

In order to find the same spot on the substrate after stretching to certain amplitude A, x- and y-displacement calibrations were necessary. The substrates (inner part 20x20 mm^2) were stretched stepwise in 1 and 2 mm intervals from the pre-stretch amplitude of 1 mm to 5 mm, and at every step an image was acquired. By moving the sample with the help of the XY-stage, the spot of interest was found again. The pattern in the first image was visually compared to each of the consequently acquired images at different strain amplitudes. This displacement measurement was carried out in 13 locations on the substrates (Figure 2.12), thus defining dependence of the displacement due to stretch with respect to the initial

location of a cell on the substrate. For simplicity, we assume that the deformation is homogeneous throughout the substrate.

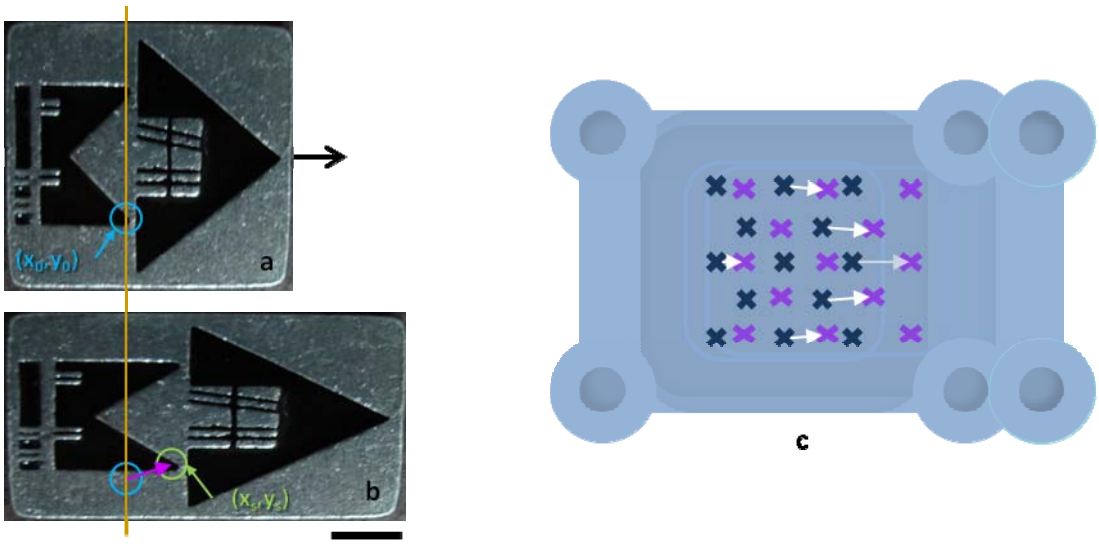

Figure 2.12. Demonstration of the displacement of a spot of interest due to stretching. (a, b) A spot of interest with coordinates of the centre (x_0, y_0) is displaced when an object is stretched in x and compressed in y direction (x_s, y_s). (c) Cartoon of a substrate: blue crosses mark calibration measurement locations before and purple – after the stretch, white arrows indicate displacement direction and magnitude (arbitrary).

The x- and y-displacements per unit stretch were averaged over each position on the substrate: and (see Appendix C for details). The after-stretch positions were calculated in each experiment, depending on the initial position and the stretch amplitude A:

If the cell did not lie exactly in the center of the field of view after the xy-correction was performed, the position was adjusted manually.

2.5.2 Z-Corrections

Similarly, the correction in z-direction was done. However, due to slight differences in substrates manufacturing and how they were clamped onto the holders, a larger scatter in z-displacements was observed. The direction of z-drift varied, although the mean absolute displacement remained the same (20 µm). An empirically deduced correction was , where A is the stretch amplitude [mm], and pS is the pre-stretch amplitude (in this case, 1 mm). For more precise focusing, an autofocus procedure was used.

2.6 Experiment: Traction Force Microscopy of a Single Cell under Constant or Transient Strains

Two kinds of experiments were carried out: stretch-and-hold (constant strain) and stretch-and-release (transient strain). In the first type of experiment, the substrates were stretched once from the pre-stretch amplitude of 1 mm to 5 mm (~20% strain) and held in that position (Figure 2.13 a). In the second type, substrates were stretched in the same manner and after a 1 s halt released back to the pre-stretch state with the same speed (Figure 2.13 b). Microscopy was performed before and after stretching. In both cases, imaging conditions were the same.

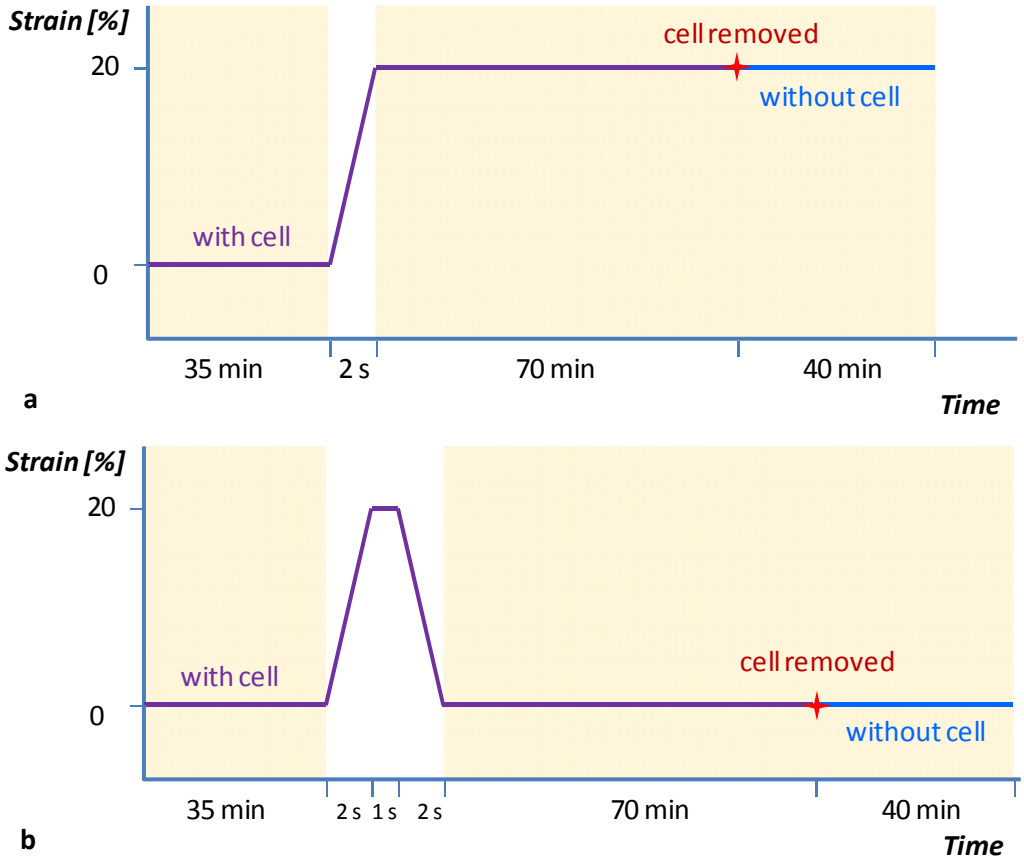

Figure 2.13. Schematic representation of the experiments. (a) Stretch-and-hold and (b) stretch-and-release sequences. Filled areas mark when imaging was performed. The red cross indicates the time point when the cell was chemically removed from the substrate. In (b) the stretch cycle follows a trapezoid stretch function with the 1 s pause duration at the maximum amplitude.

Microscopy was performed in two channels: red (denoted as "RFP") and bright field (denoted as "5%"). The images, taken with minimal time difference in all channels, formed a *set of images*. Default imaging parameters are shown in Table 2-1. Generally, focusing (see Section 2.4.2) was performed in the "RFP" with shorter exposures to reduce time between image acquisitions, and cells were imaged in bright field.

Table 2-1: Imaging parameters: exposure times for different channels

Channel	Exposure (ms)	
	Acquisition	**Focusing**
RFP	100	40
Bright field	100	80

After a substrate with cells was fixed on the stretcher, it was scanned in search for a isolated cell (Figure 2.14). A cell was regarded as single, if no other cells in its vicinity (not closer than 100 µm) were observed. To move a sample and refocus in different step sizes, an MM-script was used (see Appendix C).

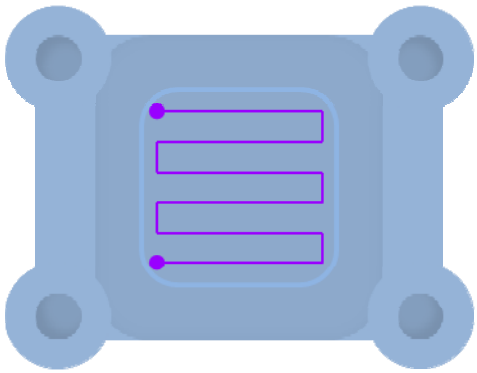

Figure 2.14. The scanning path of the substrate. The inner part of the substrate is 10x10 mm². However, because of the objective geometry and the clamping, the area available for imaging is 7x8 mm². The line is not to scale.

It was important that cells were sessile; however, minor lamelipodial dynamics was acceptable. To check cells viability and motility, images in both channels were acquired with 1 min interval for 35 min. If the cell of interest survived and satisfied the aforementioned requirements, the experiment continued. An additional set of images was acquired before stretching. In case of the stretch-and-hold experiment, the substrate was held at 5 mm throughout the experiment. In the stretch-and-release experiments, the stretcher returned to the pre-stretch position following a trapezoid stretch function. The total cycle duration of such a function was 6 s at the stretch speed of 2 mm/s, hence pause duration at the maximum amplitude was 1 s. One image in bright field was acquired right after stretching to ensure that the cell rested in the centre of the field of view. If necessary, the position was corrected and refocused. Further imaging was performed for 70 min. The first two image sets were taken with no delay; subsequent images were taken at increasing time intervals: 1 s x 10, 30 s x 10, 60 s x 10, 180 s x 16. This kind of sequencing allowed the observation of immediate and long term reactions of cells, without excessive illumination.

After the cell was removed from the substrate as described in Section 2.1, reference images without cell were acquired. In the stretch-and-hold experiments two reference

images were needed: one in the pre-stretch and another at 5 mm stretch positions, while in the stretch-and-release experiments only one reference image was required. The cells were chemically removed from the substrate by trypsinization. First, the medium was removed from the basin with a syringe, and sifted through a 100 nm sterile filter for reuse. The substrate was washed with PBS, and 300 µl of TE was given on its surface. After 5 min incubation at 37 °C, the substrate was washed with PBS again to get rid of organic debris. The basin was filled with 20 ml of purified water for further imaging. Change of media could cause shift or rotation of the substrate. To correct that, the sample was moved in either direction, until the images of beads before washing and after coincided. Imaging was performed for 40 min at equal time intervals of 5 min to let the material reach a relaxed state. After that the stretcher returned to the pre-stretch position, and was moved until the beads positions fitted to those in the very first image of the experiment. Once more, the substrate was imaged for 40 min at 5 min intervals until it relaxed.

Control experiments were performed in the similar way, however, without stretching. Thus, influence of strain on cell behavior was defined. Microscopy was performed on a single-lying cell for 105 min with the same imaging settings as described above. After that the cell was trypsinized from the substrate and the latter was imaged for another 40 min.

3. Results

Experiments on living human endothelial cells were carried out with the help of the developed setup and the corresponding software. Consequently, the mechanical response of pHUVECs to 20% single transient or constant strains was analyzed. Since all the data were acquired in the same manner, the analysis followed the same procedure. The data obtained in the experiments with cells were analyzed for the contractile moments, cell orientation and general behavioural patterns.

3.1 Setup

The first part of the current work was dedicated to the development of a setup for live cell traction force microscopy during stretch experiments and relevant software. Cells were seeded on elastic substrates made of cross-linked polydimethylsiloxane and stretched uniaxially by 20%. The cells were imaged before and after stretch, thus providing all the necessary data. The control measurements confirmed the suitability of the setup (for more details see Section 3.2). The conditions of the experiments were adjusted to meet the requirements of both live cell imaging and traction force analysis.

3.2 General analysis

In the second part of the work, an extensive work on living cells was performed. Altogether three kinds of experiments with cells were made: stretch-and-hold (SH), stretch-and-release (SR), and no-stretch as controls (C), as described in Section 2.6. All the data sets were analyzed as described in Sections 2.4.4 and 2.4.5. The displacements of beads were calculated by comparing the reference images with the images with a cell. Substrate deformations and cell forces were estimated from the displacements of beads.

In order to define the noise level in the measurements, all three types of experiments were carried out without cells. Every step was performed exactly as in the experiments with cells to ensure that no additional uncertainty was brought into the measurement by any of the procedures. These controls revealed no further uncertainty influence (Figure 3.1).

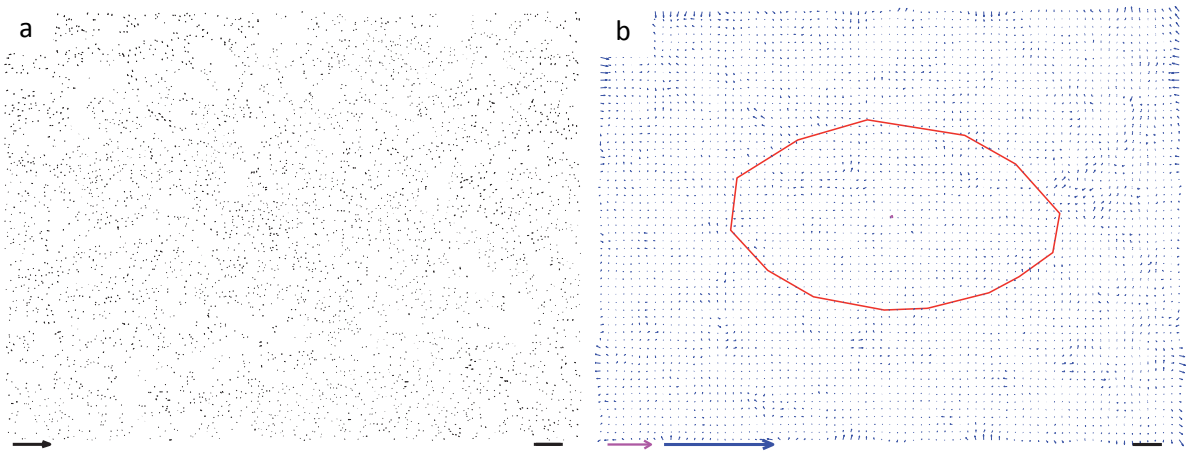

Figure 3.1. No-cell control measurements. (a) Displacement vector field with the average x-displacement 0.29 µm, average y-displacement 0.64 µm. 4580 beads were tracked. (b) Force vector field (blue) and force dipole (purple), sum of eigenvalues inside the red outline -0.03 pNm (purple). The red selection represents a typical cell outline that was necessary to restrict the area of force calculation. The only perturbations are seen along the perimeter of the image, where the beads were out of focus. All vectors are magnified 30 times for visual representation. Displacement arrow scale 1 µm. Dipole arrow scale 5 pNm, force arrow scale 50 nN. Scale bars 10 µm.

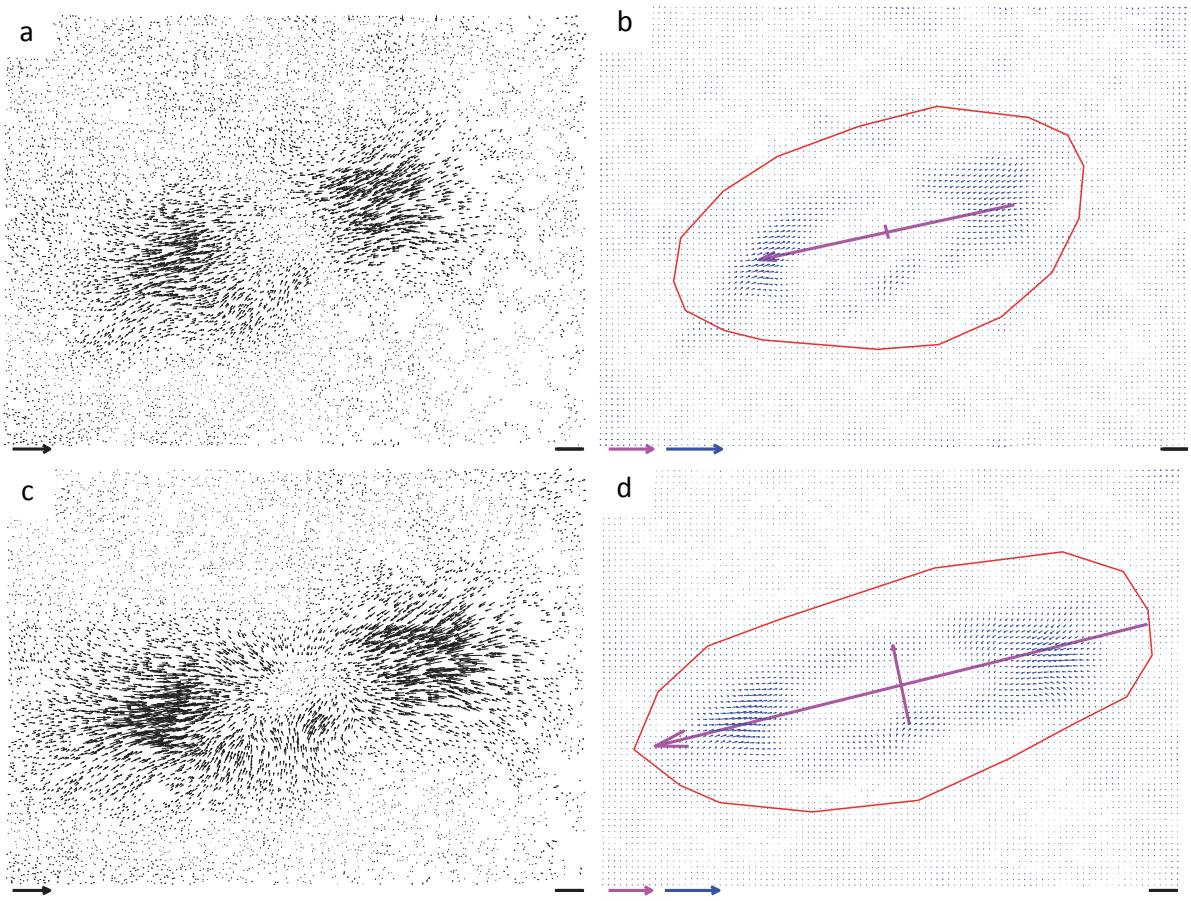

Figure 3.2. Stretch-and-hold. (a, c) Displacement vector fields. (b, d) Force vector fields (blue) and force dipoles (purple). Red contours mark the regions deformed by a cell. (a) DVF before stretching with 8290 beads tracked, average x-displacement of 2.1 µm, average y-displacement of 0.12 µm. (b) Force field and force dipole before stretching, sum of eigenvalues inside the red outline -30.81 pNm. (c) DVF right after stretch with 7443 beads tracked, average x-displacement 7.8 µm, average y-displacement 1.5 µm. (d) Force field and force dipole after the stretch, sum of eigenvalues inside the red outline -65.37 pNm. The substantial increase of tractions is observed compared to the state before stretch. All vectors are magnified 30 times for visual representation. Displacement arrow scales 1 µm. Force arrow scales 25 nN (blue). Dipole arrow scales 5 pNm (purple). Scale bars 10 µm.

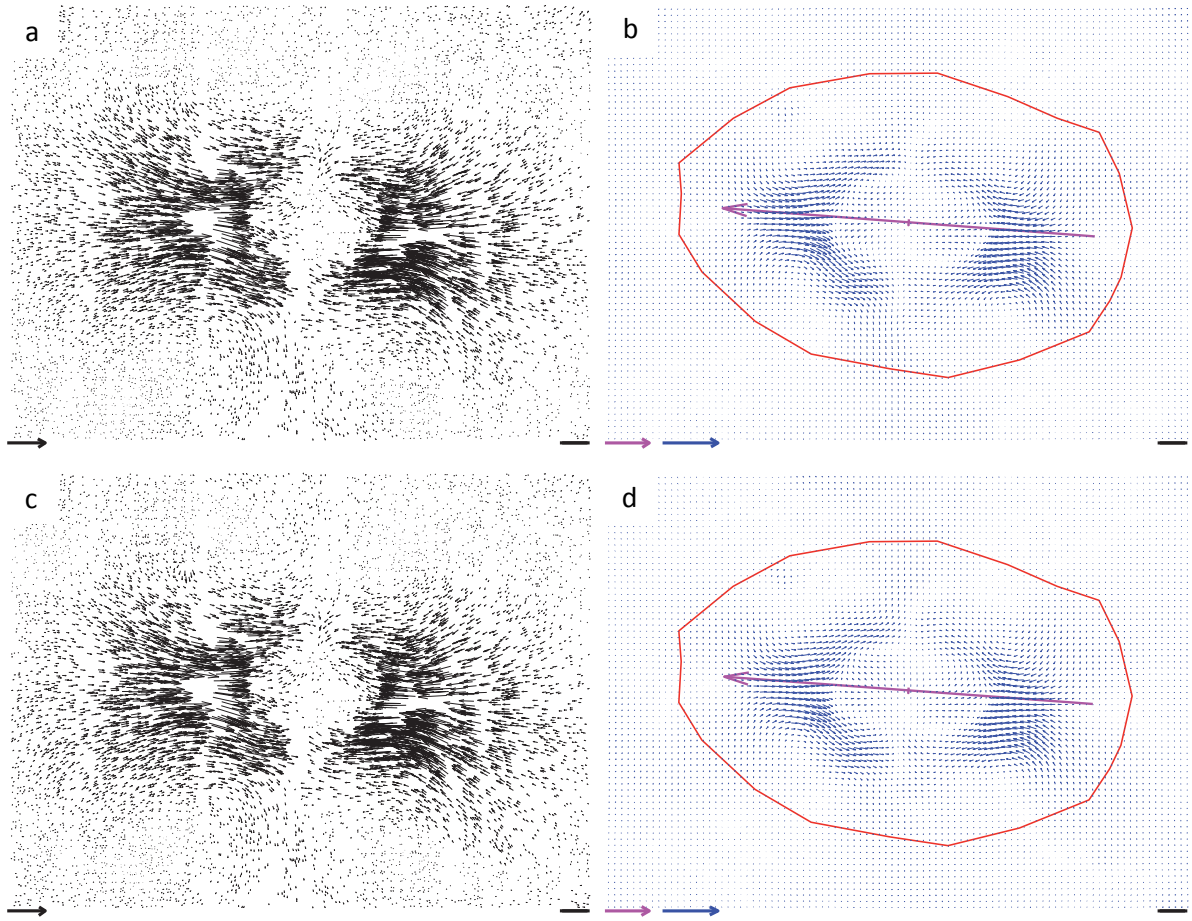

Figure 3.3. Stretch-and-release. (a, c) Displacement vector fields. (b, d) Force vector fields (blue) and force dipoles (purple). Red contours mark the regions deformed by a cell. (a) DVF before stretching with 6917 beads tracked, average x-displacement of 2.79 µm, average y-displacement of 0.47 µm. (b) Force field and force dipole before stretching, sum of eigenvalues inside the red outline -82.24 pNm. (c) DVF right after stretch with 6917 beads tracked, average x-displacement 2.85 µm, average y-displacement 0.42 µm. (d) Force field and force dipole after the stretch, sum of eigenvalues inside the red outline -60.84 pNm. No visible change of tractions is observed when comparing the states before and after the stretch. All vectors are magnified 30 times. Displacement arrow scales 1 µm. Dipole arrow scales 10 pNm. Force arrow scales 25 nN. Scale bars 10 µm.

From the visual representations of the equally scaled displacement vector fields (DVF), force vector fields and dipoles of the representative data from the no-cell control, stretch-and-hold and stretch-and-release experiments before and after stretching (Figure 3.1, Figure 3.2, and Figure 3.3, respectively).

The values obtained in the cell force analysis were addressed for quantitative information. As stated before (Section 1.3) the sum of eigenvalues of the first generalized moment (or alternatively, contractile moment, CM) was chosen as a descriptive measure of cell's contractile behaviour. All average values of the sum of eigenvalues before stretch and their standard deviations are plotted in Figure 3.4 together with no-cell experiments for comparison. It is important to note, that the experiment numbers are not a chronologically ordered. The noise level (the average sum of eigenvalues of all three no-cell control was 0.76 pNm) is indeed insignificant compared to the cell tractions. In all experiments the cells

exerted forces of the same order of magnitude (between -10 pNm and -100 pNm) with the mean around -40 pNm in stretch-and-release and control, and -30 pNm in stretch-and-hold experiments (Figure 3.5). The mean contractile moments in the stretch-and-release and controls belong to the same normal distribution (U-test, p=0.68). However, stretch-and-hold is statistically different from both of them (U-test, p=0).

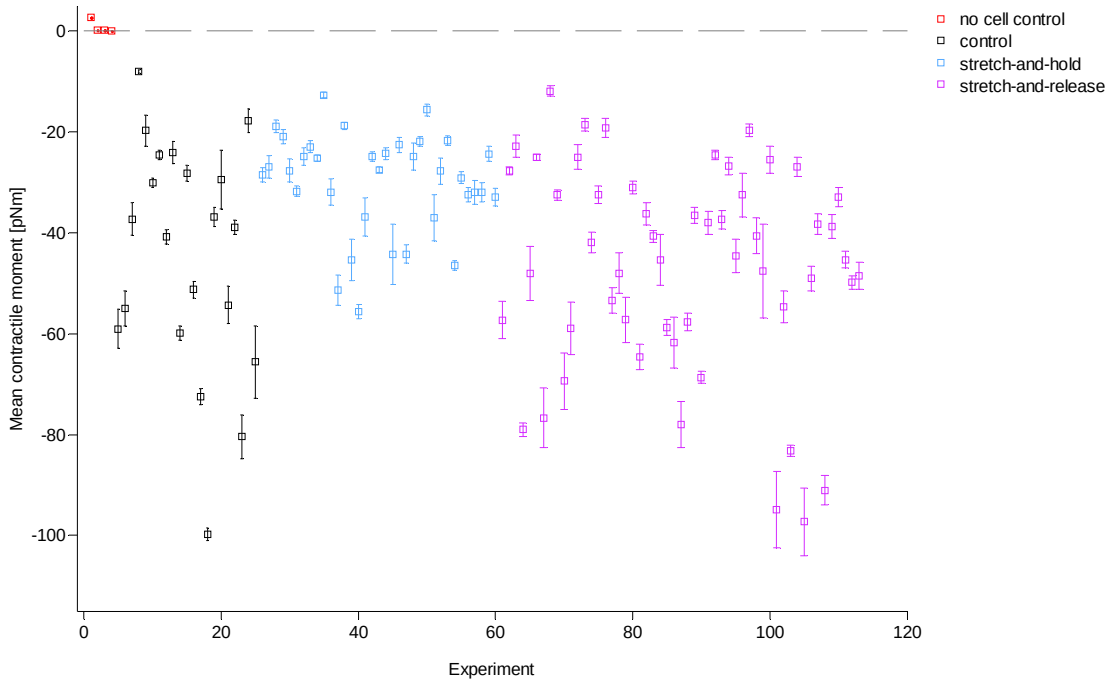

Figure 3.4. Mean contractile moments of all experiments, including no cell controls. The values are of the same order of magnitude, independent of the external factors (cell passage number, medium and PDMS components batch, and the experiment execution date). The no-cell control values approach zero (0.76 pNm), compared to the smallest value of mean contractile moments from the experiments with cells (-99 pNm).

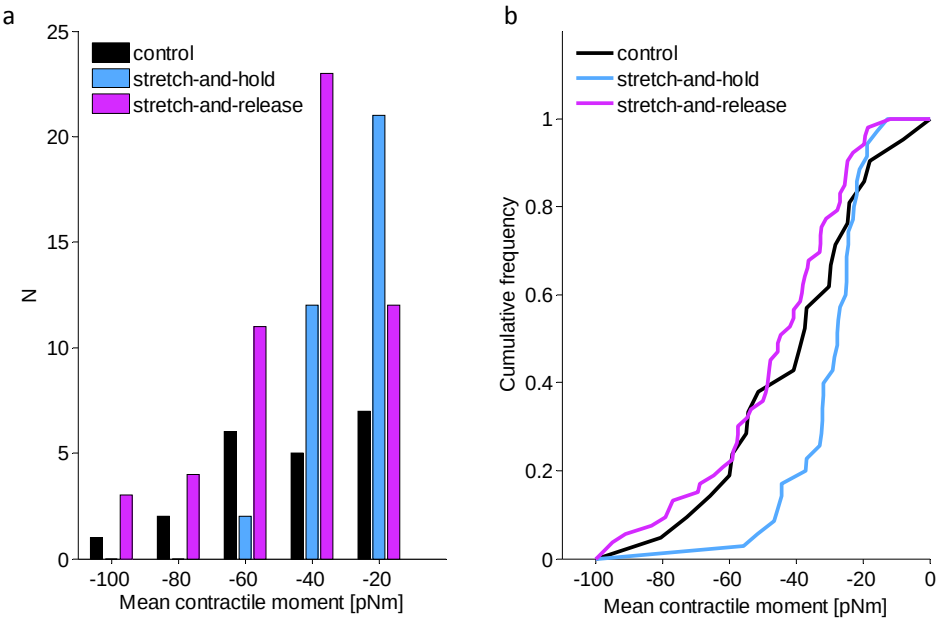

Figure 3.5. (a) Distributions and (b) cumulative frequencies of the mean contractile moments in stretch-and-hold, stretch-and-release, and control experiments. SR and C belong to the same distribution (U-test, p=0.68), SH distribution is statistically different (U-test, p=0). Square points mark quartiles in the cumulative plot.

3.3 Contractile Moments

To have a better and more comparative overview of the change of cell tractions in all experiments, the sum of eigenvalues were normalized to the mean of the sum of eigenvalues of the first part of the observation (that is, before stretch was applied) in every dataset (Figure 3.6). The time of the stretch application was set to zero for convenience.

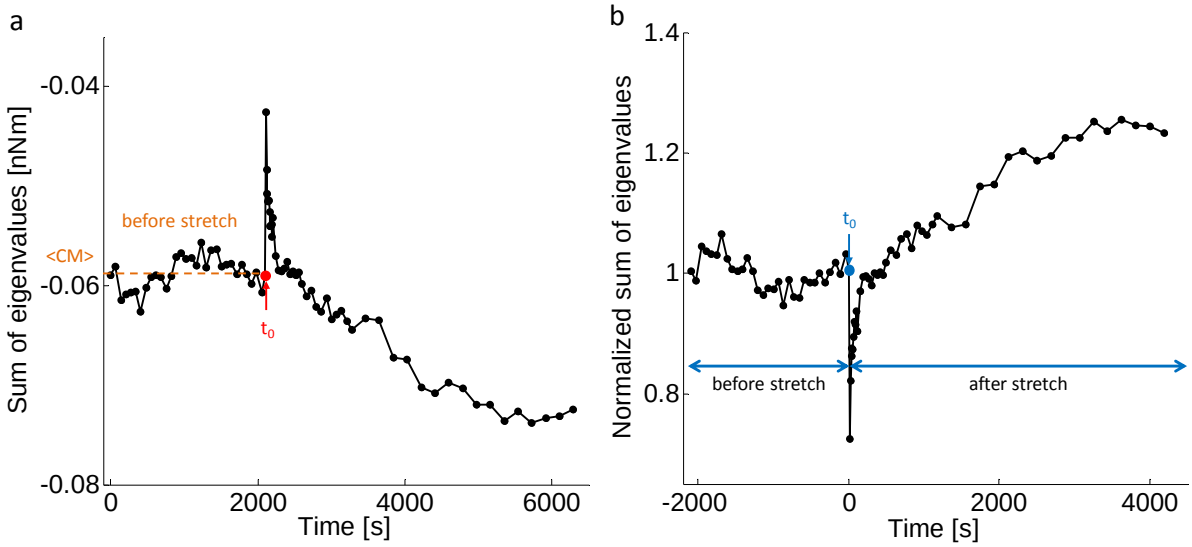

Figure 3.6. Example of normalization on a stretch-and-release experiment. (a) Sum of eigenvalues of the first generalized moment, raw data showing absolute values. (b) After normalization and setting the time of the stretch application t_0 to zero. The entire dataset was normalized to the average of the sum of eigenvalues before stretch (orange), in this case <CM>=-58 pNm.

In order to display the general behaviour upon stretch, all cell tractions were averaged over time in each type of experiment (see the average curve in bold black of the control experiments in Figure 3.7). The mean curve was calculated as follows: all values of contractile moments that fall into certain time intervals were averaged. Typically, curves were smoothed for more than one data point of a measurement could fall into one time interval. Time intervals were calculated starting from the time zero with varying lengths in both directions (red arrows in Figure 3.7). Furthermore, the cell mechanical response in the stretch-and-hold and stretch-and-release experiments was subdivided into groups according to the magnitude of change of the sum of eigenvalues and the general trend after stretch was applied.

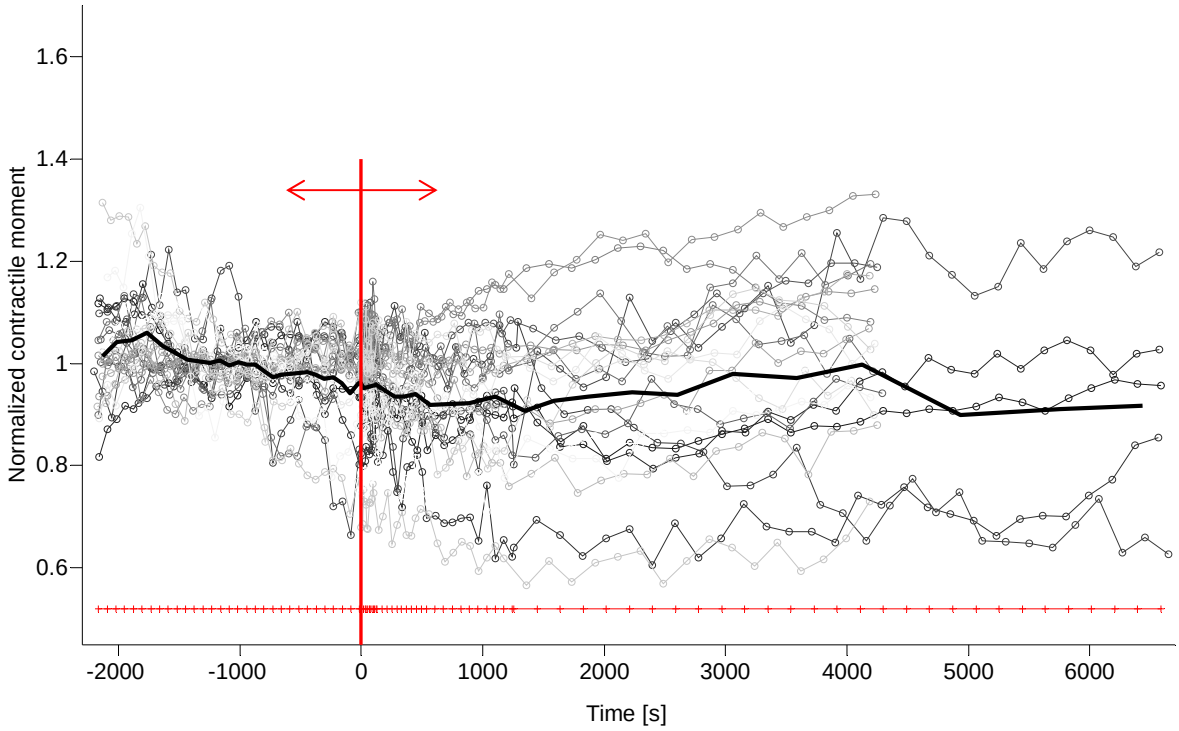

Figure 3.7. Normalized contractile moments of cells in the control experiments. The average is shown as a black bold line. The averaging was done in two 'directions' starting time zero (red bold line and arrows). Time points when image acquisition was performed are shown as a red line with ticks. Note the varying intervals. Number of experiments N=21.

The cell tractions in the control experiments were scattered around the mean (that is around 1 due to normalization). A slight decline of the averaged contractile moments was observed, however this decrease was regarded as insignificant since the number of experiments was low (N=21). In general, no great effects of illumination or experimental course on the cells were observed. They did not initiate either cell death or detachment, or an unexpected increase in cell contractility, except for the occasions equally present in all three types of experiments.

3.3.1 Single Stretch-and-Hold

In the stretch-and-hold experiments an abrupt rise in contractile moments upon stretch application was observed. It was followed by further increase of the traction forces, in most experiments concluded by a slow decrease. Hereafter in this section, an "increase" refers to the difference between the maximum value and the last value before stretch was applied (Figure 3.8).

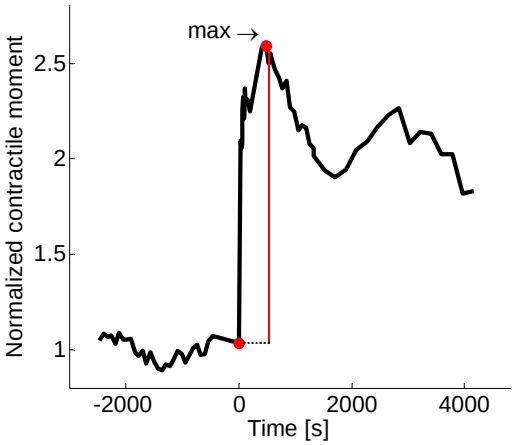

Figure 3.8. ***The after-stretch increase of contractile moments in the stretch-and-hold experiments.***

Altogether only in four cases did cells return to the pre-stretch level or lower. In the rest cases the contractile moments decreased slowly for 20 min and remained on average at the level one quarter higher than one. The mean increase was by 0.57 with a standard deviation of 0.28; the lowest increase was by 0.08 and the largest increase by 1.12.

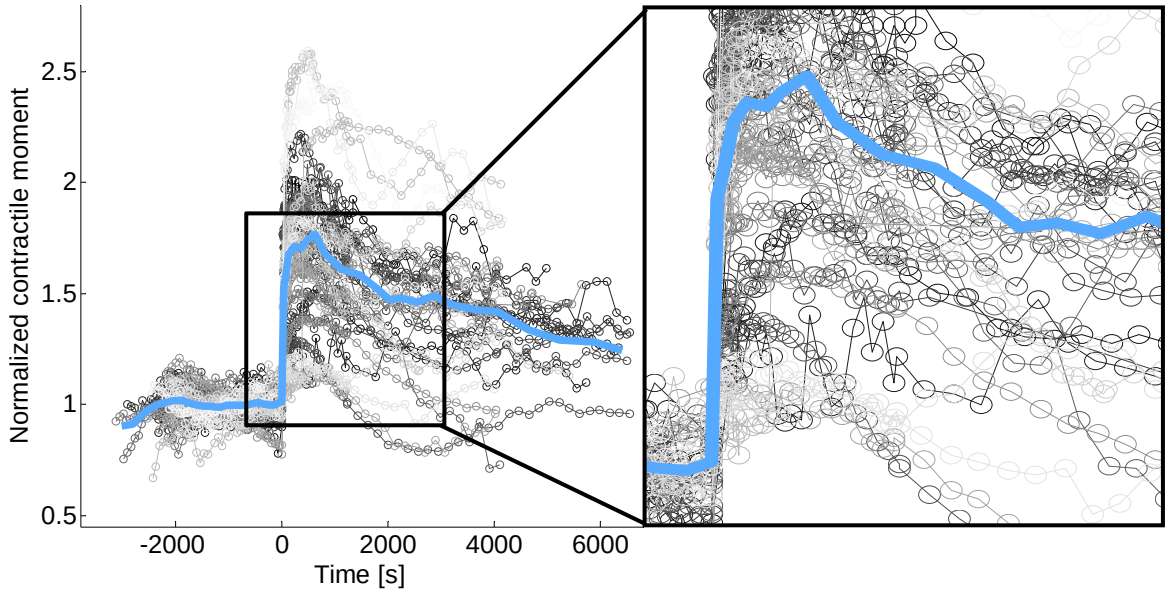

Figure 3.9. Normalized contractile moments in the stretch-and-hold experiments. Blue line depicts the averaged moments over all experiments. The maximum CM value of the averaged curve is 1.77 and is reached in 10 min after the stretch. The CM increase by 0.75, and the CM decrease to1.24. N=35.

The results were grouped according to the increase of contractile moments and typical after-stretch behaviour. Unfortunately, automated systematic classification was unsuccessful since it resulted in many groups with only few curves in each, also because of a relatively low number of experiments (N=35). Therefore, all data were sorted qualitatively. Additionally to the visual characteristics, magnitudes of change in contractile moments upon stretch and standard deviations of the sum of eigenvalues in the second half of the measurements after the stretch were taken into account. For a better overview all data were plotted in one row. The spacing between the curves was set to avoid overlapping (Figure 3.10).

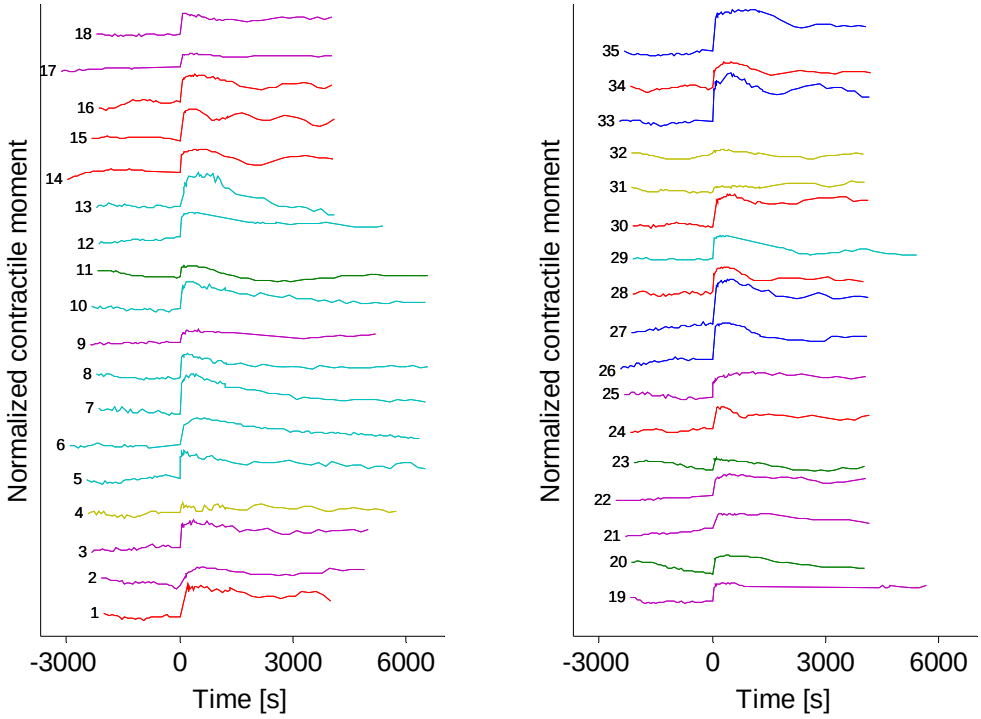

Figure 3.10. Qualitative grouping. All data of the stretch-and-hold experiments are plotted in two rows. The curves with the biggest similarities are highlighted in the same colours: blue – group a, red – group b, cyan – group c, magenta – group d, green – group e, yellow – group f).

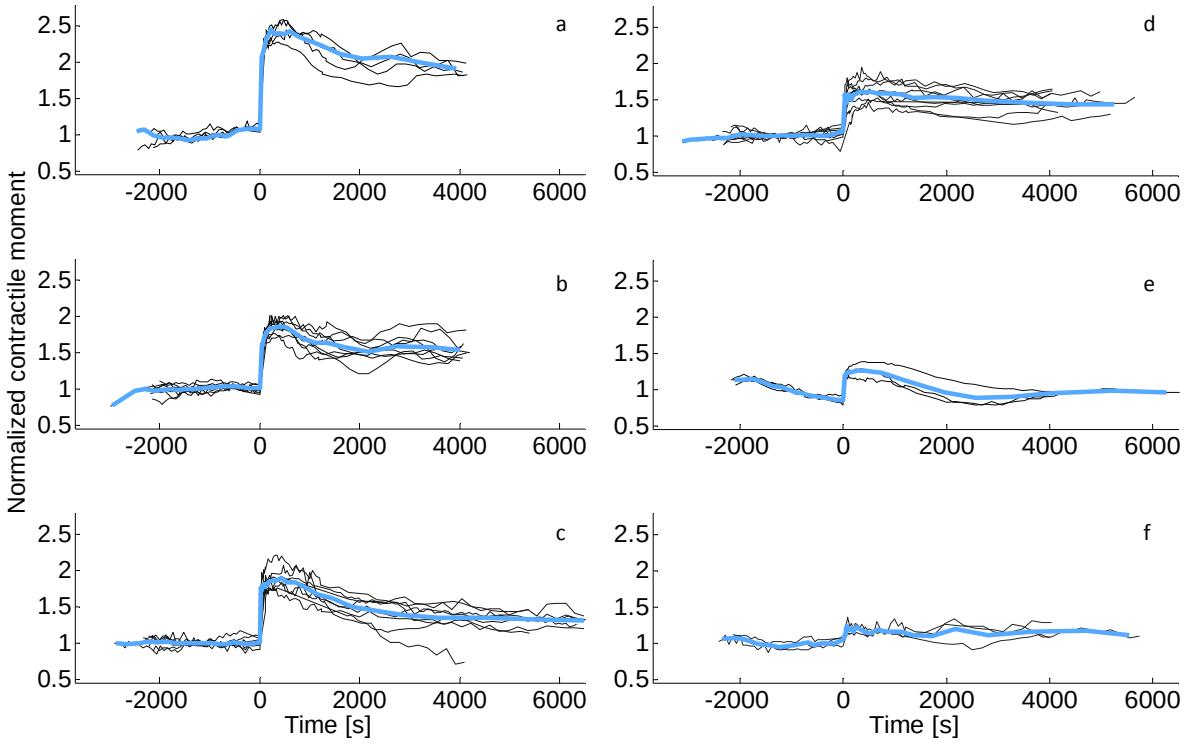

Figure 3.11. Grouped normalized contractile moments in stretch-and-hold experiments. (a) Corresponds to the first group with the largest increase in contractile moments after the stretch. (b) The second group with a significant rise of CM after stretch and an increased cell activity. (c) A slow decrease of contractile moments after the stretch. (d) The fourth group with a smaller increase of CM and almost no change in CM until the end of experiments. (e) The fifth group with decreasing CM and a small rise upon stretching. (f) The sixth group with the smallest increase of CM. The averaged curves are shown in bold blue lines for each of the groups.

Altogether, six groups were determined with their averaged characteristics (Figure 3.11):

a) the contractile moments increased the most upon the stretch compared to other cell tractions (on average by 1.39) and remained at an elevated level of 2.1; N=4;

b) a large increase of contractile moments on average by 0.89, the cells became more active after the stretch (standard deviation of the mean CM was 0.15 compared to the pre-stretch value of 0.08); N=8;

c) a large increase of contractile moments by 0.93 on average with a distinct decline by the end of observations; N=8;

d) a smaller increase by 0.63 and almost no change until the end of experiments (remains at an elevated level of 1.54 on average); N=9;

e) the contractile moments decreasing in the first part of the experiment, increased on average by 0.45 after the stretch; N=3;

f) all measurements with the smallest increase in contractile moments after the stretch (only by 0.26); N=3.

The maximum value of contractile moments was typically reached within 10 min after stretch in all experiments, except one case, in which forces persisted to increase until the end of observation (Figure 3.12). No correlation between the mean pre-stretch tractions and the time when the maximum was reached was determined. The times are normally distributed (KS test and U test α=0.05).

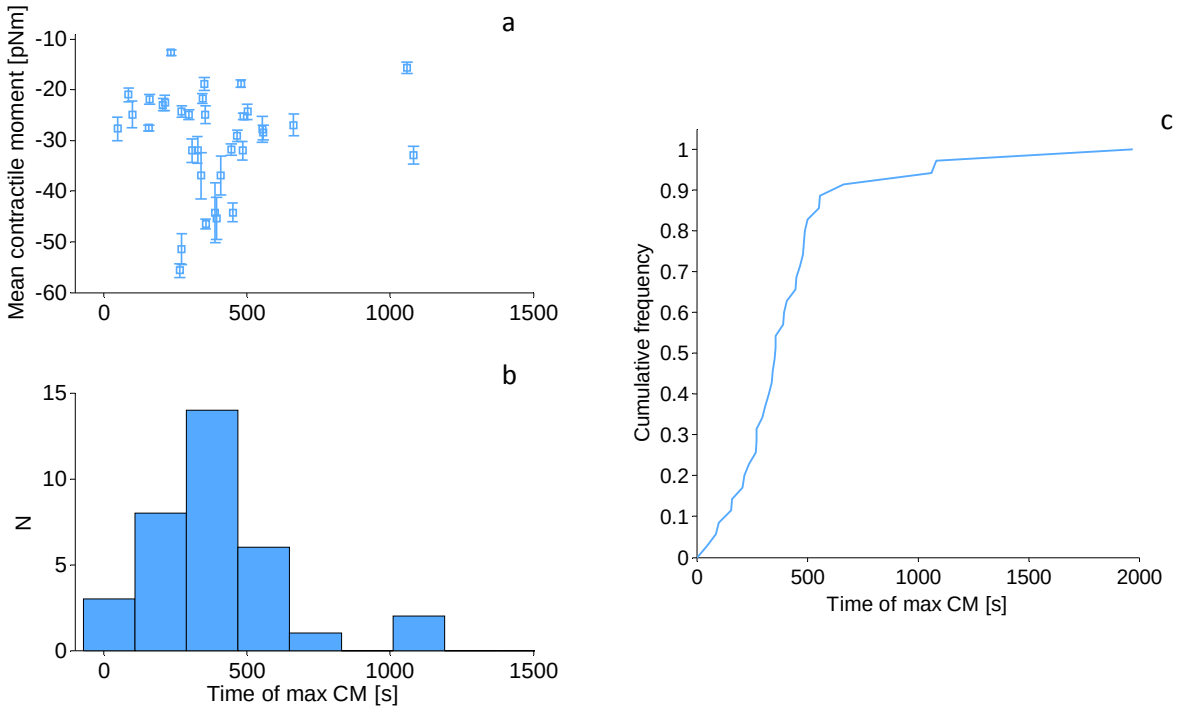

Figure 3.12. Time when the maximal contractile moments were reached after the stretch: (a) against the contractile moments before the stretch, (b) distribution, and (c) cumulative plot. No correlation between the time of the maximum and CM was defined (U test, α=0.05). One measurement showed a progressive increase in contractility, therefore its time of the maximum CM was disregarded. Error bars are standard deviations.

In the most cases, the contractile moments after the stretch increased on average by 0.75 compared to the values right before the stretch (Figure 3.13 a, b). The maximal contractile moments were as high as the normalized value of 2, with the maximal of 2.6 (Figure 3.13 c, d). The increase magnitude was independent of the cell traction forces before the stretch.

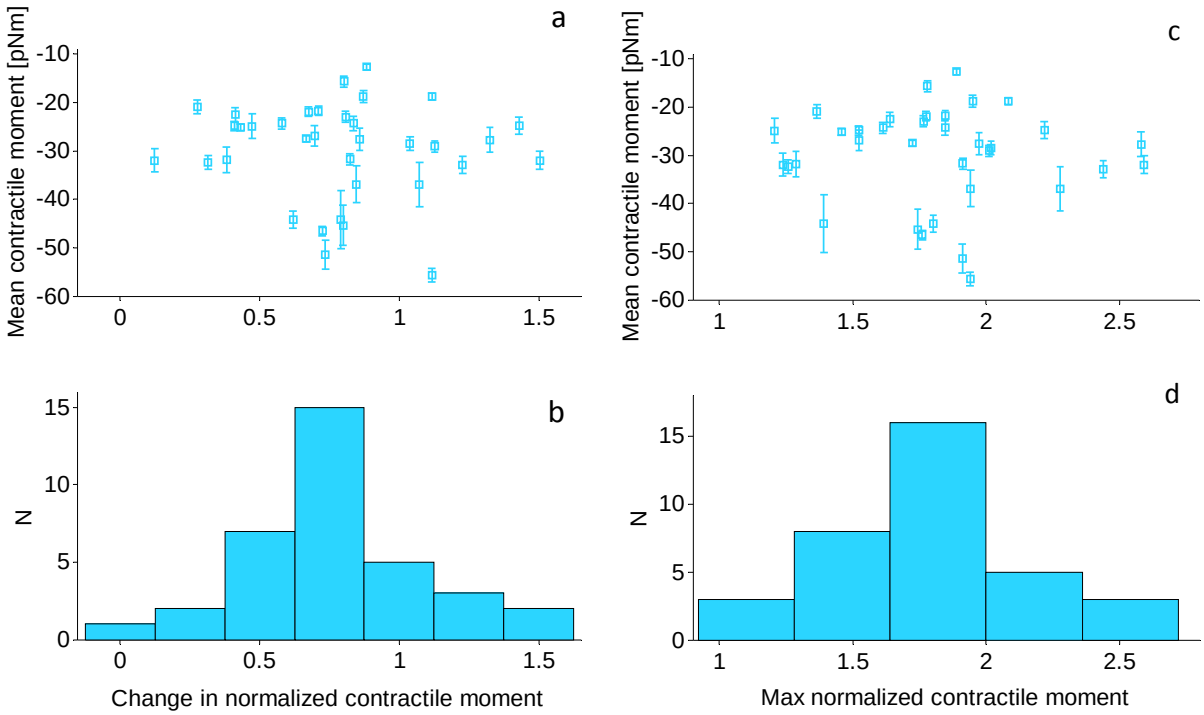

Figure 3.13. (a, b) Increase of the contractile moments relative to the pre-stretch value. (c, d) Maximal contractile moments after the stretch. Error bars are standard deviations. Both are normally distributed (U test, α=0.05).

3.3.2 Single Stretch-and-Release

The image acquisition was performed before the stretch and right after the stretch-release cycle in the stretch-and-release experiments. The data were analyzed similarly to the stretch-and-hold data analysis. Hereafter, a difference between the contractile moments before stretch and right after is referred as a "drop" (Figure 3.14), similarly to the "increase" in the stretch-and-hold data. In general, a drop in contractile moments was detected immediately after the stretch in the stretch-and release experiments. To facilitate the analysis, a baseline correction was made in cases when contractile forces were linearly decreasing. A linear regression fit was applied excluding the data points right after stretching (Figure 3.15).

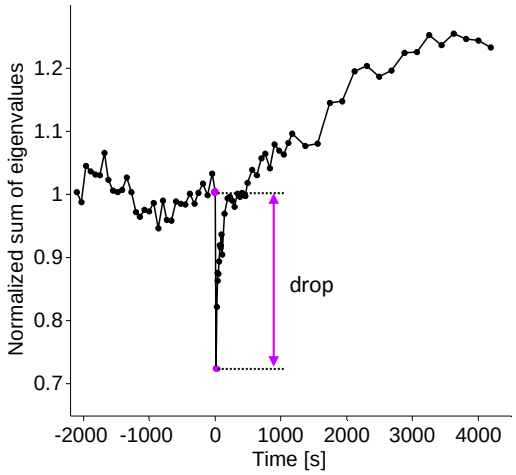

Figure 3.14. Drop of contractile moments in the stretch-and-release experiment was defined as a difference between the CM before the stretch-release cycle and right after.

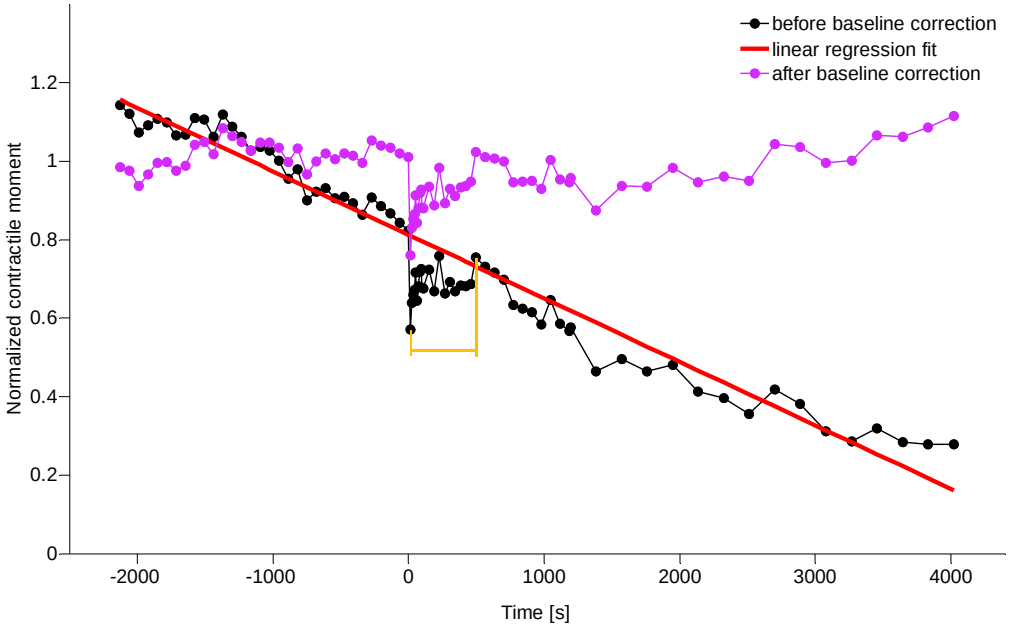

Figure 3.15. Baseline correction of the linearly decreasing contractile moment. The black dotted line indicates the initial data, red line – the corresponding linear regression, magenta – baseline corrected data. The data points in the region marked in yellow were excluded from the fit.

In order to determine the recovery time (that is the time when the values of contractile moments recovered to the pre-stretch level), an exponential fit of the first order ($y = y_0 + A \cdot \exp(-x/t)$) was applied to the manually selected region (Figure 3.16). The mean recovery time of all experiments was 160 s with a standard deviation of 133 s.

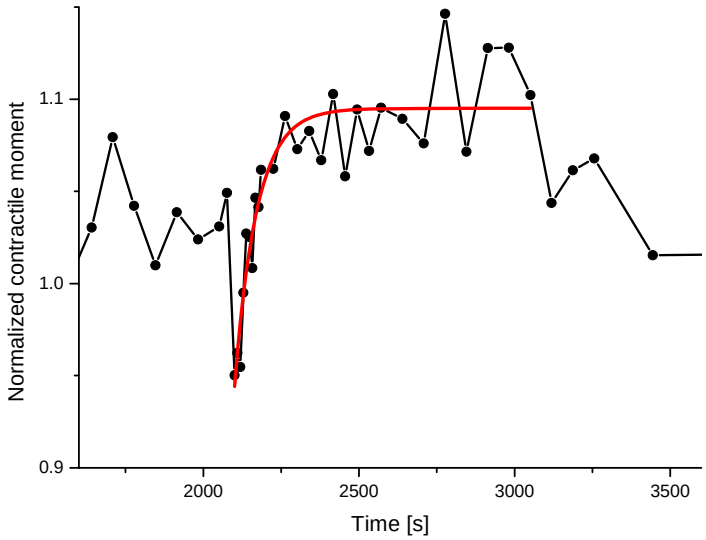

Figure 3.16. A first order exponential fit $y = y_0 + A \cdot \exp(-x/t)$ was done to determine the recovery time t of the contractile moment after the stretch (red line). The fit region was selected manually.

The results of the stretch-and-release experiments were averaged (Figure 3.17) and sorted in a similar way as those of the stretch-and-hold. Four cases out of total N=53 deviated from the trend: a minor rise of contractile moments was observed instead of a drop (by 0.025), negligible compared to the average drop by 0.16. Two more cases had drops hardly distinguishable from the overall fluctuations of the contractile moments.

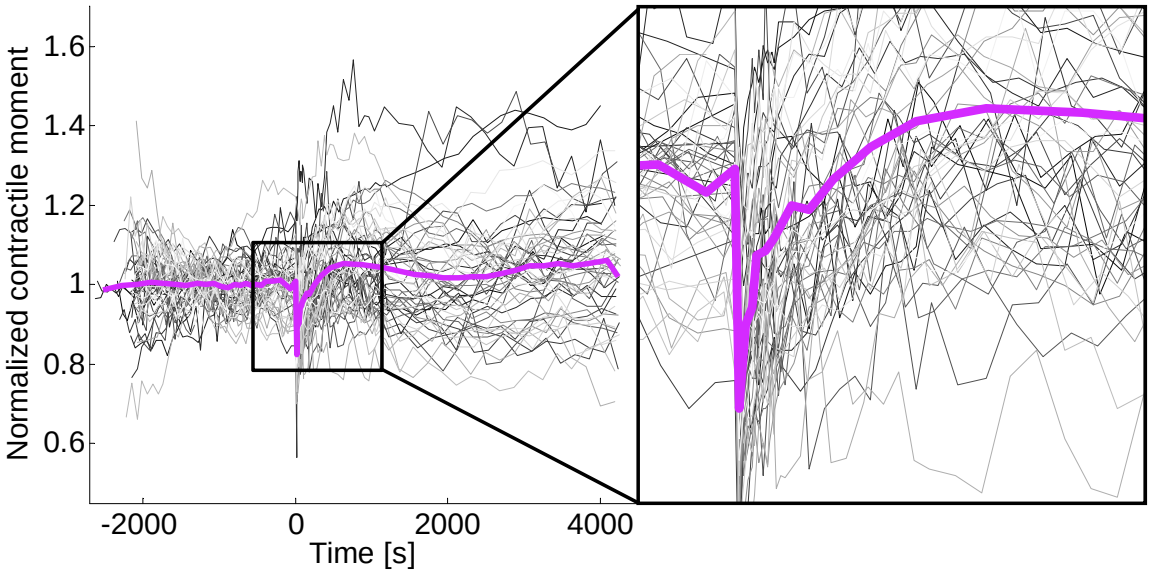

Figure 3.17. Normalized contractile moments in the stretch-and-release experiments. Magenta line depicts the averaged moments over all experiments. The CM of the average curve decreases by 0.18, and the recovery time is 120 s. The overshoot after recovery is 0.05 compared to the CM value before the stretch. N=53.

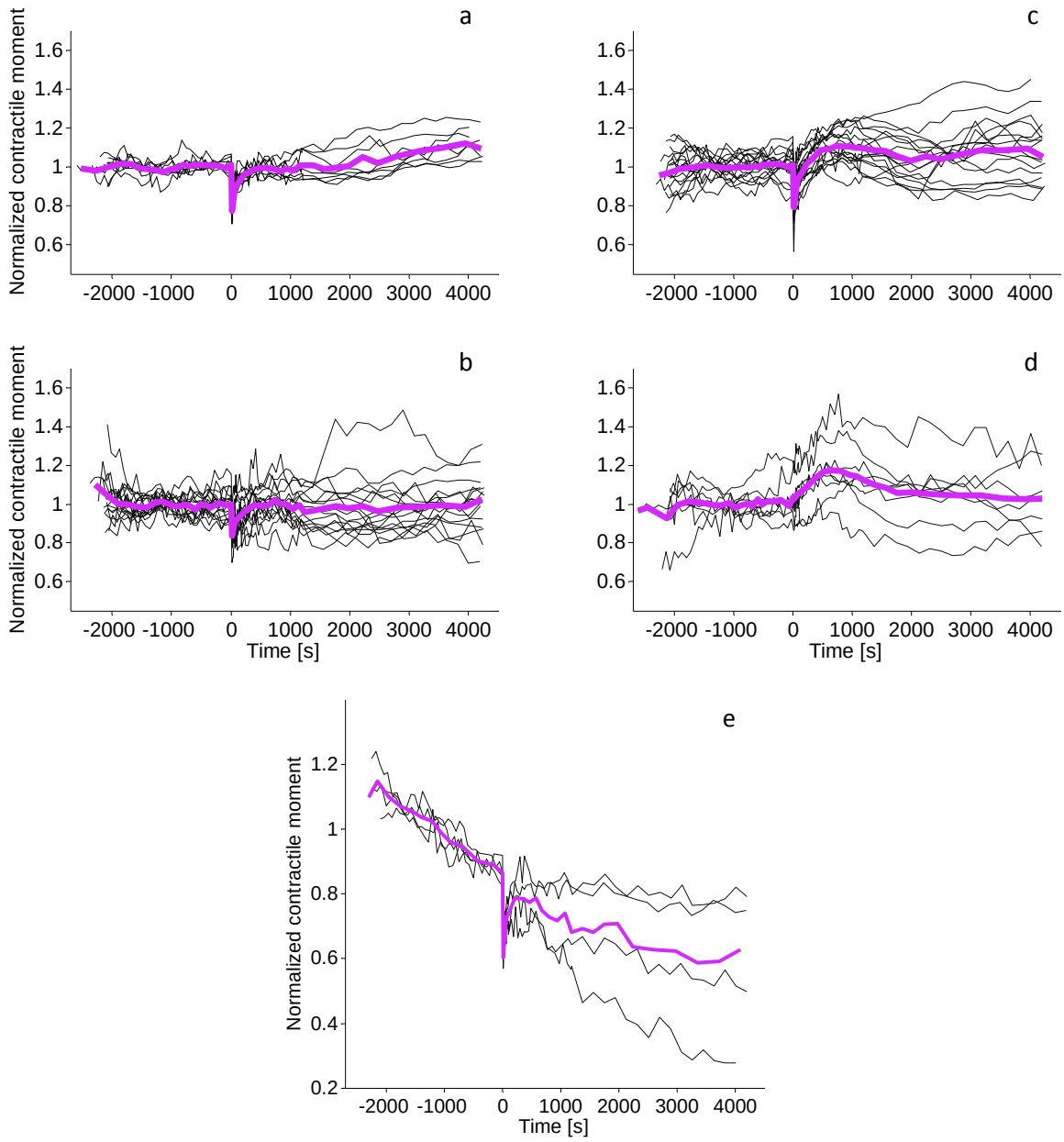

Figure 3.18. Grouped normalized contractile moments in stretch-and-hold experiments. (a) The first group with a notable drop and a slow increase in contractile moments after the stretch. (b) The second group with a smaller drop and almost no change of CM after recovery to the pre-stretch values. (c) The third group with a sharp drop and an overshoot. (d) The fourth group with no drop and generally noisy data. (e) The CM decreasing throughout the experiment. The averaged curves are shown in bold magenta lines for all groups.

The data were grouped with the averaged characteristics as follows (Figure 3.18):

a) a pronounced drop of contractile moments after the stretch by 0.2 on average and a fast recovery to the pre-stretched value (~97 s) followed by a slow increase in CM; N=8;

b) a smaller drop of CM by 0.14 on average and a longer recovery time (~164 s); N=17;

c) a sharp drop by 0.23 with an overshoot by 0.09 and a longer recovery time (~190 s); N=16;

d) no or almost negligible decrease of CM; N=8;

e) the contractile moments decreasing during the entire experiment; N=4.

It is worth to note that neither the recovery times (Figure 3.19), nor the drop of tractions (Figure 3.20) correlated with the cell pre-stretch traction history (that is mean contractile moments), similarly to the stretch-and-hold results. In most cases contractile moments recovered within 3 min. The recovery times are normally distributed (KS test, U test α=0.05).

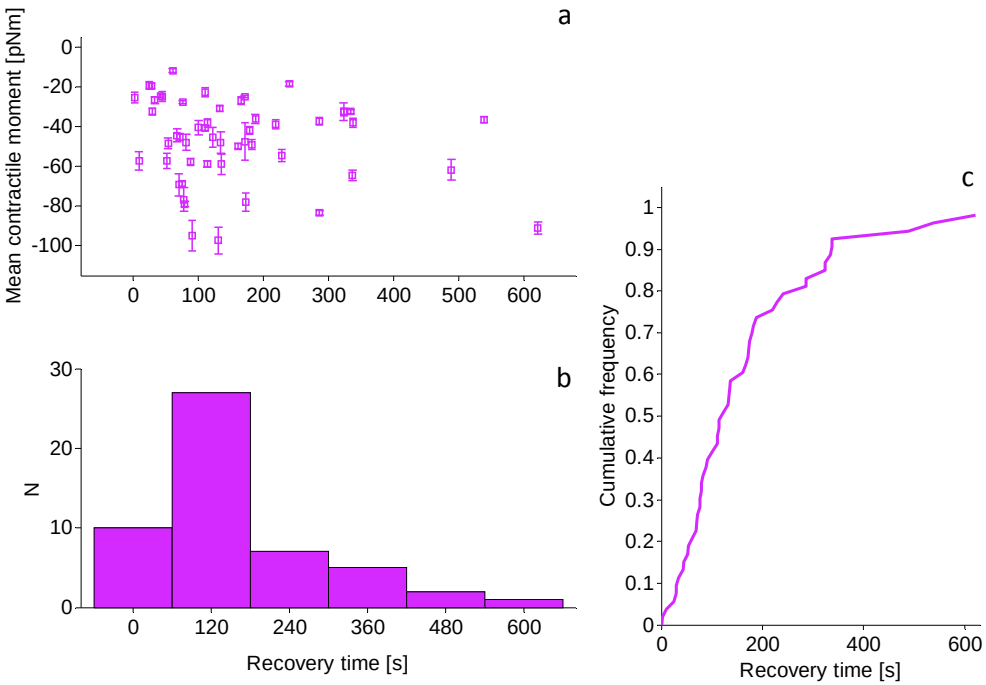

Figure 3.19. Recovery time of the contractile moments after the stretch: (a) plotted against mean CM before stretching, (b) distribution, (c) cumulative plot. Most of the cell tractions recovered within 3 min after the stretch. No obvious correlations between the mean contractile moments and recovery times or the drop in contractile moments were observed.

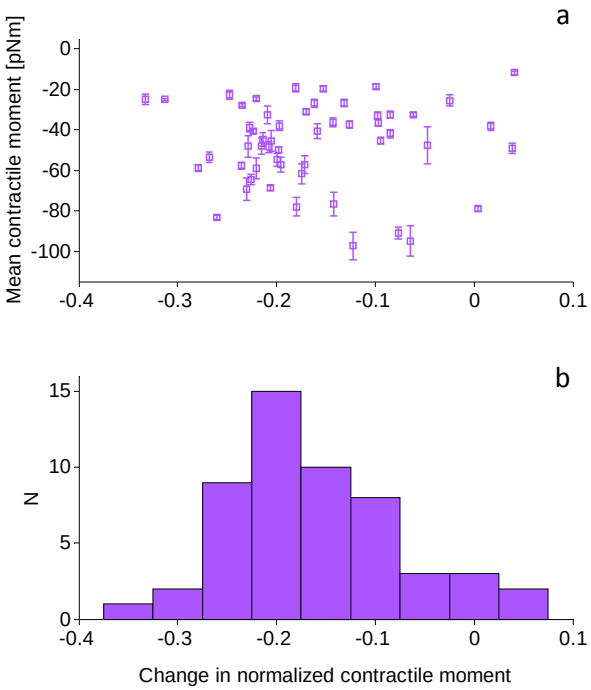

Figure 3.20. Drop of contractile moments upon stretch: (a) plotted against the mean contractile moments before stretching, (b) distribution. No correlation between mean CM and drop observed (U test, **α=0.05**).

3.4 Cell Orientation, Aspect Ratio, and Area

The experimental setup was set such that the x-axis corresponded to the stretch-axis. It is important to note, that the cells that were lying along the stretch axis were chosen for the stretch-and-hold and stretch-and-release experiments, whereas for the controls experiments orientation of cells was regardless of the stretch direction. There were two ways to determine the cell orientation: from the ellipse fit that was made around the manually selected cell outline (Figure 3.21 a, b) and from the force dipole (Figure 3.22 c, d). In the first case, the orientation can be approximated by the angle between the ellipse major axis and the x-axis (η_0 and η_s angles before and after the stretch, respectively in the SH experiment). In the second case, it is the angle between the eigenvector of the largest eigenvalues of the contractile moment and the x-axis (ψ_0 and ψ_s, similarly, before and after the stretch). The results of two methods of defining cell orientation coincided for elliptical cells, and differed for round cells, since the ellipse axes could be oriented in either way. Therefore, the second method was used in this analysis, if not stated otherwise.

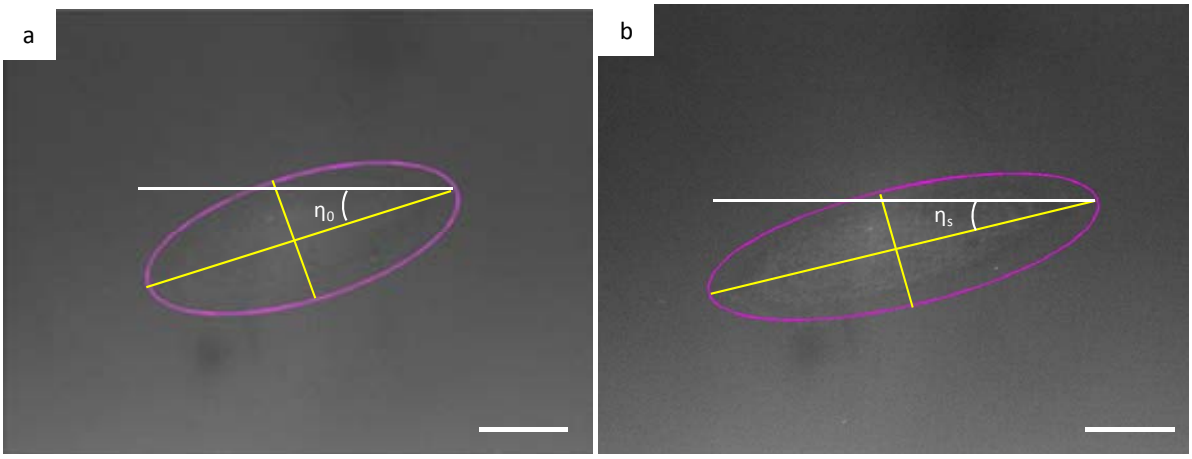

Figure 3.21. Cell orientation from ellipse fit. The angles η_0 and η_s can be assumed as the cell body orientation relative to the stretch direction. Scale bars 20 µm.

An immediate effect of stretching on the cell orientation was registered in the stretch-and-hold experiments. This was especially apparent when comparing the cell orientation before stretching and right after. To check whether this effect was solely due to the substrate deformation, a correlation between the change in angles between a line drawn on the substrate (as described in Section 2.4.5, see Figure 3.22. a, b) and the x-axis and the change in angles between the largest eigenvector and the x-axis (Figure 3.22. c, d) was investigated. This assumption was not confirmed (Figure 3.23).

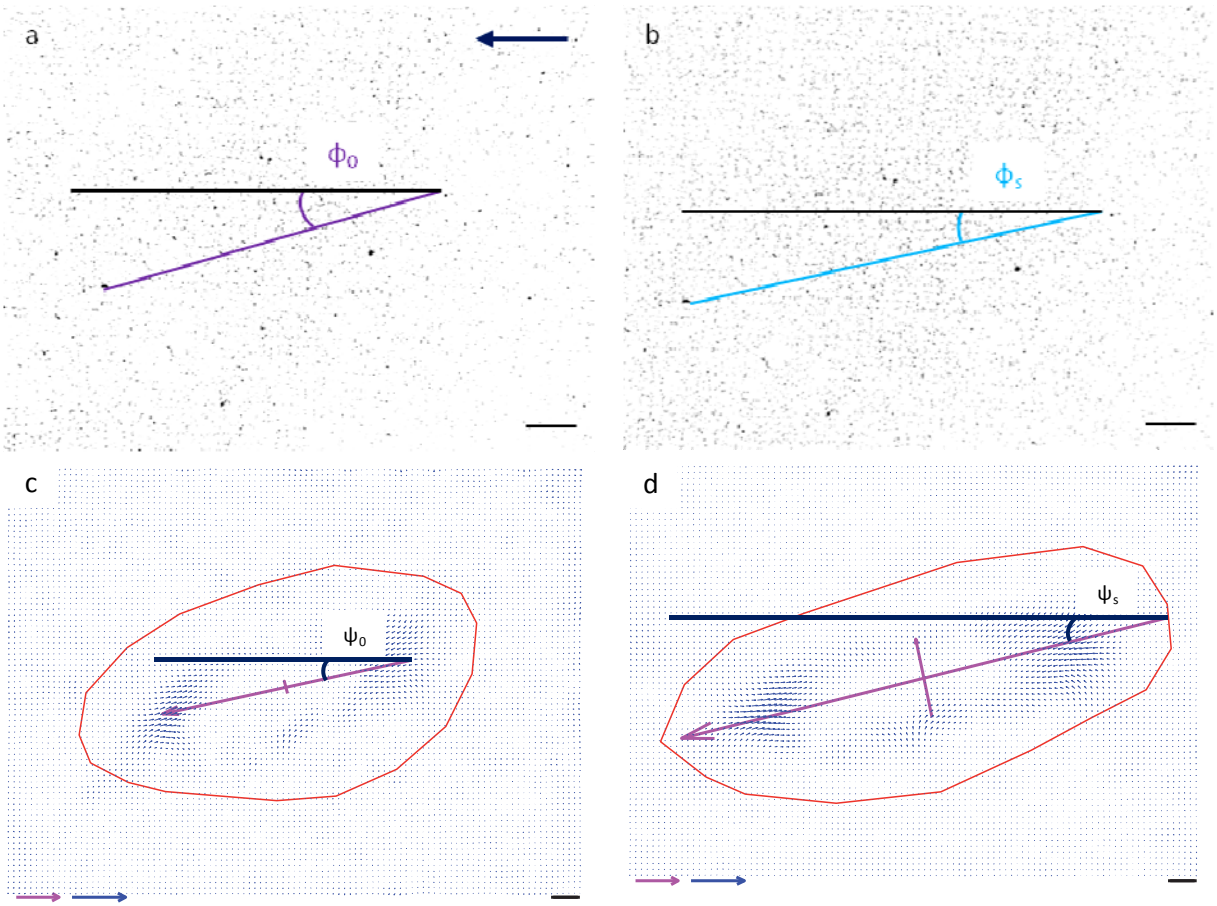

Figure 3.22. Substrate and cell deformation direction. (a, c) Before and (b, d) right after the stretch in the SH experiment. The purple line connects two distinguishable patterns on the micrograph of beads to calculate the direction of substrate deformation; φ_0 is the angle between the line and the x-axis. the blue line. The black arrow indicates the direction of stretch (or x-axis). Scale bars on the bead micrographs 20 µm, on the force dipole images 10 µm.

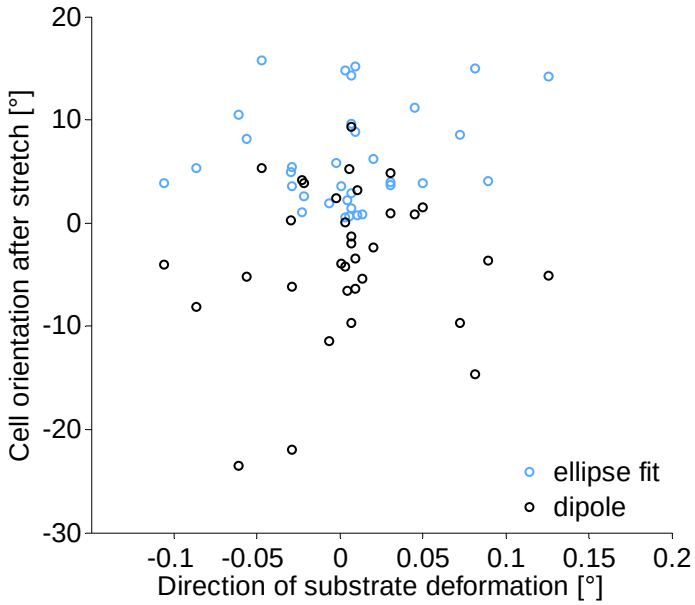

Figure 3.23. Immediate cell reorientation and direction of substrate deformation. (a) Data from the ellipse fit and the force dipole eigenvector orientation. No correlation for all data.

Mean cell orientations before and after stretch were compared in the stretch-and-hold and stretch-and-release experiments. No major change in the cell orientation initiated by the stretch event was observed in either of the experiments (Figure 3.24).

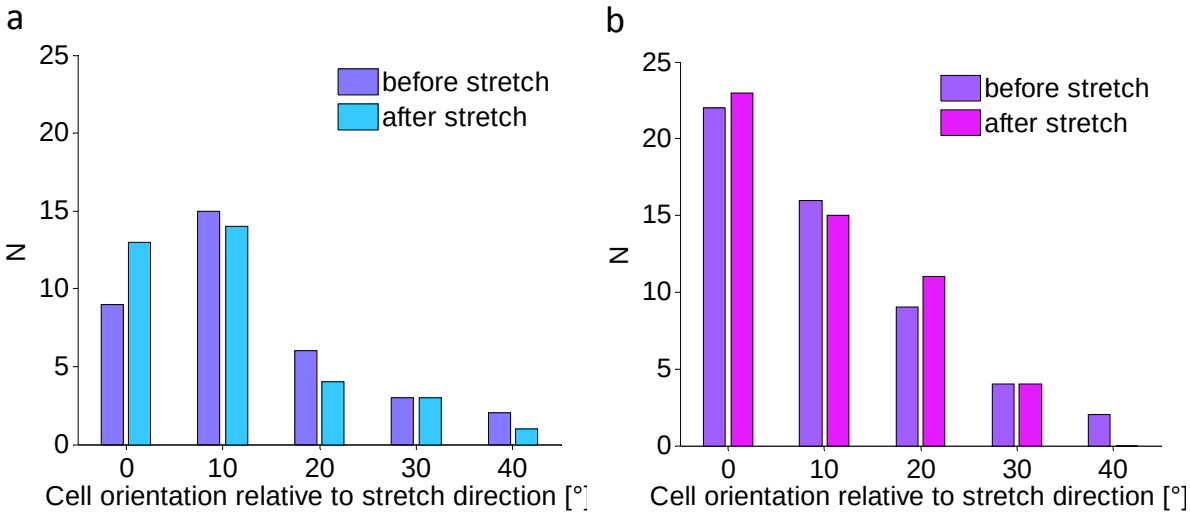

Figure 3.24. Mean cell orientation before and after the stretch. (a) Stretch-and-hold experiments, (b) stretch-and-release.

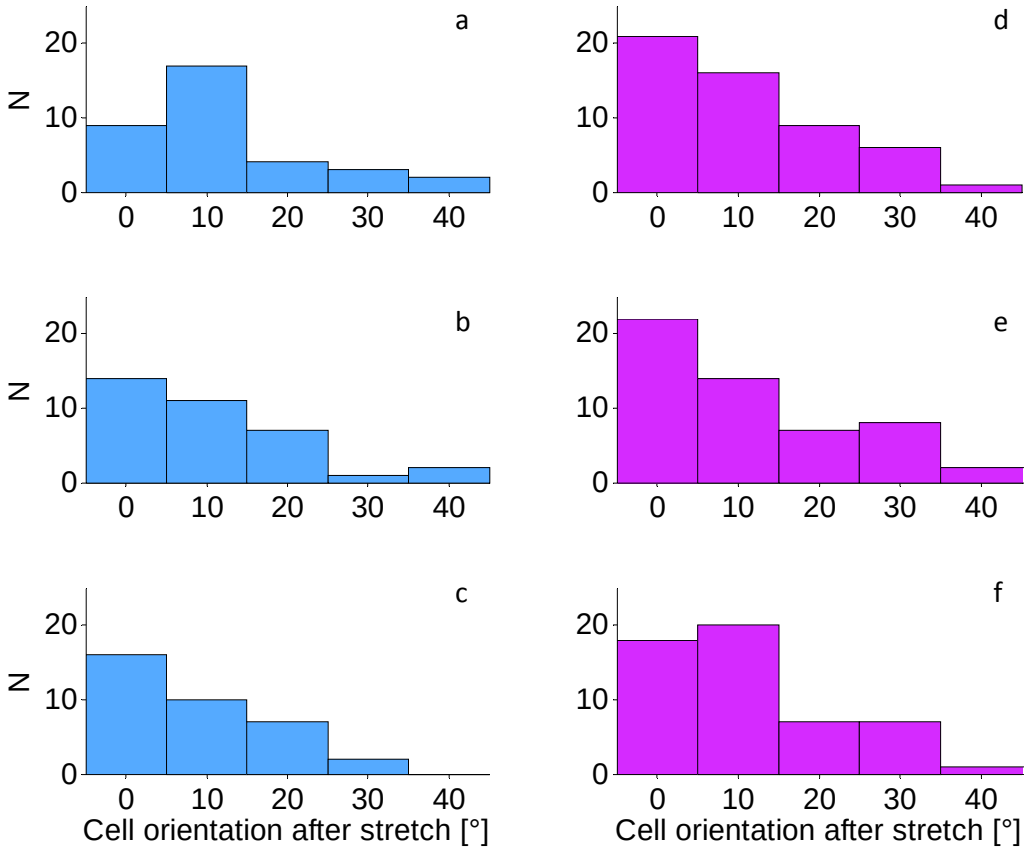

Figure 3.25. Absolute cell orientation: (a, b, c) in the stretch-and-hold and (d, e, f) in the stretch-and-release experiments. (a) and (d) before the stretch; (b) and (e) right after the stretch; (c) and (f) at the end of the observation.

It is clear, that the cells changed their orientation towards the stretch direction in the stretch-and-hold experiments (Figure 3.25 a, b), and remained oriented so until the end of the observation (Figure 3.25 c). There was a further shift towards the stretch-direction, however its significance is uncertain, because of the low statistics. The cell orientation did not change considerably upon stretch and by the end of the observation in the stretch-and release experiments.

Cumulative frequencies of the mean orientation of cells in the stretch-and-hold, stretch-and-release and control experiments are presented in Figure 3.26. The distribution of the mean angles before and after stretch in both stretch-and-release and control experiments was akin to the normal distribution (KS test, α=0.05).

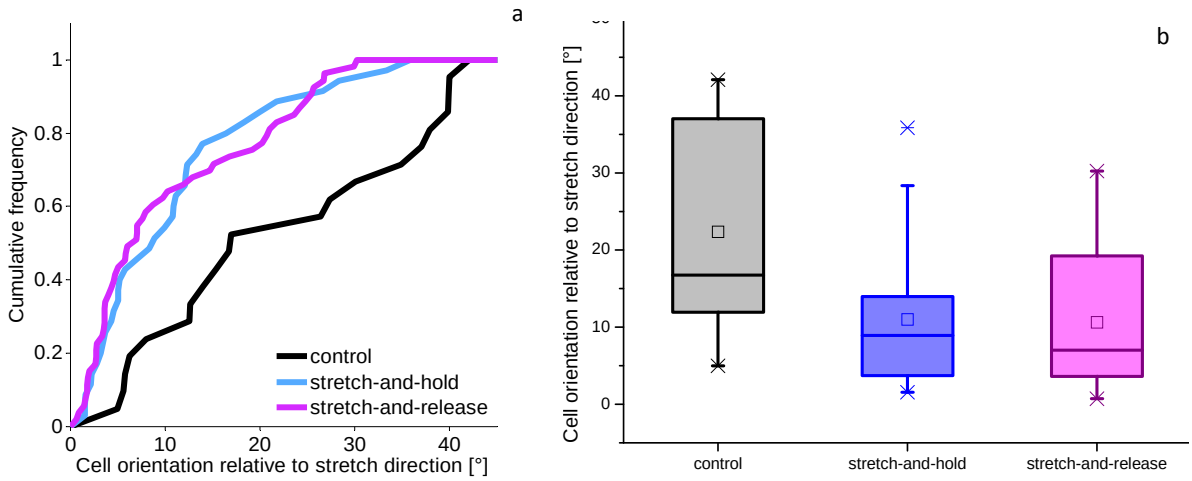

Figure 3.26. Cell orientation relative to the stretch direction. (a) Cumulative frequencies and (b) a box diagram of cell orientation in the SR, SH and control experiments.

Cell area and exerted by the cell forces did not correlate (Figure 3.27).

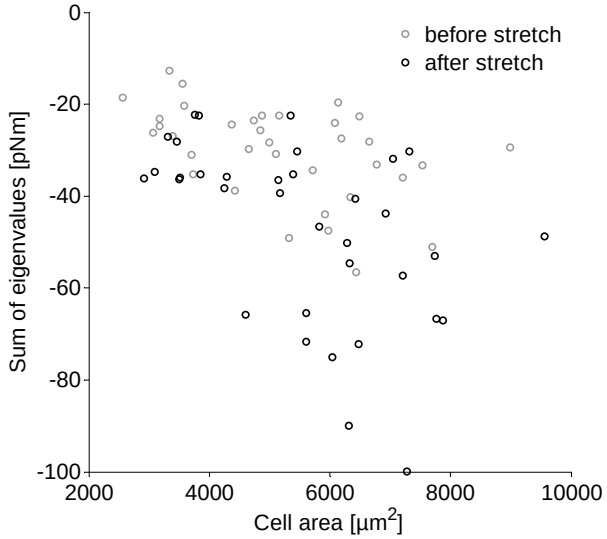

Figure 3.27. Cell area in SH. Sum of eigenvalues before and after the stretch did not correlate with cell area before (grey) and after (black).

The immediate change of elongation and aspect ratio of cells were determined from the ellipse fit performed as described in Section 2.4.5. The elongation as a shape characteristic was calculated as $l = (a - b)/(a + b)$, implying that rounder cells would have l=1, and prolate cells would have $l \rightarrow 0$. The aspect ratio was calculated as $r = a/b$, where a is the major axis of the ellipse, and b is the minor axis. In principle, both parameters indicate that cells elongated upon stretch in the stretch-and-hold experiments.

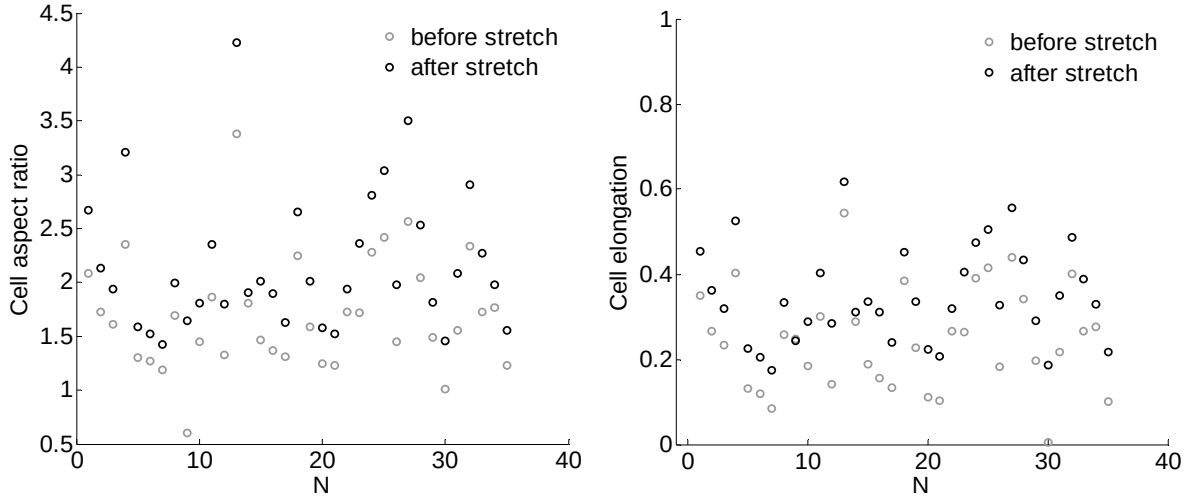

Figure 3.28. Immediate before and after the stretch aspect ratio and elongation of cells in the stretch-and-gold experiment. (a) Aspect ratio and (b) cell elongation before and right after the stretch.

4. Discussion

Mechanical reaction of human vein endothelial cells to external stresses was observed and analyzed in the current project. Cells were cultured on elastic substrates until stable adhesions were created. Subsequently, cells were subjected to a uniaxial constant or transient stretch with the strain rate of 10%/s. The cells and substrates were imaged under physiological conditions before and after stretching using the setup developed for this purposes and software. Traction forces and geometric features of cells were evaluated and discussed thereupon.

4.1 Cell Traction Forces

Interestingly, all cells displayed consistent reactions in the stretch-and-hold experiments or in the stretch-and-release experiments. Namely, the cell contractile moments increased substantially in the former type of strain protocol, and dropped promptly in the latter, independent of the cells' pre-stretch behaviour. This kind of universality indicates that the cells follow certain mechanisms to withstand mechanical loads, whether through biochemical or mechanical adaptation, irrespective of the complexity of their internal organization. Since primary objective of the present work is to analyze the mechanical response of the cells, the force-bearing and force-generating cellular structures are of the main focus of this discussion.

Actomyosin machinery together with focal adhesion protein aggregates are the active contractile units of cells. Actin cytoskeleton is a complex anisotropic structure therefore its response to external loads cannot be described by a single process, but rather by several processes happening at the same time, consecutively or competitively. Single actin filaments, cross-linked actin bundles, and actomyosin stress fibres have different organization [21], therefore, their reaction may vary upon the same type of externally applied stress. It is important to note that non-motile cells, as in these experiments, form mostly thicker stress-fibres with supposedly slower protein exchange kinetics [21].

One should take into account that both types of stretch experiments that were executed in this work have a common feature: cells were strained to the same amplitude (by 20%) therefore some of the reactions of cells could be partially identical. Here, the duration of stretch had the greatest impact on the cell behaviour.

4.1.1 Stretch-and-Hold

A significant increase of contractile moments after the stretch was observed in the SH experiments. The maximum cell forces were reached within 10 min after stretching. The contractile moments relaxed slowly in the next 30 min, however, no or rare return to the pre-stretch state in general was observed.

The observations and implications of processes that happen upon mechanical stress application are often controversial due to variety of reasons like specificity to a cell type, stress type, strain magnitude and rate, etc. Nonetheless, several possibilities could be speculated upon. Single actin filaments might disrupt due to very large loads, however this is not of any influence on the contractile moments in this case, considering the magnitude of the increase. Those filaments that break, are typically repaired within few seconds or induce formation of new adhesion sites and actin bundles [25]. Moreover, single filaments within stress-fibres might break as well, and are reported to be repaired within 120 s by recruitment of such proteins as zyxin and VASP [47]. A similar research on cardiac fibroblasts and other cell types revealed no actin polymerization at the ends of stress fibres, but simple elongation of stress-fibres and focal adhesions along stretch direction [1], [28], [48], and filaments under tension do not bind actin severing protein cofilin [24]. The stress-fibres remain elongated or contract because of the increased tension. Consequently, it causes cells stiffen by reinforcing their cytoskeleton [49], [50]. Overall cell stiffness is related to that of the actin cytoskeleton [1]. Copious research presented that cell stiffness escalated upon stress application [2], [29], [51]. T. Mizutani and colleagues [51], [52] reported a double increase of cell stiffness after an 8% single uniaxial stretch. The stiffness decreased slowly and stabilized (or not) after 2 h of observations. Generally, the remodeling of actin network due to slow cross-linker kinetics might take up from few minutes to as much as half an hour [53]. This fact could explain the slow relaxation of contractile forces after maximum was reached after the stretch.

On the other hand, myosin is activated and recruited due to the increase of external strains. The arguable influence of mechanosensitive channels activation that promotes Ca^{2+} influx could play a role, as stated by some authors [54], [55]. Yet, there have been studies that revealed no such effect [56]. In addition, it has been demonstrated that ATP is released in response to stress [57], [58]. These two could play a role in myosin recruitment and activation in the present work, which is to be proven by additional measurements. Myosin recruitment could explain the fact that in the stretch-and-hold experiments, contractile forces persist to increase until some maximum is reached.

Apart from the biochemical reactions, a simple rise in tension in the stress fibres due to load increase occurs. By analogy with a Maxwell-Voigt spring-dashpot model, a rapid increase of contractile moments due to reaction of the spring and a slow release - of the dashpot.

The author of the thesis believes, that interplay of all these processes could explain the sharp and substantial increase of contractile forces, and a slow or no relaxation to the pre-stretch levels.

4.1.2 Stretch-and-Release

Similarly to the observations in the stretch-and-hold experiments, all cells exhibited the same kind of drop in contractile forces independent of the cell behaviour before the stretch-release cycle. The contractile moments decreased abruptly on average by 15% and recovered relatively fast (within 3 min) upon stretch-and-release cycle. Analogous experiments on various cell types exposed to a maximal 10% tensile transient stretch [14], [59] showed drops of contractile moments by 50%. Nonetheless, the reported recovery times were about the same as observed here (few minutes).

In general, the transient stretch did not seem have such a great and lasting impact compared to the constant strain in the stretch-and-hold experiments. This is clearly seen from the observations of the monotonically increasing or decreasing contractile moments. The cell activity was only shortly interrupted by the stretch event (Figure 4.1), after the appropriate recovery time, cell activity resumed to that of the pre-stretch.

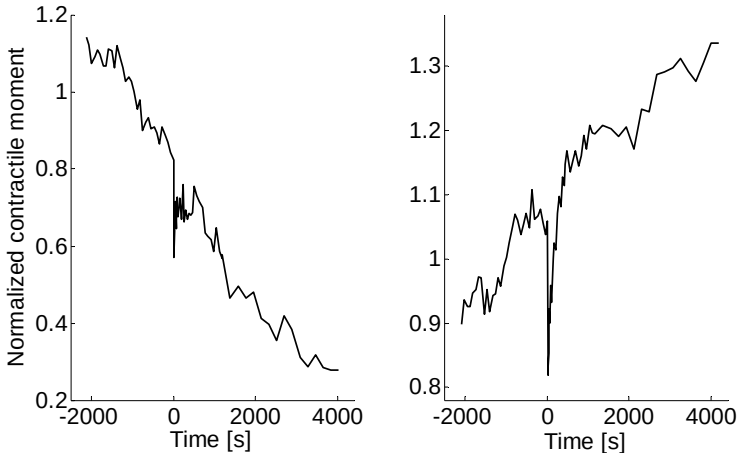

Figure 4.1. Decreasing and increasing contractile moments of cells in the stretch-and-release experiments.

As mentioned before, both stretch-and-hold and stretch-and release have a common initiating point, namely the stretch to 20% itself. This means, that the drop of contractile moments in the SR experiments was probably not only due to minor actin network disruption upon stress application. K. D. Costa and colleagues [60] demonstrated buckling, disruption and reassembling of actin stress fibres in cells that were subjected to a uniaxial 26% compression. The whole process of disassembling and reassembling of fibres was in the same time range as observed in this work (few minutes). Therefore the drop in contractile moments might be partially explained by the same phenomena. Single actin filaments might disrupt and be repaired, whereas thin stress fibres buckle and thicker ones contract at the same time [61].

The results of these experiments could be compared to those of a simple compression experiments [52]. T. Mizutani and colleagues confirmed that cell stiffness decreased, cell body compressed and therefore measured cell stiffness dropped abruptly directly after stress application. However, the reported stiffness fully recovered much slower (40 min) compared to the contractile moments estimated in the current work.

Cells reacted in the same way to the same kind of stretch irrespective of their contractile history before stress was applied in both types of experiments. Neither of observed quantities (cell areas, amplitudes of change of contractile moments, recovery time to the pre-stretch values, time when maximum was reached etc.) correlated with the contractile behaviour of the cell before stretch. Since focal adhesions seemed to have remained intact right upon stretch (Figure 4.2), the leading role in sustaining and adapting to the externally applied stresses was assigned to the actin cytoskeletal structures.

4.2 Cell Orientation, Aspect Ratio, and Area

The cell body orientation, aspect ratio, area and elongation were obtained from the manually selected cell outlines and ellipse fit results. The orientation of the eigenvector with the largest eigenvalue was taken as a traction orientation.

A more distinct impact of stretching on these cell parameters was observed in the stretch-and-hold experiments. Cell body followed the substrate deformation upon stretch, implying a geometrical effect on reorientation. When the cell initial orientation was more than 20° away from the stretch direction before stretch was applied, the cells reoriented towards the stretch direction upon stretching. Those cells that were lying along the stretch axis changed

their orientation in either direction insignificantly. In contrast to that, cell orientation, area and aspect ratio remained unchanged upon stretch in the stretch-and-release experiments. This speaks for the assumption, that transient stress (whole stretch-release cycle duration was 5 s) was not sufficient to induce biochemical reactions necessary for reorientation [62]. An extensive study has been performed on the cell behaviour in cyclic stretch experiments [56], [63], [64]. Numerous scientific reports demonstrated and elaborated theoretical models [65]–[67] that cells reorient perpendicular to the stretch direction for small stretch amplitudes and low frequencies, and about the minimum strain direction for large amplitudes and higher frequencies (which is 62° for the substrates used in this work [64]) in the cyclic stretch experiments. Contrary to that, single stretch did not initiate cell reorientation away from the stretch direction, as observed in the current work: cells simply followed substrate deformation direction and remained oriented this way. Either the cell orientation along stretch was optimal for a stretch-and-hold type of stress, or a periodic stretch is required for a major cell reorientation.

Interestingly, cell area did not correlate with the forces exerted by the cell in this study. Previous research connected cell (human pulmonary artery endothelial cells, 3T3 fibroblasts) spread area to force generation [33], [68]. These studies showed that larger cells exercise larger forces. However, the artificially controlled cell spreading area and shape might have not reflected the physiological conditions. Furthermore, those cells were spread on micropost arrays or other similar microstructure of different densities (with a varying packing parameter), but not a flat surface like in this work. Moreover, when cells are spreading on the surface, they naturally have to create contacts to it and hence the force increases until stable. In these studies another parameter was coupled to the cell force, namely stiffness of substrates. Hence, it is rather an effect of the environment rigidity on strengthening of the cytoskeleton and focal adhesions described by D. Choquet and colleagues [11].

More precise analyses compared the area of focal adhesions and the forces applied at these sites by cells (cardiac myocytes, 3T3 fibroblasts) [69]–[71]. They demonstrated a linear correlation between the two quantities: the larger the total area, the larger were the forces. Preliminary experiments made by the author of the thesis revealed that focal adhesions (cells were transfected with pEGFP-vinculin) elongated along the stretch direction (not yet quantified). Another compelling observation was that the pHUVECs did not disassemble their focal adhesions upon stretch (Figure 4.2). This might be connected to the strengthening of the linkage between cytoskeleton and integrins [11].

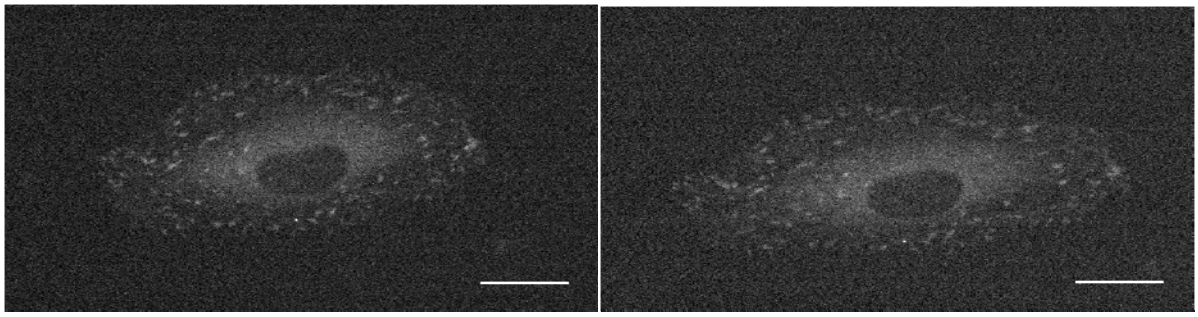

Figure 4.2. Fluorescence micrographs of pHUVECs transfected with pEGFP-vinculin. (a) before stretch and (b) right after stretch in the stretch-and-hold experiment. No obvious disassembly of focal adhesions was observed. They become elongated along the stretch direction. Scale bars 20 μm.

Summing up, the results of this work are consistent with the previous research [11], [14], [24], [29], [49], [51], [52], [59], [60]. The results require further investigations on a macromolecular scale in order to obtain a better understanding of the molecular mechanisms that govern cell behaviour upon external mechanical stress. The exchange and rearrangement of cell actomyosin structures and actin cross-linkers, as well as focal adhesion dynamics in the stretch or compression experiments are to be investigated. Moreover, to have a better understanding of the subcellular mechanisms it is necessary to resolve the apparent difference between stresses that cause long-term changes as response to repetitive or continuous action [62], [64], [72]–[74], and transient strain that appears to have no or little effect.

5. Conclusion

As a result of the first part of this work, a setup for live traction force microscopy during stretch experiments was established. The setup has proven to perform on a stable basis. Silicone elastomeric substrates of various configuration can be used in the experiments (ribbon-like without rim, as used in this work, or box-shaped with rim as described in [64]). Test measurements with living cells ensured that the parameters of the experimental environment were supported at the cell physiological level, thus, warranting that the work on living cells is possible. The setup allows multi-channel image acquisition with a minimal time between two adjacent channels of 47 ms. Therefore, experiments with transfected cells are possible and proven to be successful. Moreover, various kinds of stretch experiments can be performed on the setup: stretch-and-hold, stretch-and-release, and their counters release-and-hold, release-and-stretch, and cyclic stretch. These can be implemented with varying or constant amplitudes and frequencies. In conclusion, the developed user-friendly GUIs make the setup highly adjustable and easy to operate. Two types of experiments were performed: stretch-and-hold and stretch-and-release. For every instance a script or a graphical user interface were coded in Micro-Manager.

In the second part of the current work the response of primary human umbilical vein endothelial cells to single 20% uniaxial transient or constant strains was investigated. Cell traction forces were calculated, cell area, cell body orientation, orientation of tractions, and whole cell behaviour upon stretch were defined and inspected.

Both kinds of previously reported reactions were observed on the same cell type in two kinds of experiments. The single stretch-and-hold induced a prominent increase in contractile moments. The latter remained on an elevated level compared to the pre-stretch values throughout the most observations, implying a very slow relaxation upon load increase. The stretch-and-release prompted a transient response: an abrupt decrease of contractile moments and a fast recovery to the pre-stretch level. Interestingly, in both cases, the reaction was universal, i.e. independent of the pre-stretch cell behaviour and contractility.

As an outlook of this work, further investigation with transfected cells should be performed. Both types of experiments are to be repeated with fluorescently labeled actin cytoskeletal structures and focal adhesion associated proteins, such as vinculin, in order to obtain more detailed information on cell internal reorganization upon stress application.

Micrographs of actin labeled cells would provide direct clues on the stress fibre response. One would obtain information on the cytoskeleton reinforcement: if it is conveyed through actin polymerization, or whether it is rather an increase of load in existing actin bundles in the stretch-and-hold experiments; and whether buckling and disruption of filaments occurs in the stretch-and-release experiments.

Furthermore, a more extensive analysis of cell adhesion sites dynamics should be performed. Preliminary tests revealed that the focal adhesions oriented along strain direction and elongated by 10-20%. No major change in quantity of FA or signal increase of vinculin was observed, signifying no new focal adhesion formation. However, if amount of vinculin in FA does not change, and its distribution in FA becomes sparser, it would mean the load is increased in the same contact points and distributed over a larger area. Vinculin signal increase would imply a very fast (at least, within several seconds) creation of additional adherent points, so the net load would spread over a larger focal area. If this increase is accompanied by actin polymerization, that would speak for cytoskeleton reinforcement as discussed in [16]. It should also be confirmed whether the response in stretch-and-release experiments applies to a simple compression-and-hold or shortening experiments and to which extent.

In conclusion, as a result of this work, a setup for live cell traction force microscopy during stretch experiments has been successfully built and software supporting it has been developed. Furthermore, it proved to be suitable for the studies on the living matter. The results of the experiments were coherent with the previous research and provided new information on mechanical response of endothelial cells to external stress.

6. References

[1] K. Hayashi, "Tensile Properties and Local Stiffness of Cells," in in *Mechanics of Biological Tissue*, no. i, G. A. Holzapfel and R. W. Ogden, Eds. Springer Berlin Heidelberg, pp. 137–152, 2006.

[2] M. Sato, M. J. Levesque, and R. M. Nerem, "Micropipette aspiration of cultured bovine aortic endothelial cells exposed to shear stress," *Arterioscler. Thromb. Vasc. Biol.*, vol. 7, no. 3, pp. 276–286, 1987.

[3] J. Candiello, M. Balasubramani, E. M. Schreiber, G. J. Cole, U. Mayer, W. Halfter, and H. Lin, "Biomechanical properties of native basement membranes.," *FEBS J.*, vol. 274, no. 11, pp. 2897–908, 2007.

[4] S. Houben, N. Kirchgeßner, and R. Merkel, "Estimating Force Fields of Living Cells – Comparison of Several Regularization Schemes Combined with Automatic Parameter Choice," in in *Lecture Notes in Computer Science*, vol. 6376, M. Goesele, S. Roth, A. Kuijper, B. Schiele, and K. Schindler, Eds. Darmstadt: Springer Berlin Heidelberg, pp. 71–80, 2010.

[5] B. E. Sumpio, J. T. Riley, and A. Dardik, "Cells in focus: endothelial cell.," *Int. J. Biochem. Cell Biol.*, vol. 34, no. 12, pp. 1508–12, 2002.

[6] J. P. Califano and C. a Reinhart-King, "Exogenous and endogenous force regulation of endothelial cell behavior.," *J. Biomech.*, vol. 43, no. 1, pp. 79–86, 2010.

[7] R. Merkel, N. Kirchgessner, C. M. Cesa, and B. Hoffmann, "Cell force microscopy on elastic layers of finite thickness.," *Biophys. J.*, vol. 93, no. 9, pp. 3314–23, 2007.

[8] B. Geiger, J. P. Spatz, and A. D. Bershadsky, "Environmental sensing through focal adhesions.," *Nat. Rev. Mol. Cell Biol.*, vol. 10, no. 1, pp. 21–33, 2009.

[9] A. J. Engler, S. Sen, H. L. Sweeney, and D. E. Discher, "Matrix elasticity directs stem cell lineage specification.," *Cell*, vol. 126, no. 4, pp. 677–89, 2006.

[10] J. Z. Gasiorowski, S. J. Liliensiek, P. Russell, D. a Stephan, P. F. Nealey, and C. J. Murphy, "Alterations in gene expression of human vascular endothelial cells associated with nanotopographic cues.," *Biomaterials*, vol. 31, no. 34, pp. 8882–8, 2010.

[11] D. Choquet, D. P. Felsenfeld, and M. P. Sheetz, "Extracellular matrix rigidity causes strengthening of integrin-cytoskeleton linkages.," *Cell*, vol. 88, no. 1, pp. 39–48, 1997.

[12] C. M. Nelson, R. P. Jean, J. L. Tan, W. F. Liu, N. J. Sniadecki, A. a Spector, and C. S. Chen, "Emergent patterns of growth controlled by multicellular form and mechanics.," *Proc. Natl. Acad. Sci. U. S. A.*, vol. 102, no. 33, pp. 11594–9, 2005.

[13] C. F. Deroanne, C. M. Lapiere, and B. V Nusgens, "In vitro tubulogenesis of endothelial cells by relaxation of the coupling extracellular matrix-cytoskeleton.," *Cardiovasc. Res.*, vol. 49, no. 3, pp. 647–58, 2001.

[14] C. Chen, R. Krishnan, E. Zhou, A. Ramachandran, D. Tambe, K. Rajendran, R. M. Adam, L. Deng, and J. J. Fredberg, "Fluidization and resolidification of the human bladder smooth muscle cell in response to transient stretch.," *PLoS One*, vol. 5, no. 8, pp. 1–7, 2010.

[15] R. Krishnan, E. P. Canovic, A. L. Iordan, K. Rajendran, G. Manomohan, A. P. Pirentis, M. L. Smith, J. P. Butler, J. J. Fredberg, and D. Stamenovic, "Fluidization, resolidification, and reorientation of the endothelial cell in response to slow tidal stretches.," *Am. J. Physiol. Cell Physiol.*, vol. 303, no. 4, pp. C368–75, 2012.

[16] R. Krishnan, C. Y. Park, Y.-C. Lin, J. Mead, R. T. Jaspers, X. Trepat, G. Lenormand, D. Tambe, A. V Smolensky, A. H. Knoll, J. P. Butler, and J. J. Fredberg, "Reinforcement versus fluidization in cytoskeletal mechanoresponsiveness.," *PLoS One*, vol. 4, no. 5, p. e5486, 2009.

[17] N. Rosenblatt, S. Hu, J. Chen, N. Wang, and D. Stamenović, "Distending stress of the cytoskeleton is a key determinant of cell rheological behavior.," *Biochem. Biophys. Res. Commun.*, vol. 321, no. 3, pp. 617–22, 2004.

[18] P. Fernández, P. a Pullarkat, and A. Ott, "A master relation defines the nonlinear viscoelasticity of single fibroblasts.," *Biophys. J.*, vol. 90, no. 10, pp. 3796–805, May 2006.

[19] P. Kollmannsberger, C. T. Mierke, and B. Fabry, "Nonlinear viscoelasticity of adherent cells is controlled by cytoskeletal tension," *Soft Matter*, vol. 7, no. 7, pp. 3127–3132, 2011.

[20] S. Pellegrin and H. Mellor, "Actin stress fibres.," *J. Cell Sci.*, vol. 120, no. Pt 20, pp. 3491–9, 2007.

[21] P. Hotulainen and P. Lappalainen, "Stress fibers are generated by two distinct actin assembly mechanisms in motile cells.," *J. Cell Biol.*, vol. 173, no. 3, pp. 383–94, 2006.

[22] N. Wang, I. M. Tolić-Nørrelykke, J. Chen, S. M. Mijailovich, J. P. Butler, J. J. Fredberg, and D. Stamenović, "Cell prestress. I. Stiffness and prestress are closely associated in adherent contractile cells.," *Am. J. Physiol. Cell Physiol.*, vol. 282, no. 3, pp. C606–16, 2002.

[23] S. Deguchi, T. Ohashi, and M. Sato, "Tensile properties of single stress fibers isolated from cultured vascular smooth muscle cells.," *J. Biomech.*, vol. 39, no. 14, pp. 2603–10, 2006.

[24] K. Hayakawa, H. Tatsumi, and M. Sokabe, "Mechano-sensing by actin filaments and focal adhesion proteins.," *Commun. Integr. Biol.*, vol. 5, no. 6, pp. 572–7, 2012.

[25] J. Colombelli, A. Besser, H. Kress, E. G. Reynaud, P. Girard, E. Caussinus, U. Haselmann, J. V Small, U. S. Schwarz, and E. H. K. Stelzer, "Mechanosensing in actin stress fibers revealed by a close correlation between force and protein localization.," *J. Cell Sci.*, vol. 122, no. Pt 10, pp. 1665–79, 2009.

[26] S. Deguchi and M. Sato, "Biomechanical properties of actin stress fibers of non-motile cells.," *Biorheology*, vol. 46, no. 2, pp. 93–105, 2009.

[27] Harris A. K., Wild P., Stopak D., and (University of North Carolina), "Silicone Rubber Substrata: A New Wrinkle in the Study of Cell Locomotion," *Science (80-.).*, vol. 208, no. 4440, pp. 177–179, 1980.

[28] L. Trichet, J. Le Digabel, R. J. Hawkins, S. R. K. Vedula, M. Gupta, C. Ribrault, P. Hersen, R. Voituriez, and B. Ladoux, "Evidence of a large-scale mechanosensing mechanism for cellular adaptation to substrate stiffness.," *Proc. Natl. Acad. Sci. U. S. A.*, vol. 109, no. 18, pp. 6933–8, 2012.

[29] R. M. Hochmuth, "Micropipette aspiration of living cells.," *J. Biomech.*, vol. 33, no. 1, pp. 15–22, 2000.

[30] P. Kollmannsberger, C. T. Mierke, and B. Fabry, "Contractile prestress controls stiffening and fluidization of living cells in response to large external forces," pp. 2–5, 2010.

[31] O. du Roure, A. Saez, A. Buguin, R. H. Austin, P. Chavrier, P. Silberzan, P. Siberzan, and B. Ladoux, "Force mapping in epithelial cell migration.," *Proc. Natl. Acad. Sci. U. S. A.*, vol. 102, no. 7, pp. 2390–5, 2005.

[32] K. A. Beningo and Y.-L. Wang, "Flexible substrata for the detection of cellular traction forces.," *Trends Cell Biol.*, vol. 12, no. 2, pp. 79–84, 2002.

[33] J. L. Tan, J. Tien, D. M. Pirone, D. S. Gray, K. Bhadriraju, and C. S. Chen, "Cells lying on a bed of microneedles: an approach to isolate mechanical force.," *Proc. Natl. Acad. Sci. U. S. A.*, vol. 100, no. 4, pp. 1484–9, 2003.

[34] C. M. Cesa, N. Kirchgessner, D. Mayer, U. S. Schwarz, B. Hoffmann, and R. Merkel, "Micropatterned silicone elastomer substrates for high resolution analysis of cellular force patterns.," *Rev. Sci. Instrum.*, vol. 78, no. 3, p. 034301, 2007.

[35] Y.-C. Lin, D. T. Tambe, C. Y. Park, M. R. Wasserman, X. Trepat, R. Krishnan, G. Lenormand, J. J. Fredberg, and J. P. Butler, "Mechanosensing of substrate thickness," *Phys. Rev. E*, vol. 82, no. 4, p. 041918, 2010.

[36] P. C. Hansen and M. R. Zaglia, "Regularization tools: A Matlab package for analysis and solution of discrete ill-posed problems," *Numer. Algorithms*, vol. 6, no. I 994, pp. 1–35, 1994.

[37] U. S. Schwarz, N. Q. Balaban, D. Riveline, a Bershadsky, B. Geiger, and S. a Safran, "Calculation of forces at focal adhesions from elastic substrate data: the effect of localized force and the need for regularization.," *Biophys. J.*, vol. 83, no. 3, pp. 1380–94, 2002.

[38] P. E. Hockberger, T. a Skimina, V. E. Centonze, C. Lavin, S. Chu, S. Dadras, J. K. Reddy, and J. G. White, "Activation of flavin-containing oxidases underlies light-induced production of H2O2 in mammalian cells.," *Proc. Natl. Acad. Sci. U. S. A.*, vol. 96, no. 11, pp. 6255–60, 1999.

[39] SCHNEIDER ELECTRIC MOTION, "Programming and Software. Reference for MCode and MCode/TCP.pdf." [Online]. Available: http://motion.schneider-electric.com/downloads/manuals/MCode.pdf. [Accessed: 15-Apr-2013].

[40] A. Edelstein, N. Amodaj, K. Hoover, R. Vale, and N. Stuurman, "Computer control of microscopes using μManager.," *Curr. Protoc. Mol. Biol.*, vol. Chapter 14, no. October, p. Unit14.20, 2010.

[41] W. S. Rasband, "ImageJ." [Online]. Available: http://rsb.info.nih.gov/ij/. [Accessed: 14-Apr-2013].

[42] C. A. Schneider, W. S. Rasband, and K. W. Eliceiri, "NIH Image to ImageJ: 25 years of image analysis," *Nat. Methods*, vol. 9, no. 7, pp. 671–675, 2012.

[43] P. Niemeyer, "BeanShell - Lightweight Scripting for Java." [Online]. Available: http://www.beanshell.org/. [Accessed: 14-Apr-2013].

[44] P. Subsoontorn, H. Garcia, and N. Amodaj, "Autofocusing plug-in for micro-manager and ImageJ," 2007. [Online]. Available: https://valelab.ucsf.edu/svn/micromanager2/trunk/autofocus/Autofocus.java. [Accessed: 14-Apr-2013].

[45] M. V. Kunnavakkam, F. M. Houlihan, M. Schlax, J. a. Liddle, P. Kolodner, O. Nalamasu, and J. a. Rogers, "Low-cost, low-loss microlens arrays fabricated by soft-lithography replication process," *Appl. Phys. Lett.*, vol. 82, no. 8, p. 1152, 2003.

[46] R. Hal and J. Flusser, "Numerically stable direct least squares fitting of ellipses," in *Proc. 6th International Conference in Central Europe on Computer Graphics and Visualization*, vol. 98, no. WSCG, pp. 125–132, 1998.

[47] M. a Smith, E. Blankman, M. L. Gardel, L. Luettjohann, C. M. Waterman, and M. C. Beckerle, "A zyxin-mediated mechanism for actin stress fiber maintenance and repair.," *Dev. Cell*, vol. 19, no. 3, pp. 365–76, 2010.

[48] D. Kirchenbüchler, S. Born, N. Kirchgessner, S. Houben, B. Hoffmann, and R. Merkel, "Substrate, focal adhesions, and actin filaments: a mechanical unit with a weak spot for mechanosensitive proteins.," *J. Phys. Condens. Matter*, vol. 22, no. 19, p. 194109, 2010.

[49] M. Sato, M. J. Levesque, and R. M. Nerem, "The Effect of a Fluid-Imposed Shear Stress on the Mechanical Properties of Cultured Endothelial Cells," in in *Role of Blood Flow in Atherogenesis*, Y. Yoshida, T. Yamaguchi, C. G. Caro, S. Glagov, and R. M. Nerem, Eds. Springer Japan, pp. 189–194, 1988.

[50] G. Giannone and M. P. Sheetz, "Substrate rigidity and force define form through tyrosine phosphatase and kinase pathways.," *Trends Cell Biol.*, vol. 16, no. 4, pp. 213–23, 2006.

[51] T. Mizutani, K. Kawabata, Y. Koyama, M. Takahashi, and H. Haga, "Regulation of cellular contractile force in response to mechanical stretch by diphosphorylation of

myosin regulatory light chain via RhoA signaling cascade.," *Cell Motil. Cytoskeleton*, vol. 66, no. 7, pp. 389–97, 2009.

[52] T. Mizutani, H. Haga, and K. Kawabata, "Cellular stiffness response to external deformation: tensional homeostasis in a single fibroblast.," *Cell Motil. Cytoskeleton*, vol. 59, no. 4, pp. 242–8, 2004.

[53] T. D. Pollard and G. G. Borisy, "Cellular motility driven by assembly and disassembly of actin filaments.," *Cell*, vol. 112, no. 4, pp. 453–65, 2003.

[54] K. Hayakawa, H. Tatsumi, and M. Sokabe, "Actin stress fibers transmit and focus force to activate mechanosensitive channels.," *J. Cell Sci.*, vol. 121, no. Pt 4, pp. 496–503, 2008.

[55] T. S. Matsui, R. Kaunas, M. Kanzaki, M. Sato, and S. Deguchi, "Non-muscle myosin II induces disassembly of actin stress fibres independently of myosin light chain dephosphorylation.," *Interface Focus*, vol. 1, no. 5, pp. 754–66, 2011.

[56] K. Hayakawa, N. Sato, and T. Obinata, "Dynamic reorientation of cultured cells and stress fibers under mechanical stress from periodic stretching.," *Exp. Cell Res.*, vol. 268, no. 1, pp. 104–14, 2001.

[57] C. Luna, G. Li, J. Qiu, P. Challa, D. L. Epstein, and P. Gonzalez, "Extracellular release of ATP mediated by cyclic mechanical stress leads to mobilization of AA in trabecular meshwork cells.," *Invest. Ophthalmol. Vis. Sci.*, vol. 50, no. 12, pp. 5805–10, 2009.

[58] J. A. Eldred, J. Sanderson, M. Wormstone, J. R. Reddan, and G. Duncan, "Stress-induced ATP release from and growth modulation of human lens and retinal pigment epithelial cells.," *Biochem. Soc. Trans.*, vol. 31, no. Pt 6, pp. 1213–5, 2003.

[59] X. Trepat, L. Deng, S. S. An, D. Navajas, D. J. Tschumperlin, W. T. Gerthoffer, J. P. Butler, and J. J. Fredberg, "Universal physical responses to stretch in the living cell.," *Nature*, vol. 447, no. 7144, pp. 592–5, 2007.

[60] K. D. Costa, W. J. Hucker, and F. C.-P. Yin, "Buckling of actin stress fibers: a new wrinkle in the cytoskeletal tapestry.," *Cell Motil. Cytoskeleton*, vol. 52, no. 4, pp. 266–74, 2002.

[61] S. Deguchi, T. S. Matsui, and M. Sato, "Simultaneous contraction and buckling of stress fibers in individual cells.," *J. Cell. Biochem.*, vol. 113, no. 3, pp. 824–32, 2012.

[62] A. M. Goldyn, B. A. Rioja, J. P. Spatz, C. Ballestrem, and R. Kemkemer, "Force-induced cell polarisation is linked to RhoA-driven microtubule-independent focal-adhesion sliding.," *J. Cell Sci.*, vol. 122, no. Pt 20, pp. 3644–51, 2009.

[63] J. H. Wang, P. Goldschmidt-Clermont, J. Wille, and F. C. Yin, "Specificity of endothelial cell reorientation in response to cyclic mechanical stretching.," *J. Biomech.*, vol. 34, no. 12, pp. 1563–72, 2001.

[64] U. Faust, N. Hampe, W. Rubner, N. Kirchgessner, S. Safran, B. Hoffmann, and R. Merkel, "Cyclic stress at mHz frequencies aligns fibroblasts in direction of zero strain.," *PLoS One*, vol. 6, no. 12, pp. 1–16 e28963, 2011.

[65] S. A. Safran and R. De, "Nonlinear dynamics of cell orientation," *Phys. Rev. E*, vol. 80, no. 6, pp. 4–7, 2009.

[66] S. A. Safran, A. Zemel, and R. De, "Orientational Polarizability and Stress Response of Biological Cells," in in *IUTAM Symposium on Cellular, Molecular and Tissue Mechanics*, vol. 16, K. Garikipati and E. M. Arruda, Eds. Dordrecht: Springer Netherlands, pp. 91–101, 2010.

[67] J. Qian, H. Liu, Y. Lin, W. Chen, and H. Gao, "A mechanochemical model of cell reorientation on substrates under cyclic stretch.," *PLoS One*, vol. 8, no. 6, p. e65864, 2013.

[68] S. J. Han, K. S. Bielawski, L. H. Ting, M. L. Rodriguez, and N. J. Sniadecki, "Decoupling substrate stiffness, spread area, and micropost density: a close spatial relationship between traction forces and focal adhesions.," *Biophys. J.*, vol. 103, no. 4, pp. 640–8, 2012.

[69] N. Q. Balaban, U. S. Schwarz, D. Riveline, P. Goichberg, G. Tzur, I. Sabanay, D. Mahalu, S. Safran, a Bershadsky, L. Addadi, and B. Geiger, "Force and focal adhesion assembly: a close relationship studied using elastic micropatterned substrates.," *Nat. Cell Biol.*, vol. 3, no. 5, pp. 466–72, 2001.

[70] A. D. Rape, W.-H. Guo, and Y.-L. Wang, "The regulation of traction force in relation to cell shape and focal adhesions.," *Biomaterials*, vol. 32, no. 8, pp. 2043–51, 2011.

[71] A. Saez, A. Buguin, P. Silberzan, and B. Ladoux, "Is the mechanical activity of epithelial cells controlled by deformations or forces?," *Biophys. J.*, vol. 89, no. 6, pp. L52–4, 2005.

[72] M. Skutek, G. J. Zeichen, N. Brauer, and U. Bosch, "Cyclic mechanical stretching modulates secretion pattern of growth factors in human tendon ® broblasts," pp. 48–52, 2001.

[73] L. P. Desai, S. R. White, and C. M. Waters, "Cyclic mechanical stretch decreases cell migration by inhibiting phosphatidylinositol 3-kinase- and focal adhesion kinase-mediated JNK1 activation.," *J. Biol. Chem.*, vol. 285, no. 7, pp. 4511–9, 2010.

[74] T. S. Matsui, K. Ito, R. Kaunas, M. Sato, and S. Deguchi, "Actin stress fibers are at a tipping point between conventional shortening and rapid disassembly at physiological levels of MgATP.," *Biochem. Biophys. Res. Commun.*, vol. 395, no. 3, pp. 301–6, 2010.

Appendix A: Hardware

Microscopic setup

Microscope: Axiotech Vario	Carl Zeiss AG, Jena, Germany
Filter set 79 HE ms: (1) Excitation DBP 470/27 nm + 556/25 nm Beamsplitter DFT 490 nm + 575 nm (2) Emission BP 512/30 nm and BP 630/98 nm Beam combiner BC 565 nm	Carl Zeiss AG, Jena, Germany
Filter: GG 475, d=25 mm	Schott AG, Mainz, Germany
Objective: LUMPLFLN 40x Water, NA 0.8, WD 3.3 mm	Olympus Corp., Tokyo, Japan
Camera: SensiCam qe	pco.imaging AG, Kelheim, Germany
Lamp: X-Cite ® 120	EXFO, Quebec, Canada
Motorized fast filter wheel: 500-HF110	Prior Scientific GmbH, Jena, Germany
Linear stage (“Stretcher”) motor type: MT 63	Steinmeyer GmbH, Albstadt, Germany
Multiaxis motorized XY-stage motor type: KT 205	Steinmeyer GmbH, Albstadt, Germany
Z-stage: P-725.1CD Controller: PI-655	PI, Karlsruhe/Palmbach, Germany
Tilt stage: M-044.00	PI, Karlsruhe/Palmbach, Germany
Incubator	FZ Jülich GmbH, Germany
Tempcontrol 37-2 digital, heating unit	PeCon GmbH, Erbach, Germany

Further Hardware

Incubator: Heracell 150i	Thermo Scientific, Germany
Laboratory scales: JB1603-C/FACT	Mettler-Toledo, Gießen, Germany
Vacuum desiccators, d=200 mm	Duran Group, Wertheim, Germany

Vacuum pump: RC6	Vucuumbrand, Wertheim, Germany
Laminar flow cabinet: H12	Heraeus, Osterode, Germany
Centrifuge: Heraeus Labofuge 400	Thermo Scientific, Germany
Centrifuge: 5415-R	Eppendorf,Wesseling-Berzdorf, Germany
Oven: E 400	Memmert, Schwabach, Germany
MilliQ: Gradient A10	Millipore, Billerica, USA
Laboratory water bath: WB-22	Memmert, Schwabach, Germany
Microscope: Axiovert 40 CFL	Zeiss, Jena, Germany

Appendix B: Materials

Consumable materials

Pipette tips: 2 µl, 20 µl, 1 ml, 5 ml, 10 ml	VWR, Darmstadt, Germany
Conical tubes: 15 ml and 50 ml	Greiner Bio-one, Frickenhausen, Germany
Cell culture dishes:	Nunc, Wiesbaden, Germany
6-well plates	Greiner Bio-one, Frickenhausen
Glass Pasteur pipettes	Brand, Wertheim, Germany
Cell culture flasks: 25 cm^2, 75 cm^2	Nunc, Wiesbaden, Germany
Kimtech science wipers	Kimberley Clark, UK
Parafilm	Pechiney Plastic Packaging, Chicago, IL, USA

Chemicals

Cryo-SFM (Cryopreservation Serum Free Medium)	PromoCell, Heidelberg, Germany
EDTA (Ethylenediaminetetraacetic Acid)	Sigma-Aldrich, München, Germany
Ethanol	Merck, Darmstadt, Germany
FBS (Fetal Bovine Serum)	Sigma-Aldrich, Munich, Germany
Fibronectin from human placenta	BD Bioscience, Fernwald, Germany
HBSS (Hank's Balanced Salt Solution)	Sigma-Aldrich, Munich, Germany
HEPES (4-(2-Hydroxyethyl)-1-Piperazineethanesulfonic Acid)	Sigma-Aldrich, Munich, Germany
Isopropanol	Merck, Darmstadt, Germany
PenStrep Solution: - 10000 units/ml Penicillin - 10 mg/ml Streptomycin	Sigma-Aldrich, Munich, Germany
Carboxilated Fluorospheres crimson, Ø 0.2 µm	Life Technologies, Darmstadt, Germany

Carboxilated Fluorospheres red, ∅ 0.1 µm	Life Technologies, Darmstadt, Germany
Trypsin-EDTA Solution: - 5 g/l Trypsin - 2 g/l EDTA 4Na	Sigma-Aldrich, Munich, Germany
PDMS	Sylgard 184, Dow Corning, Wiesbaden, Germany

Buffers and Media

EGM-2 (Endothelial Cell Growth Medium 2), prepared by adding Bulletkit to EBM-2 (Endothelial Cell Basal Medium 2): - GA-1000 (gentamicin sulfateamphotericin-B) 0.5 ml; - hydrocortisone 0.2 ml; - heparin 0.5 ml; - ascorbic acid 0.5 ml; - R3–IGF–1 (recombinant long R insulin-like growth factor 1) 0.5 ml; - VEGF (endothelial growth factor vascular human recombinant) 0.5 ml; - rhEGF (epidermal growth factor human recombinant in a buffered saline solution) 0.5 ml; - rhFGF–B (r human fibroblast growth factor - B) 2.0 ml; - FBS (Fetal Bovine Serum) 10 ml	Lonza, Cologne, Germany
PBS (phosphate buffered saline): - 8 g/l NaCl - 1 g/l D-Glukose - 400 mg/l KCl - 350 mg/l NaHCO3 - 60 mg/l KH2PO4 - 47.88 mg/l Na2HPO4	

Appendix C: List of Micro-Manager Scripts

Main MMscripts

FullConfig.bsh	Set initial configurations, load XY-stage and stretcher's positions from a .txt file
Close.bsh	Exit system and close XY-stage and stretcher's positions to a .txt file
30_min_Cell_Dyn_W.bsh[1]	Acquisition of a cell to check dynamics. Duration 35 min.
XYStrCellT_NRB_1to45_W.bsh	Stretch-and-hold experiment. Duration 70 min.
StrCntract_NRB_W_noS.bsh	Stretch-and-release experiment. Duration 70 min.
40_min_TE_W.bsh	Acquisition sequence after a cell was chemically removed from a substrate. Duration 40 min.
Control_2h_noShtr.bsh	Control experiment script (no stretching). Duration 105 min.
SingleAcqonly_W.bsh	Only acquisition sequence
XY_MA_back.bsh	Move XY-stage to x and y absolute positions (MA stands for "move absolute")
StretcherMA.bsh	Move stretcher to an absolute position
XYZListener.bsh	XY and Z-stages controlling script with substrate inner borders set as limits
XYZListenerNoLim.bsh	XY and Z-stages controlling script without limitations
XYReset.bsh	Script that resets XY-stage positions
StrReset.bsh	Script that resets stretcher position

[1] "W" stands for „White", meaning acquisition of a cell is performed only in the bright field. Similar scripts designated for transfected cells acquisition have both "GFP" (green fluorescent protein) and "W".

Auxiliary MM scripts

ZAF_start.bsh	Autofocus settings for the first acquisition
ZAF_afterStretch.bsh	Autofocus settings for the after stretch acquisition
ZAF_loop.bsh	Autofocus settings for the loop acquisition
PosFromFile.bsh	Read XY and stretcher positions from a .txt file

Autofocus settings

	Start autofocus	After stretch focus	Loop autofocus
Coarse step size (µm)	2.0	2.5	2.0
Coarse step number	10	34	6
Fine step size (µm)	0.3	0.3	0.05
Fine step number	2	2	4
Crop ratio	0.3	0.4	0.4
Threshold	0.02	0.02	0.02

XY-Stage Displacement Calibration

$dx = -6602 + 0.05 \cdot x_0 \quad [\mu st]$	$dx = -516 + 4 \cdot 10^{-3} \cdot x_0 \quad [\mu m]$
$dy = -457 - 0.02 \cdot y_0 \quad [\mu st]$	$dy = -16 - 2 \cdot 10^{-3} \cdot y_0 \quad [\mu m]$

Appendix D: List of Abbreviations

Units

°C	degree Celsius
mm	millimeter
ms	millisecond
mM	millimolar
nm	nanometer
µm	micrometer
µst	microstep

General

API	application programming interface
CFA	cell force analysis
CTF	cell traction forces
DVF	displacement vector field
EBM-2	endothelial cell basal medium 2
ECM	extracellular matrix
EDC	1-ethyl-3-(3-dimethylaminopropyl) carbodiimide
EDTA	ethylenediaminetetraacetic acid
EGM-2	endothelial cell growth medium 2
FA	focal adhesion
FBS	fetal bovine serum
GFP	green fluorescent protein
GUI	graphical user interface
HEPES	4-(2-hydroxyethyl)-1-piperazineethanesulfonic acid
IJ	ImageJ
IDE	integrated development environment
MM	Micro-Manager
pEGFP	plasmid enhanced green fluorescent protein
PEI	polyethyleneimine
PBS	phosphate buffered saline
PDMS	polydimethylsiloxane

pHUVEC	primary human umbilical vein endothelial cell
RFP	red fluorescent protein
SH	stretch-and-hold
SR	stretch-and-release
TE	trypsin – EDTA
TFM	traction force microscopy